A Study of Mass Reconstruction in $H^0 \rightarrow \mu^+\mu^-$

Master Thesis in Experimental Particle Physics

By

Rasmus J. Brekke

Department of Physics and Technology

University of Bergen

June 14, 2021

Acknowledgements

I would like to thank my supervisor Bjarne Stugu, for guiding me through what has been the most interesting and challenging project I have taken on in my life. I'm also extremely grateful to Graham Lee, for his experience with the software and seemingly endless patience with dumb questions from my side. This project could not have been completed without your help. I will also thank Gerald Eigen for valuable input and feedback throughout the project. I would also like to thank my lovely girlfriend for her infinite support during what has undoubtedly been a very tough time for us all. Lastly, I want to acknowledge the COVID-19 pandemic. You're an idiot.

Table of Content

Table of figures

Abstract

The goal of the thesis is to reconstruct the mass of the Higgs boson based on $H^0 \rightarrow \mu^+\mu^-$ events from the ATLAS experiment which is part of the Large Hadron Collider (LHC) at CERN in Geneva, Switzerland. The biggest challenge with this is the extremely small cross section of this decay, which means we will need a lot of data to potentially see a peak. In order to get to that we will use the much more common $Z^0 \rightarrow \mu^+\mu^-$ decay to learn about what we can expect from the signal, and to get measures of how well the detector is performing. By comparing to real data we can build up a signal from MC's to be comparable to what a real event would look like, and use that to calculate the luminosity and cross section of the Z^0 decay. That is useful when we look for the Higgs, where we can try to fit the signal and repeat the same calculation to try to estimate the luminosity and cross section of the $H^0 \rightarrow \mu^+\mu^-$.

Introduction

Ever since the Higgs boson was discovered in 2012, physicists have tried to learn more and more about it. Its status as the final part of the standard model puzzle made it very important for our understanding of how everything in the subatomic world is connected. This study aims to contribute to this by analysing a rarer decay channel of the Higgs, namely $H^0 \rightarrow \mu^+\mu^-$, which is not a common decay channel for the Higgs given the muon's comparatively small mass. However, for reasons that will be discussed later, it should be a cleaner interaction than the more dominant decay channels, making it easier to reconstruct and calculate. This is partly due to the lack of involved neutrinos or quarks, and partly due to the muons comparatively long lifespan in the microsecond range, meaning it can traverse large sections of the detector before decaying. This makes muons a lot easier to detect, and thus recreating the event becomes much simpler. The drawback is that this decay is so rare that it can be difficult to distinguish it from the background.

CERN

CERN (European Organization for Nuclear Research) was established in 1954 as a cooperation between the countries in Europe to further nuclear and particle research. It is based in Geneva, Switzerland, right on the Swiss-French border (1). Currently it has 23 member states, with Israel being the only state outside Europe (2). The magnitude of this cooperation has allowed CERN to become the biggest particle research facility in the world. It first became home to the Synchrocyclotron in 1957, which could accelerate particles to 600 MeV (3). It was used for experiments in both nuclear and particle physics, continuing to be used for nuclear research until 1990. The particle physics were left to the Proton Synchrotron (PS) in 1964, after it was built in 1959 (4). The PS could accelerate protons up to 25 GeV and is now used to accelerate beams and feed

them on the way to the LHC. It was succeeded by the Super-Proton Synchrotron (SPS) in 1976 with a 7 km circumference, able to accelerate protons to 450 GeV (5). Today it forms the last stage in the proton acceleration before being delivered to the LHC. Before the LHC was built, the 27 km circumference tunnel in which it sits was built to house the Large Electron-Positron collider (LEP) in 1985, before opening in 1989 (6). In the beginning it was operating at 91 GeV, topping out at 209 GeV in 2000 when it was closed in order to build the LHC, which started up in 2008.

Large Hadron Collider

The Large Hadron Collider (LHC) is what today sits in the 27 km circumference tunnel originally excavated for LEP. It is capable of accelerating protons up to a speed of 99,9999991% of the speed of light, at which speed the protons have an energy of around 6,5 TeV (7). They are accelerated up to this speed through three phases, starting with a bottle of hydrogen gas. The electrons are stripped off the protons before they are then sent into the linear accelerator LINAC2 and accelerated up to 50 MeV. From there they are sent to the PSB (Proton Synchrotron Booster) and accelerated to 1,6 GeV, collecting more bunches of protons in 4 synchrotron rings to increase the proton density before being sent to the next stage. After reaching a sufficient density of up to 100 billion protons per bunch, they are sent into the PS (Proton Synchrotron), accelerating them to 25 GeV before sending them to the bigger SPS (Super Proton Synchrotron). Here, they are accelerated further to 450 GeV, before entering the LHC. Here the protons are accelerated to the maximum energy of 6,5 TeV. Transferring from the SPS to the LHC, the pile of protons is also split into two beams, one clockwise and one anti-clockwise by the time they reach the LHC. The protons are kept going in a circle by massive electromagnets, cooled by superfluid helium to -271,3 ℃ to keep them superconducting. The magnets deliver a magnetic field strength of 8,3 T to allow the protons to stay on track at such high speed. At 4 points around the accelerator the tubes containing the protons intersect, where they can be smashed together so that physicists can study the outcome. These 4 experiments are ATLAS, CMS, ALICE, and LHCb. The goal is to find new heavy particles which might lead to discoveries of dark matter particles or supersymmetry. This is also teaching us about what the universe looked like in the extreme temperatures right after the big bang.

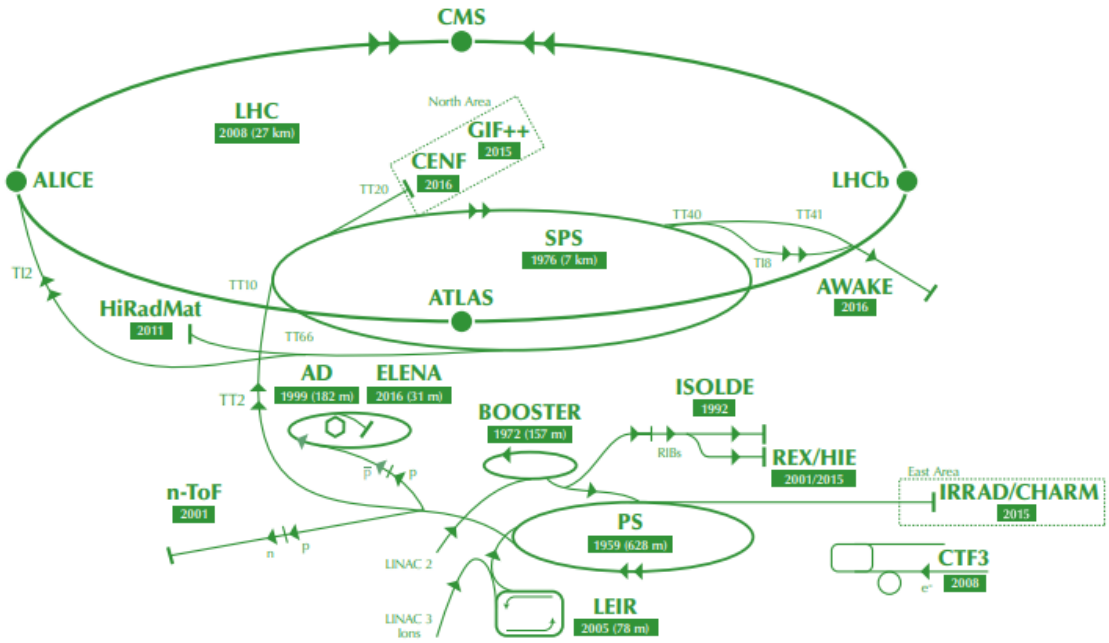

Figure 1: LHC complex at CERN (Credit: CERN (7))

ATLAS

ATLAS (A Toroidal LHC ApparatuS) is one of the four sites where the protons are smashed together. It is a massive detector built to pick up as much information as possible from the collision site and the resulting soup of exotic particles and decay products. In fact, ATLAS is the largest of the four LHC experiments, measuring 46 m in length and 25 m across (8). As is usual with this type of detectors, it is cylindrical, with layers of various sub-detectors to measure various properties of the particles and decay processes resulting from the collision in the centre. It also contains end caps at each end to catch particles leaving with a very narrow angle relative to the beam. Closest to the inside are tracking detectors to track the position of any escaping particles. The detector is also surrounded by powerful magnets in order to separate charged and neutral particles travelling through the detector, since charged particles will bend in the magnetic field. Because the path of a charged particle in a magnetic field is related to the momentum of the particle, if you can track the particle as it flies out from the collision, you can find both the position and momentum of the outgoing particle. Outside the Inner Tracker are the calorimeters. These have higher density in order to absorb the outgoing particles by slowing them down, measuring the energy the particle deposits in the detector. After the calorimeters comes the muon detectors. Since muons have a longer lifetime and more mass than electrons, they lose less energy to bremsstrahlung. They do not interact hadronically either, so they are not significantly slowed down by the calorimeters.

Inner detector

A particle produced in an event inside ATLAS will first meet the inner detector. It is cylindrical, measuring 7 m in length with a radius of 1,15 m. It is made up of three sub-detectors, a pixel detector, the Semiconductor Tracker and the Transition Radiation Tracker. As the particle enters the inner detector it is bent by a 2T magnetic field, which is helpful as it means we can calculate its momentum based on the curve of the path it takes. This will be explained in the next section. The first encounter is with the pixel detector, which is made up of four layers of pixels which very accurately can determine the position of the muon as it passes through. The fourth layer was added

in 2015 in the form of the Insertable B-Layer, closest to the beam (9). This layer provides even smaller pixels than the other three layers, to give more precise track measurements. Behind the pixel detector is the Semiconductor Tracker. It consists of 4 layers of silicon strip detectors designed to give more 2-dimensional information about the path of the particle, however with slightly lower resolution. The final part of the inner detector is the Transition Radiation Tracker. It is made up of parallel 4 mm thick straws, which are drift tube detectors filled with a mix of Xenon, Carbon dioxide and Oxygen. It is not as accurate as the Semiconductor Tracker, and it can only measure the transverse part of the path the particle takes. However, it can make a larger number of measurements than the pixel detector and the Semiconductor Tracker. The primary goal of the Transition Radiation Tracker is to recreate the tracks of charged particles as they pass through the detector, producing ionization radiation as they ionize the Xenon atoms in the straw. The electrons produced by the ionization will move to the wall of the straw where it is detected, and then the track can be reconstructed based on which straws are triggered. Another feature of the Transition Radiation Tracker is that it can identify electrons passing through the straw, because they will also produce transition radiation as they transition between the different layers of the straw.

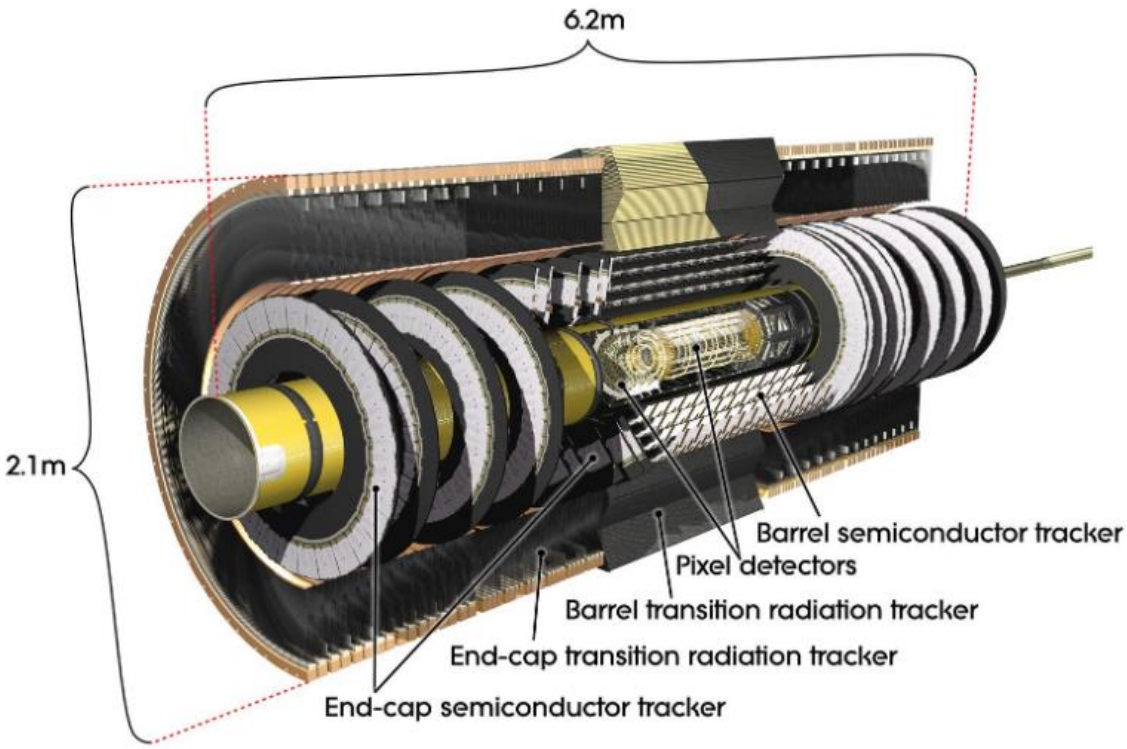

Figure 2: The ATLAS Inner Detector (Credit: CERN (9))

Calorimeters

The main goal of the calorimeter is to measure the energy of the particle entering it. It does this by absorbing it in the material of the detector and measuring the energy it deposits. The typical way to do this is to let the particle create a shower of secondary particles as it slows when entering the material. An electron entering the material will produce bremsstrahlung as it slows down, inducing a cascade of particles and antiparticles being created and annihilated. A photon entering the calorimeter would do this more directly, producing pairs of electrons and positrons that cascade deeper into the material. Calorimeters are often layered in alternating layers of dampening material

and sensors to measure the energy deposited. The sensors tend to be scintillators, where a photomultiplier reads out the electric pulses created in the scintillator. This type of calorimeter is called sampling calorimeters, unlike homogenous calorimeters, which are made up of a single type of material that combines the properties of the dampening material and the sensors. These types of calorimeters work predominantly for electrons and photons and are thus called electromagnetic calorimeters. Bigger and heavier hadrons also produce showers as they interact hadronically with atomic nuclei in the material. However, the material in an EM calorimeter usually is not enough to stop this type of particle, thus a denser hadron calorimeter is needed to measure them by maximising the effect of the hadronic showers. In ATLAS, the EM-calorimeter is a liquid Argon calorimeter, consisting of a barrel plus two end caps. This makes sure the calorimeter covers the full circle around the point of collision. The hadron calorimeter consists of a scintillator tile calorimeter in the barrel, with two liquid Argon calorimeters in the end caps (10).

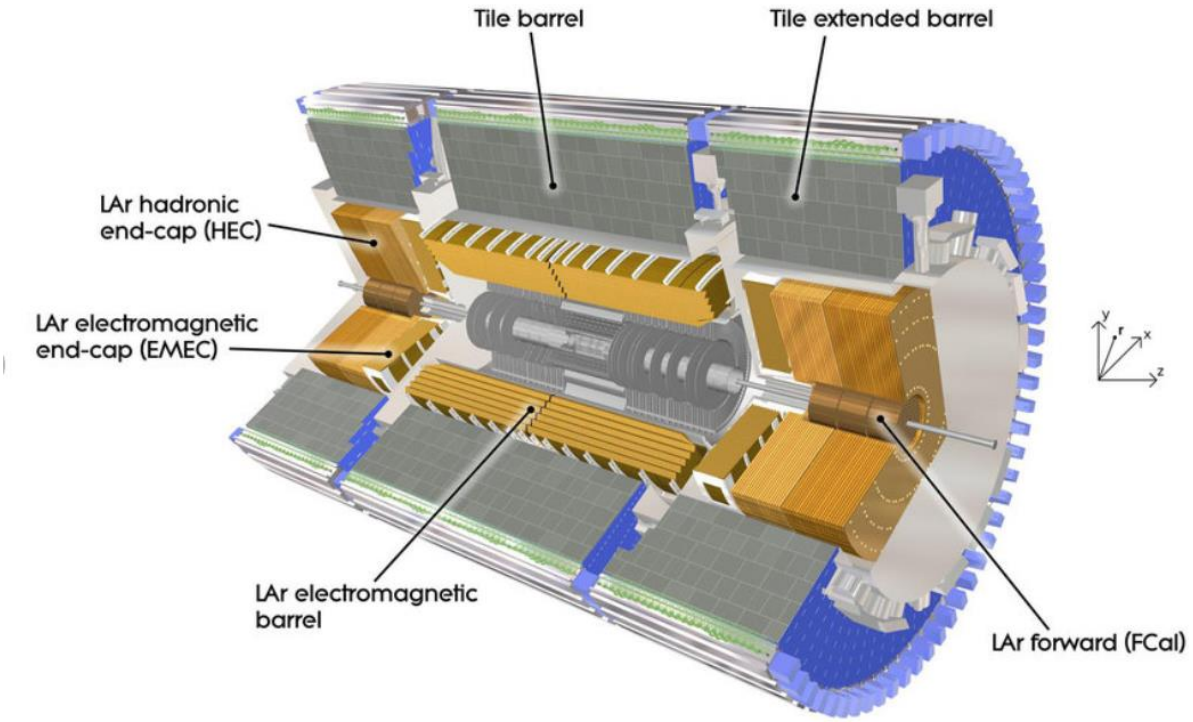

Figure 3: ATLAS Calorimeters (Credit: ResearchGate (11))

Muon Spectrometer

The calorimeters are good at picking up most particles produced in the collisions in the centre. Electrons and photons get picked up in the EM-calorimeter because they lose all their energy creating showers in the absorber material. Bigger, heavier hadrons lose their energy in the denser hadronic calorimeter through hadronic showers. However, because muons are about 200 times heavier than electrons, they do not lose much of their energy in the EM calorimeter, and they do not interact hadronically either, allowing them to pass through the hadronic calorimeter without a trace. Because muons have a lifetime of about $2{,}2 * 10^{-6}\ s$ (12), they have enough time to pass through the inner detector and calorimeters, so the muon spectrometer can form the outermost part of the ATLAS detector. Like the inner detector, the muon spectrometer measures the momenta of the muons by bending them in a magnetic field. The muons are tracked with monitored drift tubes and cathode strip chambers, arranged in layers both in the barrel and the end caps in order to track and identify the muons. The muons can then be identified using resistive plate chambers in the barrel, with thin gap chambers mounted in the end caps.

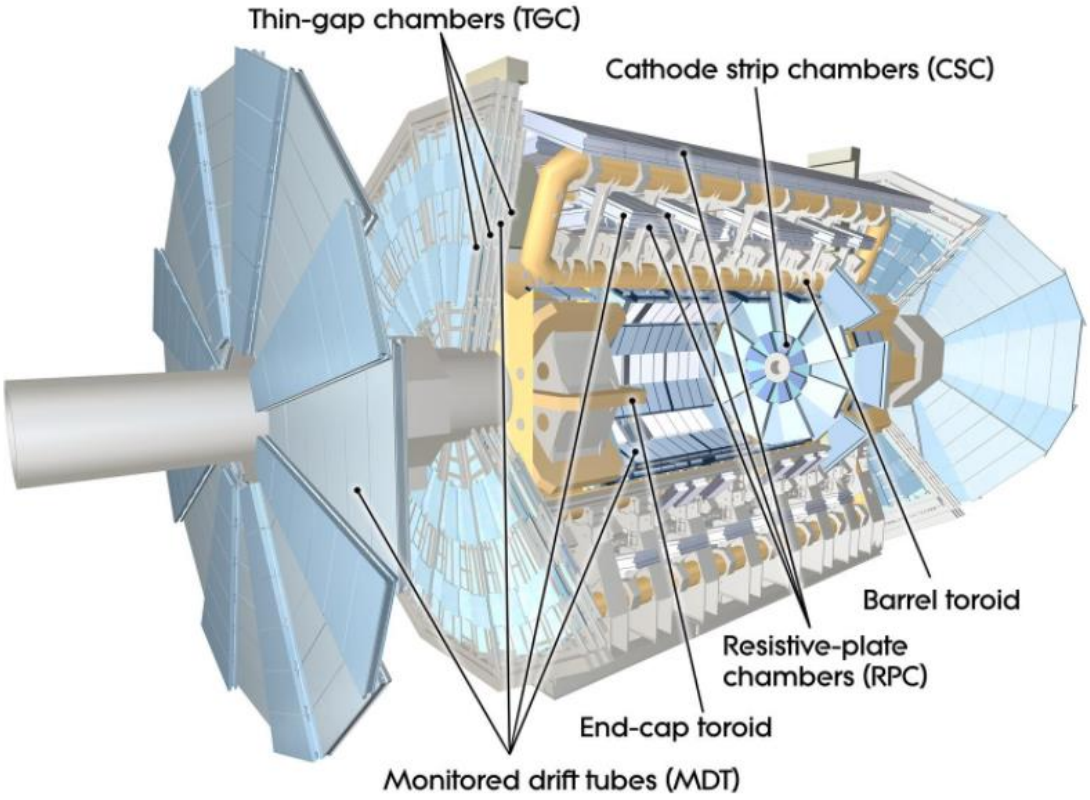

Figure 4: The ATLAS Muon Spectrometer (Credit: CERN (13))

Data Acquisition and Triggering

With the LHC running at its designed luminosity of $\mathcal{L} = 10^{34}\ cm^{-2}s^{-1}$, there will be about 40 million bunch crossings per second (14). On average, every time two bunches cross, 20 events happen where two protons collide. With each event on average producing 1000 particles, if ATLAS were to store the information, every event would take up 1 MB of space. This means the events in ATLAS would generate in the region of 1 PB of data per second, which is far too much to handle with any sort of efficiency. Thankfully, the vast majority of the generated events does not contain anything interesting, so by setting up various triggers and filters, a lot of this uninteresting information can be filtered out. This process consists of three different stages of filters that take information both from the sensors in the detector layers, and from the software used to process the information. The first stage is the level 1-trigger, taking information from the calorimeters and the muon spectrometer. It uses the information to select high p_T muons, electrons and photons, as well as jets and tau leptons decaying hadronically. This information is used to define more specific regions in the detector, where the more interesting parts of the interaction comes from. The data that makes it past this filter makes its way to the level 2- trigger, the rest is rejected. The level 1-trigger reduces the amount of data from about 1 billion collisions per second to around 75k. The level 2-trigger focuses on the parts of the data defined in the level 1-trigger. Using more refined filter criteria, it reduces the amount of data further to about 2k events per second. The final step is the event filter, which can analyse the data more closely and reconstruct tracks and vertices. This final trigger has a lot more time to analyse and decide whether to keep of reject the data, around 4 seconds compared to level 1 and 2 which decides in a fraction of a second. This further reduces the amount of data to around 10% of the amount after level 2, or about 200 hopefully interesting events per second.

Particle identification

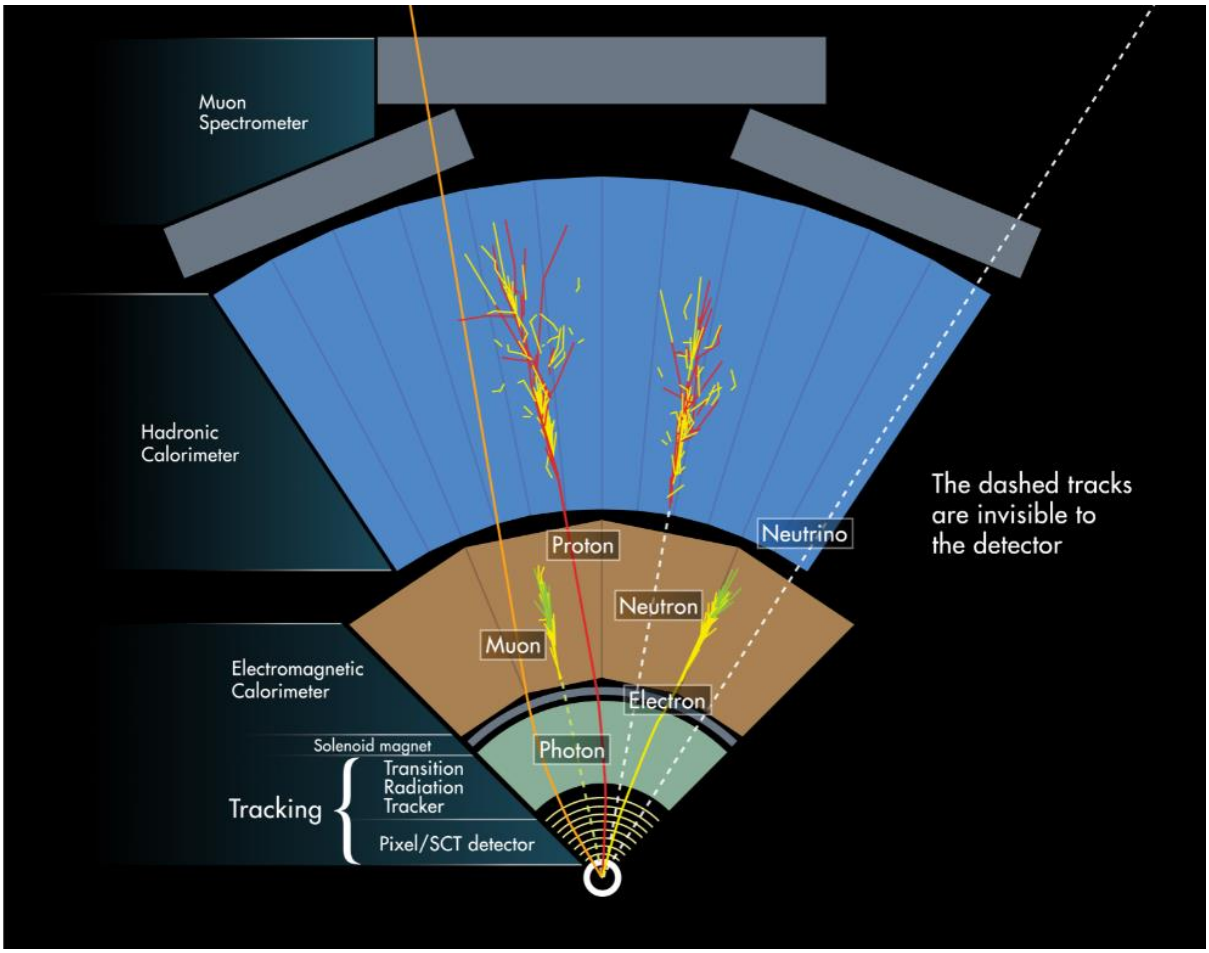

Figure 5: Particles traversing the ATLAS detector (Credit: CERN (15))

The proton-proton collisions happen in the centre of the detector, producing various particles that will traverse different parts of the surrounding detector. The inner detector can reconstruct the paths of all charged particles as they are being curved in the magnetic field, as well as identify electrons in the Transition Radiation Tracker. While the main use of the calorimeters is to measure the energy of the particles entering by absorbing them, they can also be used to identify particles combined with measurements from the inner detector. The Electromagnetic Calorimeter can also identify electrons as well as photons as they produce showers of electrons and photons when interacting with the material in the calorimeter. They can be distinguished since photons will not leave a trace in the inner detector due to its neutral charge. The Hadronic Calorimeter will absorb and identify hadrons like protons and neutrons, as well as other mesons like pions and kaons that are created in the event. While the proton can be traced in the inner detector due to its charge, the neutron will be totally invisible until it hits the hadronic calorimeter. Muons can be tracked in the Inner Detector, but it will pass straight through both calorimeters, and only in the Muon Spectrometer can they be identified. Neutrinos have no charge, and since they do not interact strongly either, they will leave no trace in any part of the detector.

ATLAS coordinates and units

The ATLAS detector uses certain coordinates and quantities to describe the events happening. Since the detector itself is cylindrical, it makes sense to use cylindrical coordinates, defining a point in the detector by the azimuthal angle ϕ, the polar angle θ, and the point z along the centre of the

cylinder. The azimuthal angle ϕ is the angle the particle follows relative to a plane perpendicular to the beam axis. This angle will thus go from $\phi \in [-\pi, \pi]$ to cover the full circle. The polar angle θ is the angle of the particle relative to the beam travelling along the Z-axis.

When describing the angle of the particle relative to the beam axis, ATLAS uses pseudorapidity, derived from the polar angle. The pseudorapidity is defined as

$$\eta = -\ln \tan \frac{\theta}{2} \tag{1}$$

Which depends on the polar angle θ (16). If a particle has $\eta = 0$ it is travelling perpendicular to the beam, and a particle travelling parallel to the beam will have $\eta = \infty$. The ATLAS detector can register muons with $-2{,}7 \leq \eta \leq 2{,}7$.

The transverse momentum is defined as the deviation of the curved path of the particle from a straight line. It can be defined as

$$p_T = |q|Br \approx \frac{|q|Bl^2}{8s} \tag{2}$$

Where q is the charge, B is the magnetic field strength, r is the radius of the path, and l is the arc length of the curved path. p_T is therefore proportional to the charge of the particle and the magnetic field strength. If the arc only takes up a small part of the circle, the radius can be approximated as $r \approx \frac{l^2}{8s}$ where s is the sagitta of the arc the muon follows in the magnetic field inside the detector. The sagitta refers to the height or depth of the arc, which depends on the radius of the circle the arc forms a part of and the angle the arc spans like this: (17)

$$s = 2r \sin^2 \frac{\alpha}{2} \tag{3}$$

The total energy is the energy as defined from special relativity,

$$E^2 = m^2 + p^2 \tag{4}$$

Written in natural units, it is just the sum of the squares of the mass and momentum.

The Standard Model

Note about units

Normally in classical mechanics you are used to using SI units (kilograms, meters, seconds) to define properties of objects. However, in the world of quantum mechanics, this is cumbersome, because many equations depend on the speed of light c or the Planck constant $\hbar$. Therefore, it is useful when working with this to define a new system of units, where these constants are equal to 1. This simplifies many equations, but the trade-off is that it introduces new units for a lot of properties. This means that quantities like mass, energy and momentum, which we traditionally define in kg, J and kg m/s are now all defined in eV, and time and length is defined in 1/eV instead of the previously familiar seconds and metres.

When trying to reconstruct a mother particle from two outgoing children, it is helpful to work with each particle's 4-momentum. The 4-momentum is a 4-vector represented like this in classical units:

$$p = \begin{bmatrix} \frac{E}{c} \\ \vec{p} \end{bmatrix} \tag{5}$$

Which, expanded and in natural units, becomes

$$p = \begin{bmatrix} E \\ p_x \\ p_y \\ p_z \end{bmatrix} \tag{6}$$

In our case, since the two muons are produced as decay products from the same mother particle, we can choose the reference frame of the mother, thus the 3-momentum of the muons must be opposite to each other:

$$p_{\mu_1} = \begin{bmatrix} E_1 \\ \vec{p} \end{bmatrix} \wedge p_{\mu_2} = \begin{bmatrix} E_2 \\ -\vec{p} \end{bmatrix} \tag{7}$$

This means the total 3-momentum of the mother is 0, and its 4-momentum must be

$$p_Z = \begin{bmatrix} E_1 + E_2 \\ \vec{0} \end{bmatrix} \tag{8}$$

This means the mother has the total energy equal to the sum of the energy of the outgoing muons, which means that the total energy is as defined by special relativity:

$$E^2 = m^2 + p^2 \tag{9}$$

Since we are in the reference frame of the mother, the momentum is 0, therefore

$$E^2 = m^2 \rightarrow E = m \tag{10}$$

Thus, we can calculate the mass of the mother in question, whether it is a Z^0, Higgs, or anything else.

Overview

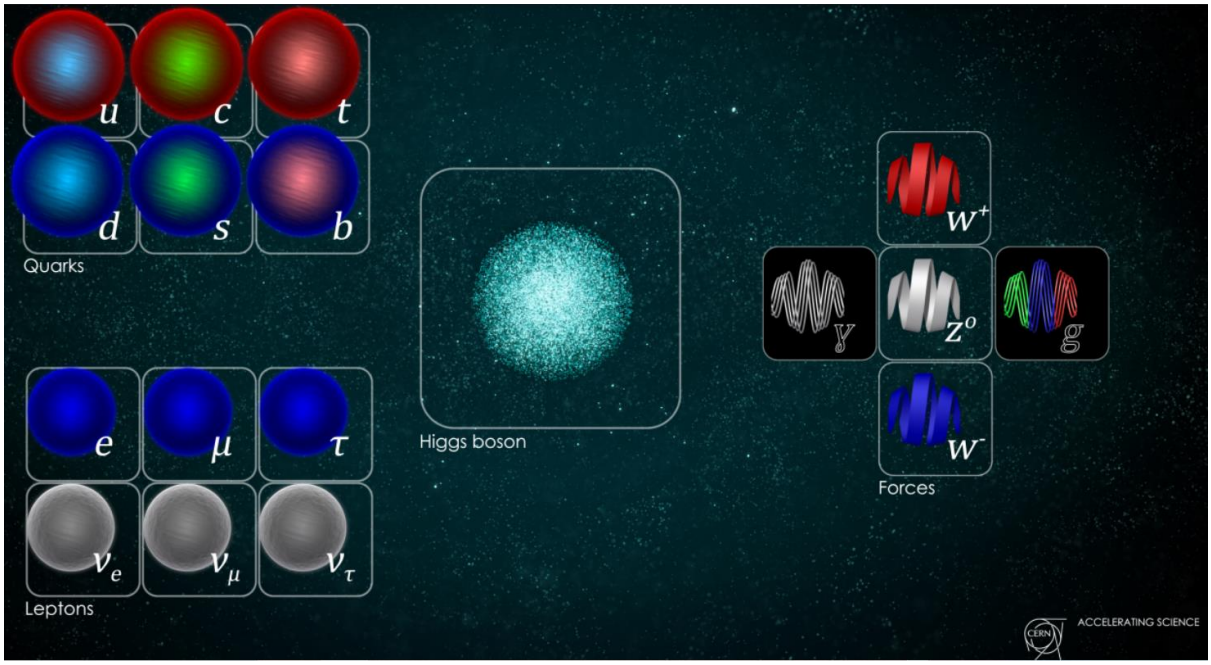

Figure 6: Standard Model of Particle Physics (Credit: CERN (18))

The standard model came about in the 1970s because physicists were discovering more and more new particles in the new particle accelerators of the time. The familiar proton and neutron were joined by several new particles which looked to have a vaguely similar structure, with the common denominator being that they all decayed in a fraction of a second. It was therefore suggested that these new particles were not in fact elementary, but compounds of sub-particles, called quarks. The new particles were classified in two different groups, baryons consisting of three quarks, and mesons consisting of a quark and an anti-quark. Since the standard model was proposed, physicists have discovered 6 flavours divided into 3 generations. These are the up, down, charm, strange, top and bottom quarks. Up and down are the only stable ones, with the 4 others decaying quickly. The up and down as well as the strange quark were theorised in 1964 by Murray Gell-Mann and George Zweig, with all three subsequently discovered by SLAC at Stanford in 1968 (19). The charm was theorized a few years later in 1970 by Glashow, Illiopoulos and Maiani, before being discovered in 1974, also at SLAC (20). The Bottom came next, being theorized in 1973 by two Japanese physicists before being discovered at Fermilab in 1977 (21). The top was theorized at the same time as the bottom, but it proved more challenging to discover. Its extreme mass of 173 GeV meant it took until 1995 to be confirmed after repeated experiments and upgrades at Fermilab (22). Assembling quarks into hadrons added another problem, as it created the possibility to break the Pauli exclusion principle. It states that two fermions (which quarks are) cannot occupy the same quantum state. However, it was discovered that certain of these compound particles had three identical quarks, which would violate the Pauli principle because the three quarks could only have two different spin directions. The solution to this was to give the quarks another property called colour, so each of the three quarks could take on one of the colours red, green or blue, with the only criteria being that the sum of the colours had to be white (all three combined or a single colour/anti colour). The quarks interact with each other primarily through the strong nuclear force, binding them together to form into hadrons (baryons and mesons). Since they have electric charge, they also interact electromagnetically, and they can also interact through the weak nuclear force when changing flavour. We will get back to what this all means later.

Table 1: Quarks in the Standard Model

Quark	Symbol	Mass	Charge	Colour	Spin
Up	u	2,2 MeV	+2/3	Yes	1/2
Down	d	4,7 MeV	-1/3	Yes	1/2
Charm	c	1275 MeV	+2/3	Yes	1/2
Strange	s	95 MeV	-1/3	Yes	1/2
Top	t	173 GeV	+2/3	Yes	1/2
Bottom	b	4,18 GeV	-1/3	Yes	1/2

In the standard model, the quarks are joined by the leptons, which include the electron, which was discovered to be an elementary particle in the late 1800s after experiments on the atom. It has since been joined by the muon and tau, which are similar in nature but much more massive, thus they decay relatively quickly. The muon, which is around 200 times heavier than the electron, was discovered in 1936 (23), and the tau followed it in 1975 being over 15 times heavier than the muon (24). These three interact only electromagnetically and weakly since they do not have colour charge.

Each of the electron, muon and tau are accompanied by a ghostly sibling, the neutrino. The neutrinos are almost massless, and have no charge, so they hardly interact with anything else, since they have neither colour nor electric charge. This means they can only interact weakly, making them near impossible to observe (25). The neutrinos are also leptons which, like the quarks, are also fermions. This means they have half integer spin, but they do not have a magnetic moment due to their lack of electric charge. Because neutrinos are so hard to observe, the first of them were only discovered in 1956 despite being theorized as early as 1930. The tau-neutrino was theorized in the 1970s, but not discovered until 2000. Neutrinos are so light that they were initially thought to be massless, but after the discovery that they can change flavour through the weak interaction it was concluded that they had to have some mass due to special relativity. The sum of the mass of all three flavours has since been refined down to less than one millionth of the electron.

Table 2: Leptons in the Standard Model

Lepton	Symbol	Mass	Charge	Colour	Spin
Electron	e^-	0,511 MeV	-1	No	1/2
Muon	μ^-	105,7 MeV	-1	No	1/2
Tau	τ^-	1777 MeV	-1	No	1/2
Electron Neutrino	ν_e	> 0	0	No	1/2
Muon Neutrino	ν_μ	> 0	0	No	1/2
Tau Neutrino	ν_τ	> 0	0	No	1/2

The last group in the table of elementary particles is the bosons. They are responsible for mediating the different forces discussed earlier. Bosons are different from fermions in that they have integer spins, thus they do not need to comply with the Pauli principle, and they are governed by slightly different rules. The family of bosons is divided into two subcategories, with all but one being vector bosons. These include the mediators of all the forces mentioned earlier. The strong nuclear force responsible for binding quarks together is mediated by the gluon, which is a massless, colour charged, electrically neutral, spin 1 vector boson. The gluon was theorized in 1962 and then discovered in the late 1970s (26). Because all hadrons must be colour neutral, it is very difficult to study individual quarks and gluons, because they can only be found in compounds that are colour neutral.

The weak nuclear force responsible for the decay of heavier particles is mediated by several particles, the W^+, W^- and Z^0. All three are necessary in different events, in order to conserve charge, as the $W^\pm$ are electrically charged, while the Z^0 is neutral (27). All three are relatively heavy, with the $W^\pm$ weighing around 80 GeV and the Z^0 around 91 GeV. All three were theorized in 1968 as the standard model was in the process of being finished, but their large masses meant it took until 1983 for them to be discovered at CERN. The weak force is involved when particles decay, for example beta decay, where one of the down-quarks in the neutron emits a W^- which in turn decays to an electron and an anti-neutrino.

The electromagnetic force is responsible for the repulsion and attraction between electrically charged particles. It is mediated by the familiar photon, which you will know is also the particle that makes up electromagnetic radiation. Like the gluon, it is massless and has spin 1, but it is colour and electrically neutral (28). The photon has been known since the early 1900s, when Einstein theorized it to explain the photoelectric effect, and it has since been validated by experiments. The photon shows up in several different events, for example various forms of scattering, creation and annihilation of particle/antiparticle pairs.

Table 3: Vector Bosons in the Standard Model

Vector Bosons	Symbol	Mass	Charge	Colour	Spin
W	W^+, W^-	80,379 GeV	+1, -1	No	1
Z	Z^0	91,188 GeV	0	No	1
Photon	γ	0	0	No	1
Gluon	g	0	0	Yes	1

The final piece of the standard model puzzle is the Higgs boson. It is a scalar rather than a vector boson because it has spin 0, unlike its vector boson cousins. It is responsible for giving particles mass as they interact with the field associated with it. The Higgs boson is one of the heaviest in the standard model, with a mass around 125 GeV, meaning it is extremely short-lived and all the more difficult to discover. It was first theorized in the 1960s by Peter Higgs and Francois Englert, and then at last discovered in 2012 simultaneously by ATLAS and CMS at CERN. The confirmation of its discovery gave the team that discovered it as well as Higgs and Englert themselves the Nobel prize in physics that year. The Higgs is normally produced in one of two ways. 90% of the time this is through the fusion of two gluons produced in the proton-proton collision. 8% of the time the Higgs is created by fusing two heavy vector bosons. Despite the significantly smaller cross section of the vector boson fusion, this channel is often more commonly used to analyse the Higgs because it tends to contain more useful handles to use in the selection process. This could for example be two high-energy quark jets going in different directions, with a Higgs emerging with high transverse momentum. With more data it is also possible to find a Higgs produced together with another vector boson (29). As mentioned briefly in the introduction, a lot of the common decay channels of the Higgs are messy and complicated to study. The most common channel is $H^0 \rightarrow b\bar{b}$, which has the problem that it is difficult to identify because the bottom-quarks will quickly decay and interact to form jets of quarks and hadrons, which looks very similar to the background in such an event. Another common decay channel is $H^0 \rightarrow WW$, but this too is complicated, since the $W^\pm$ will decay into quarks, giving the same problems as the bottom-channel, or they can decay into a lepton and a neutrino. This is difficult as well because these events cannot be fully reconstructed because the neutrinos are so hard to detect and will leave no sign in the detector. The Higgs can also directly decay to leptons, the $H^0 \rightarrow \tau^+\tau^-$ being most common due to the tau's large mass. However, this has the same problem as the $W^\pm$ decaying to leptons, creating traceless neutrinos that mean

reconstruction is near impossible due to the taus short lifetime. The most important decay channels used to identify the Higgs is $H^0 \to \gamma\gamma$ or $H^0 \to Z^0 Z^0$, where both Z^0's decay to either two electrons or two muons. Both these channels happen on the order 1/1000 Higgs decays each. For Higgs decays to fermions, the decay rate is proportional to the square of the mass of the fermion. For that reason, decays to muons are so rare because the muon mass is small compared to other fermions. For example, the tau is 17 times heavier than the muon, so the Higgs is 17 times as likely to decay to taus compared to muons.

Table 4: Scalar Bosons in the Standard Model

Scalar Bosons	Symbol	Mass	Charge	Colour	Spin
Higgs	H^0	125,10 GeV	0	No	0

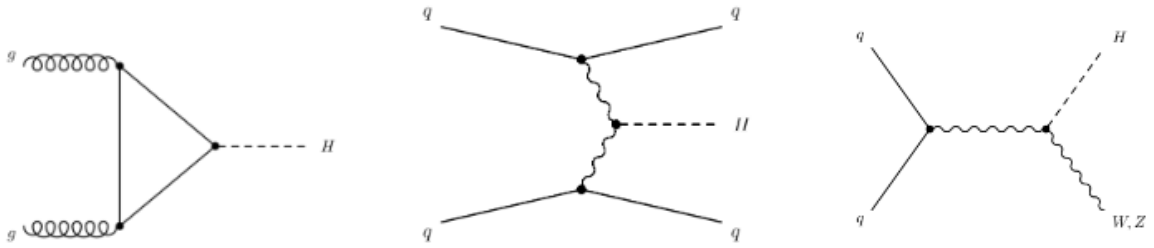

Figure 7: Common Higgs production channels: gluon-gluon fusion, vector boson fusion, vector boson-Higgs production

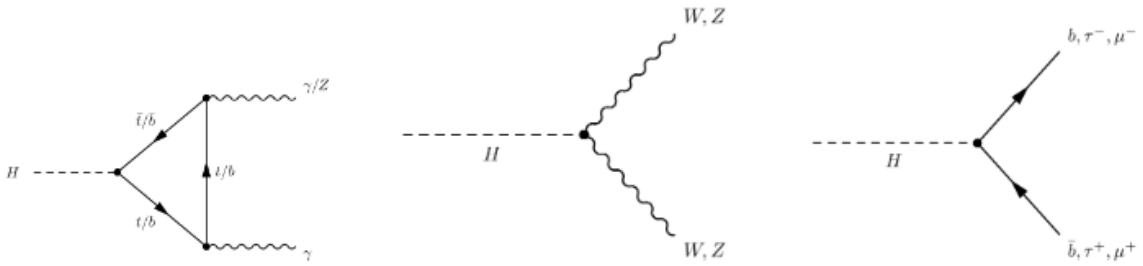

Figure 8: Common Higgs decay channels: two photons, two vector bosons, or two fermions

Software and samples used

The setup to complete this project is based on the ATLAS software tutorial inside LxPlus. That gives us the opportunity to download samples from datasets of real data as well as Monte Carlo simulations, which we can run through an algorithm we created using Athena. The MC samples are created by simulating a series of events of proton-proton collisions based on the knowledge we have about those interactions from theory and previous experiments. It is then simulated how each event is reconstructed based on knowledge of how the ATLAS detector works. This means that we end up with a file that contains information about the event as it happened, as well as how it was reconstructed in the detector. The samples are AODs (Analysis Object Data) or DAODs (Derived Analysis Object Data), meaning the particles in the events has been sequenced and labelled, making it easier to analyse them because the algorithm can look for specific particles by looking at the tag on each particle. In our case we want to look at muons, so we ask the algorithm to look inside the AOD and find all the particles in the muon container. These will have a PDG-ID of 13 or -13 depending on whether they are μ^- or μ^+. In the case of the MC samples, we can also choose to just select the muons that have decayed from a specific particle, meaning in our case we can plot just the

muons coming from a Z (identifying the Z by its PDG-ID of 23). Because all the particles are labelled, the sample contains information about each particle from the simulated event as it is reconstructed in the detector, allowing us to compare distributions before and after reconstruction, and analyse how each particle is reconstructed in the detector.

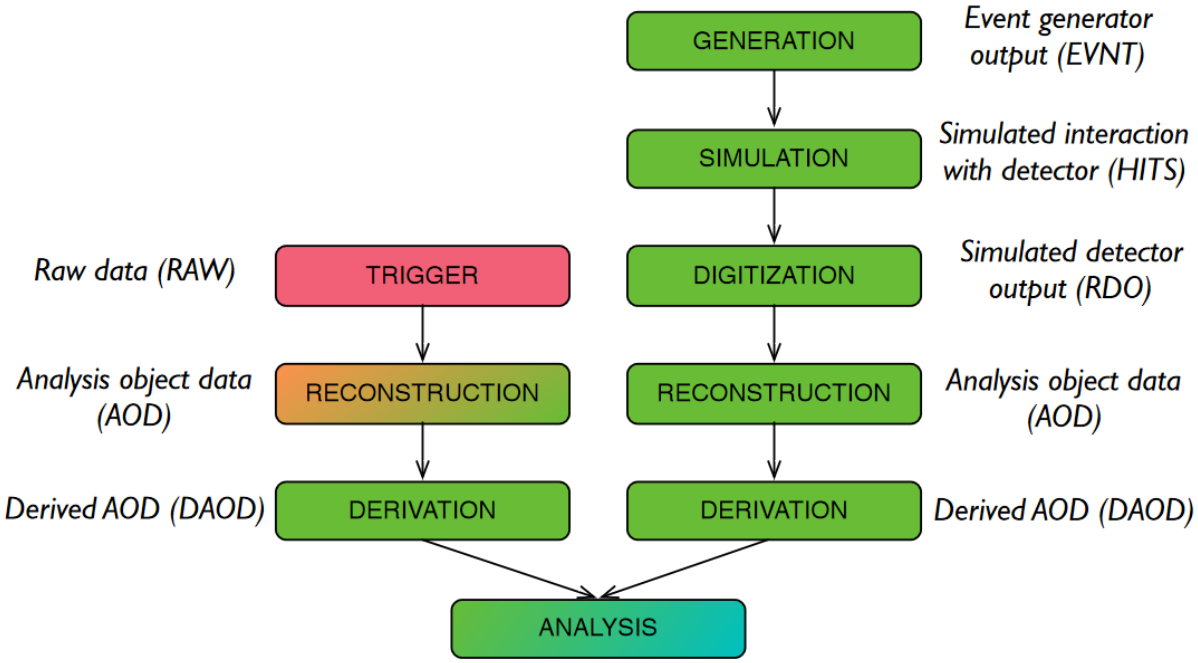

Figure 9: How AOD-files are generated (Credit: James Catmore, UIO (30))

The main challenge we faced with this project is that it required a basic understanding of the Linux operating system, since that is used by CERN, and we are accessing it locally from our computers through the terminal. The project also required an understanding of C++ programming, as that is the language used to build the algorithm and plot the information. This was needed because we had to start from scratch, building the algorithm ourselves to run through the data, store the information in ntuples, and then process it to create the plots. The datasets we used for this project were small enough that we could process everything locally, however it is possible for bigger datasets to send the algorithm to the grid and ask the central computers at CERN to process the data.

A full list of the samples used in this project with relevant information as well as how the algorithm is built can be found in “Source code and data samples”.

Learning the detector - $Z \rightarrow \mu\mu$

In order to get meaningful results from the eventual Higgs sample, it is important to know how our results might look. Therefore, we start with a pure $Z^0 \rightarrow \mu^+\mu^-$ sample, which is generated from a Monte Carlo simulation. The benefit of this is that you can access information about the actual, simulated event (truth information) in addition to the simulated reconstruction of the event through the simulated ATLAS detector. This allows you to compare the results you would see in the detector to the actual event, giving you the opportunity to tune the measurements to make the reconstruction look more like the real event. The Z^0 was chosen because it behaves reasonably similar to the Higgs, being both heavy and electrically neutral, as well as decaying in similar

circumstances. Firstly, we look at the sample, picking out the variables η, ϕ, transverse momentum p_T and total energy E of all the muons. The sample selected gives the following plots:

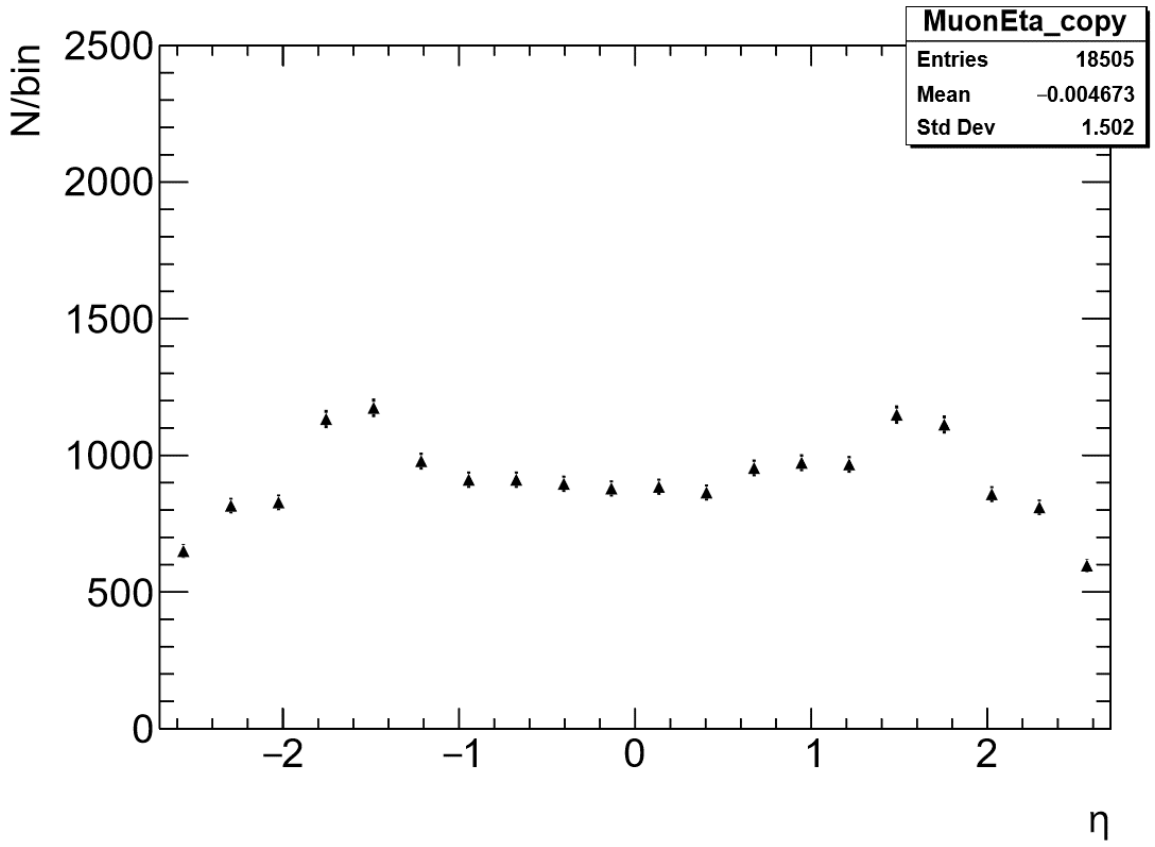

Figure 10: Reconstructed η of all muon candidates produced from Z-μμ events

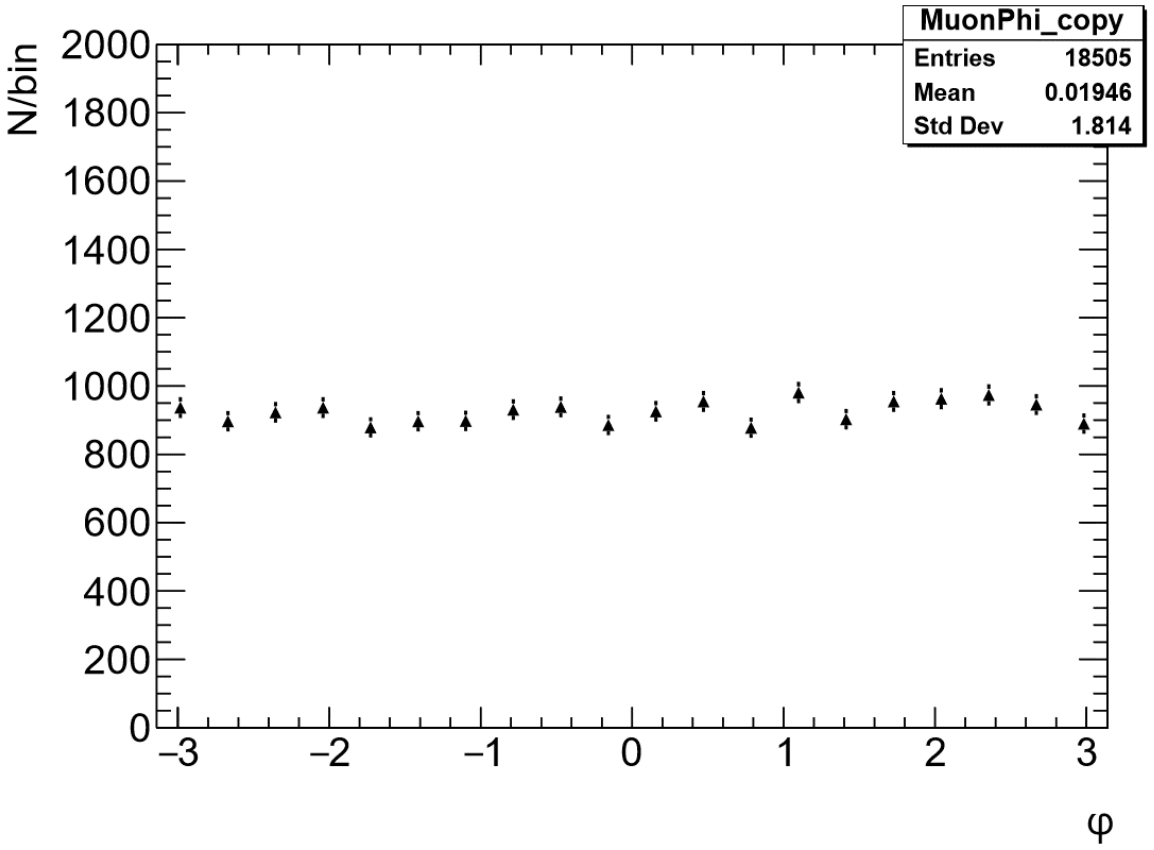

Figure 11: Reconstructed ϕ of all muon candidates produced from Z-μμ events

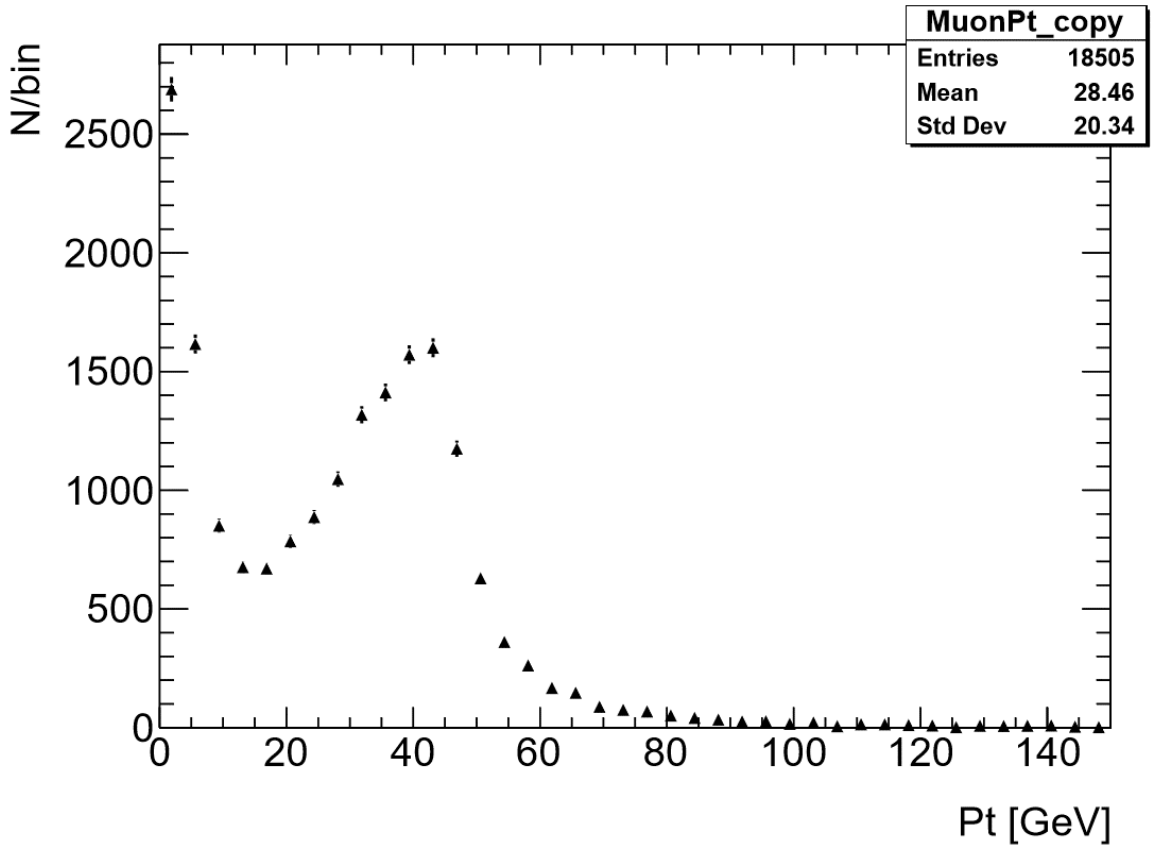

Figure 12: Reconstructed p_T of all muon candidates produced from Z-μμ events

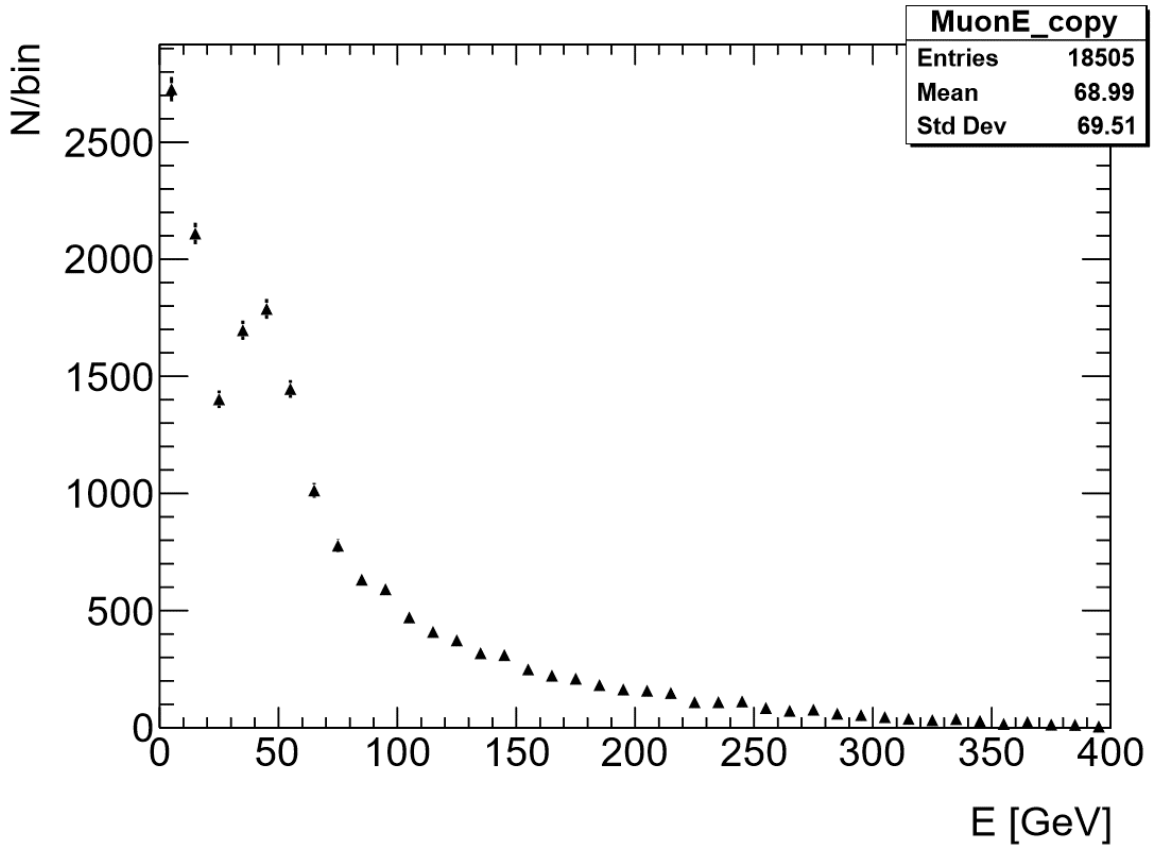

Figure 13: Reconstructed E of all muon candidates produced by Z-μμ events

The η and ϕ distribution acts mostly as sanity checks, and they look roughly as they should. The η distribution seen in figure 10 would be expected to be smoother with most muons in the centre around $\eta = 0$, however the two visible peaks can be attributed to another source of muons which will be discussed later. The ϕ distribution seen in figure 11 should be uniform, and it pretty much is, which is a good sign. The p_T and E plots are more interesting, knowing that the Z^0 mass we are looking for is 91 GeV, we would expect to register more muons with energy and momentum about half of that. In the p_T-plot in figure 12 this is clear, with a peak around 40-45 GeV, and we also see the same peak in the energy distribution in figure 13. The p_T-plot reveals a large amount of low p_T muons as well, which are the same muons mentioned in the η-distribution. In order to calculate the Z^0 mass, we need to know a bit more. It is helpful to see how many muons are in each event, this will give a hint of what needs to be done to find the Z^0.

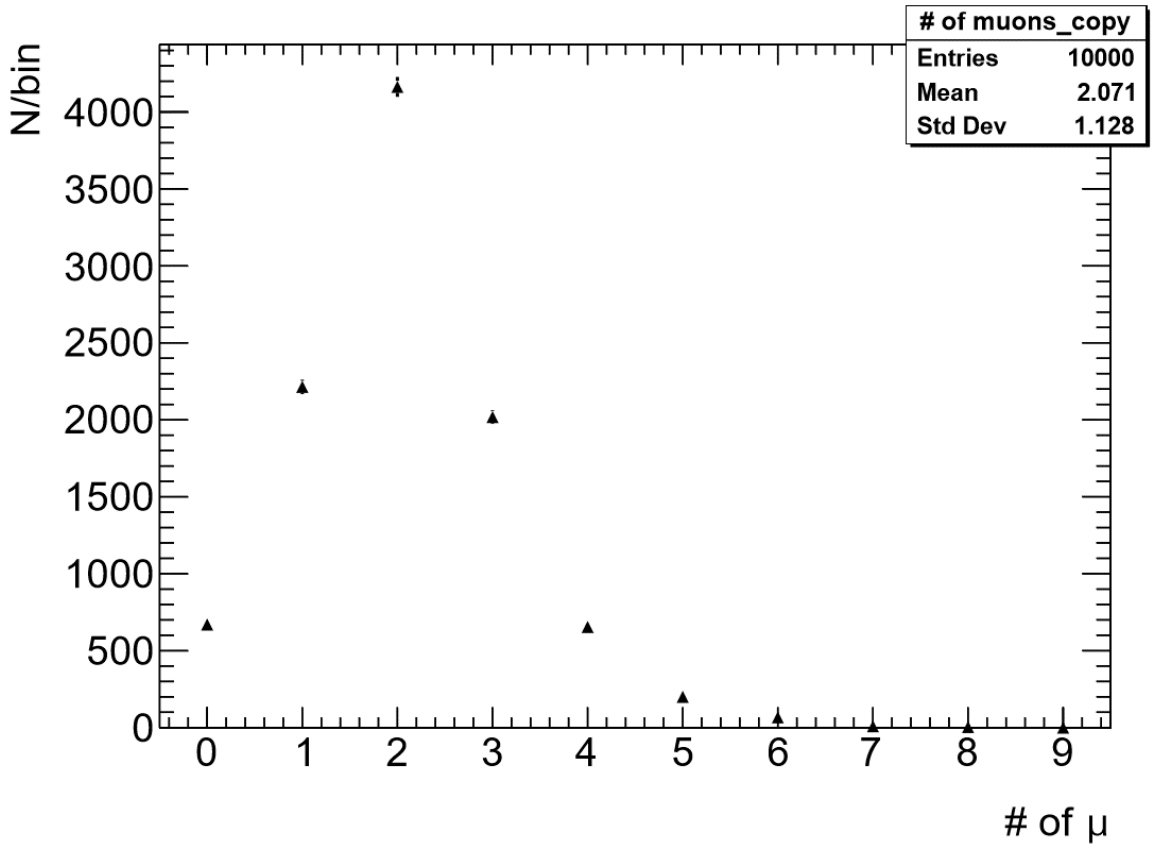

Figure 14: Number of muon candidates from Z decay reconstructed per event

As we can see from figure 14, most events contain exactly two muons, which is a good sign. However, we can also see several events with only one or no muons at all, which means that some muons are lost in the detector for various reasons we will get back to. There are also many events with more than two muons, which means there is some source of background muons that we need to filter out. The simplest solution to reconstruct the Z^0 is to choose the two muons with the most p_T from all events with two or more muons. We can then extract the 4-vector for them both and add them together to calculate the Z^0-mass, as shown with equations 5-10. The two muons, which are referred to as the leading and sub-leading muons, have the following p_T-distributions:

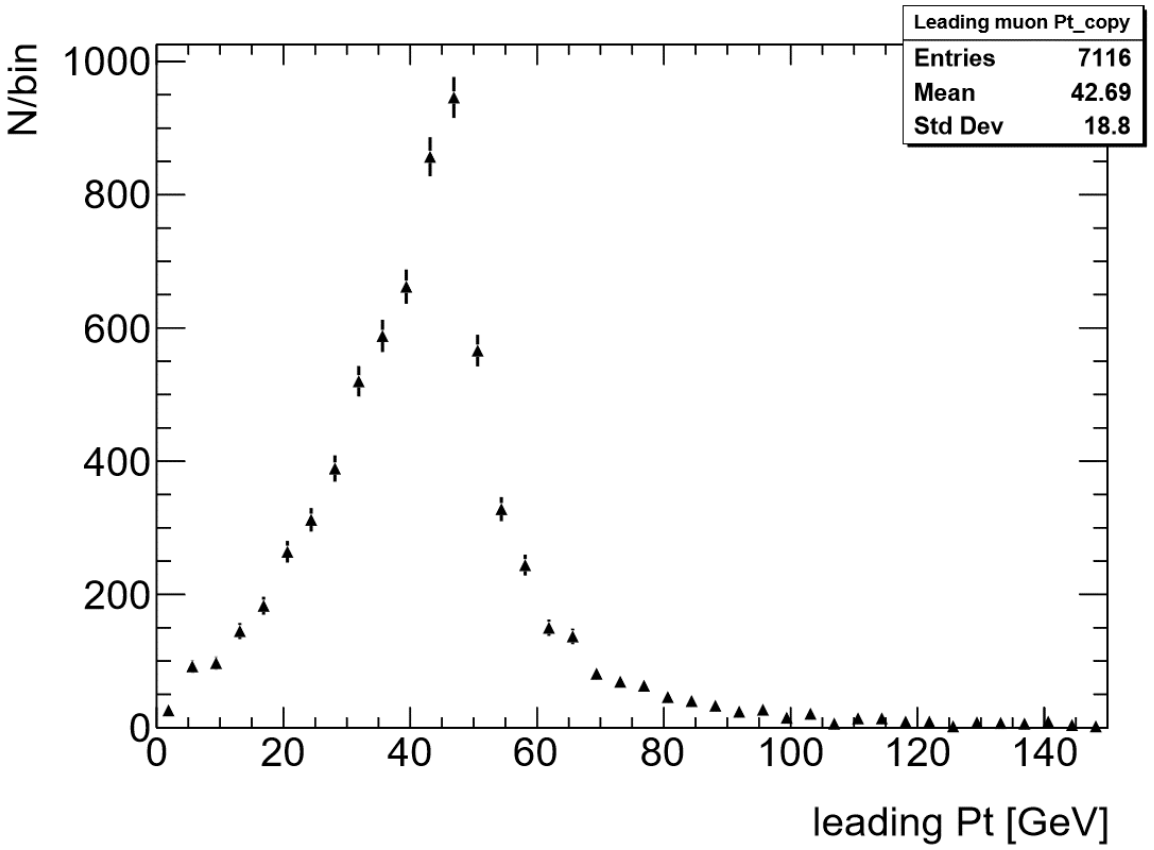

Figure 15: p_T of leading muon candidate

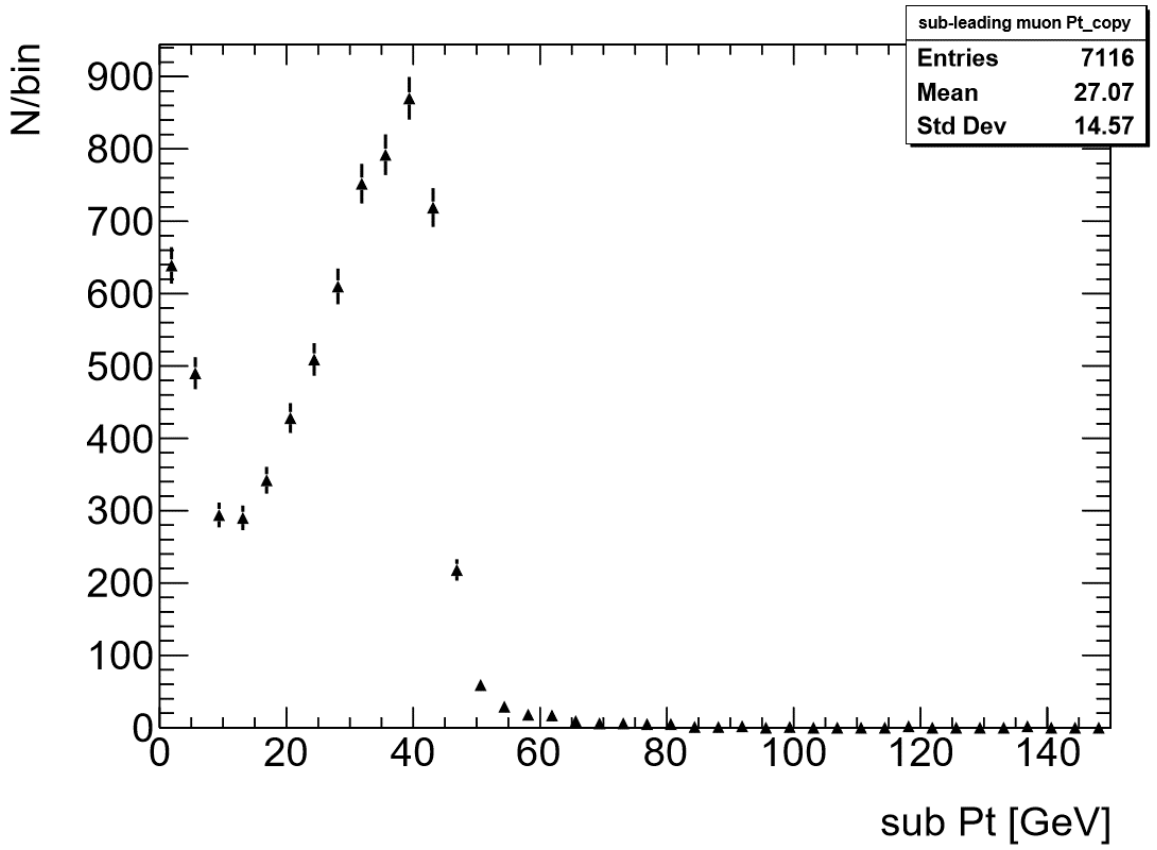

Figure 16: p_T of sub-leading muon candidate

It is apparent from figure 15 and 16 that the plots have the peaks in the same region where we would expect, but it is also clear that we are picking up a tail of background as sub-leading muons in figure 16. Adding them up and extracting the Z^0-mass, we get the following distribution:

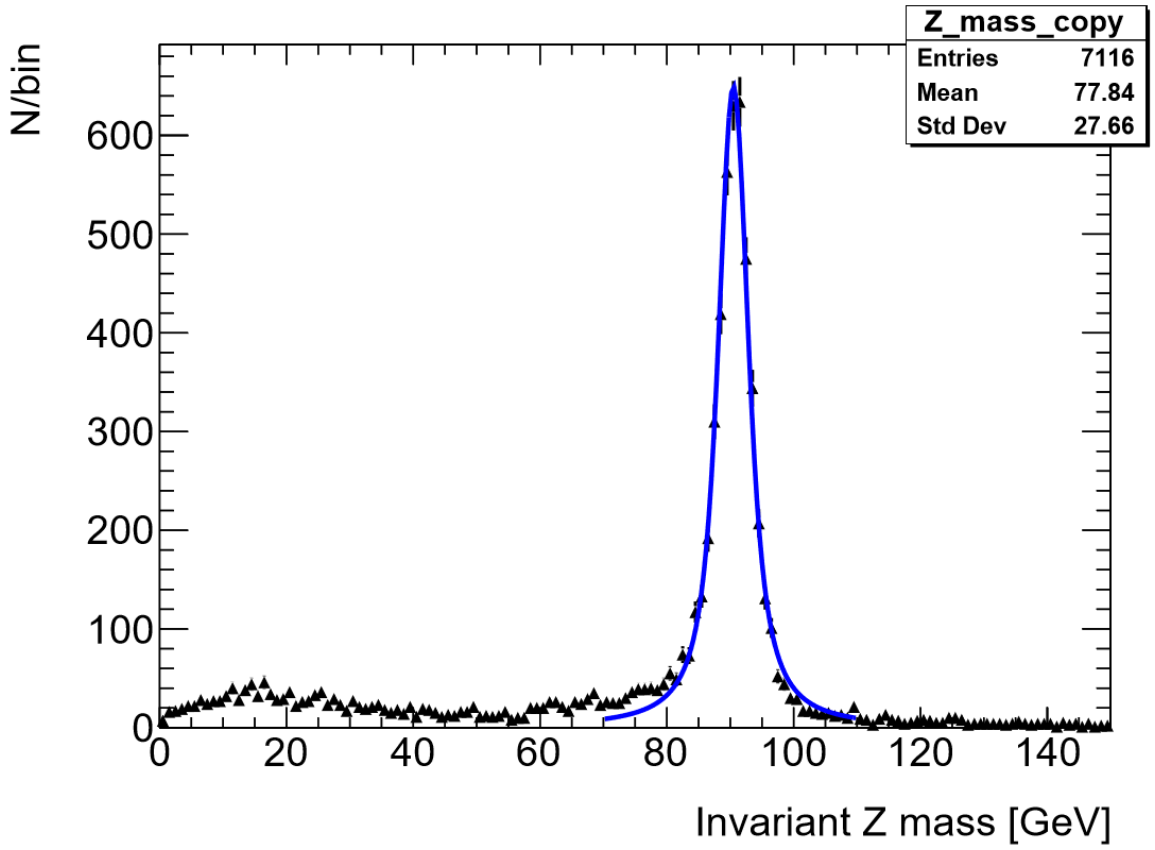

Figure 17: Z mass as calculated from leading and sub-leading muon candidates with gauss/BW convoluted fit

We use a convoluted Gauss+Breit Wigner function to fit the peak. The Gaussian looks like this:

$$f_{Gauss}(x) = p_0 e^{-\frac{1}{2}\left(\frac{x-p_1}{p_2}\right)^2} \tag{11}$$

In eq. 11 we have p_0 as the magnitude of the peak, p_1 as the mass, and p_2 as the standard deviation of the peak. The Breit Wigner function looks like this:

$$f_{BW}(x) = \frac{p_0}{(x^2 - p_1^2)^2 + p_1^2 p_2^2} \tag{12}$$

Here p_0 is also the magnitude of the function, p_1 gives the mass, and p_2 is the full width of the peak at half maximum. We use a convolution between them which generates a single function by reversing and shifting one of the functions and then integrating the sum of the overlapping area between them as one function is shifted. This generates a third function that expresses how the shape of one of the initial functions is modified by the other (31). Our convoluted function has 4 parameters, which is the mass, full width from the BW, the area under the function, and the standard deviation of the Gaussian.

The convoluted fit gives the following parameters for the plot in figure 17:

Table 5: Parameters for Gauss+BW convoluted fit on Reconstruction

Parameter	Value	Error
Mass	90,5021	0,0506255
FWHM	4,29347	0,174105
Area	5336,92	77,1470
Sigma	1,18507	0,139093

The result is clear, with most leading and sub-leading muons adding up to $m_Z = 90{,}50 \pm 0{,}05\ GeV$, with the width of the peak being $4{,}3 \pm 0{,}2\ GeV$ as shown in table 5. The background mentioned earlier is known as minimum bias. It shows up as the peaks in the η distribution, and the tail of low p_T muons that sometimes is selected as a sub-leading muon. This also creates the tail of low mass entries in the mass plot. The Minimum Bias comes from the selection criteria because we are not using a specific working point to select the muons. This means the muons will by default be selected with a very loose working point with as few biases as possible (hence minimum bias). This means muon candidates from inelastic events are also included and selected by the algorithm. More relevant background contributions will be discussed in more detail later.

In order to get a clearer view of the efficiency of the detector and to fully exclude the minimum bias, we can dig deeper into the Monte Carlo and look at the truth information. This tells you about the simulated event as it happened, without being filtered through the simulated detector. This allows us to compare the true distributions to the reconstructed distributions.

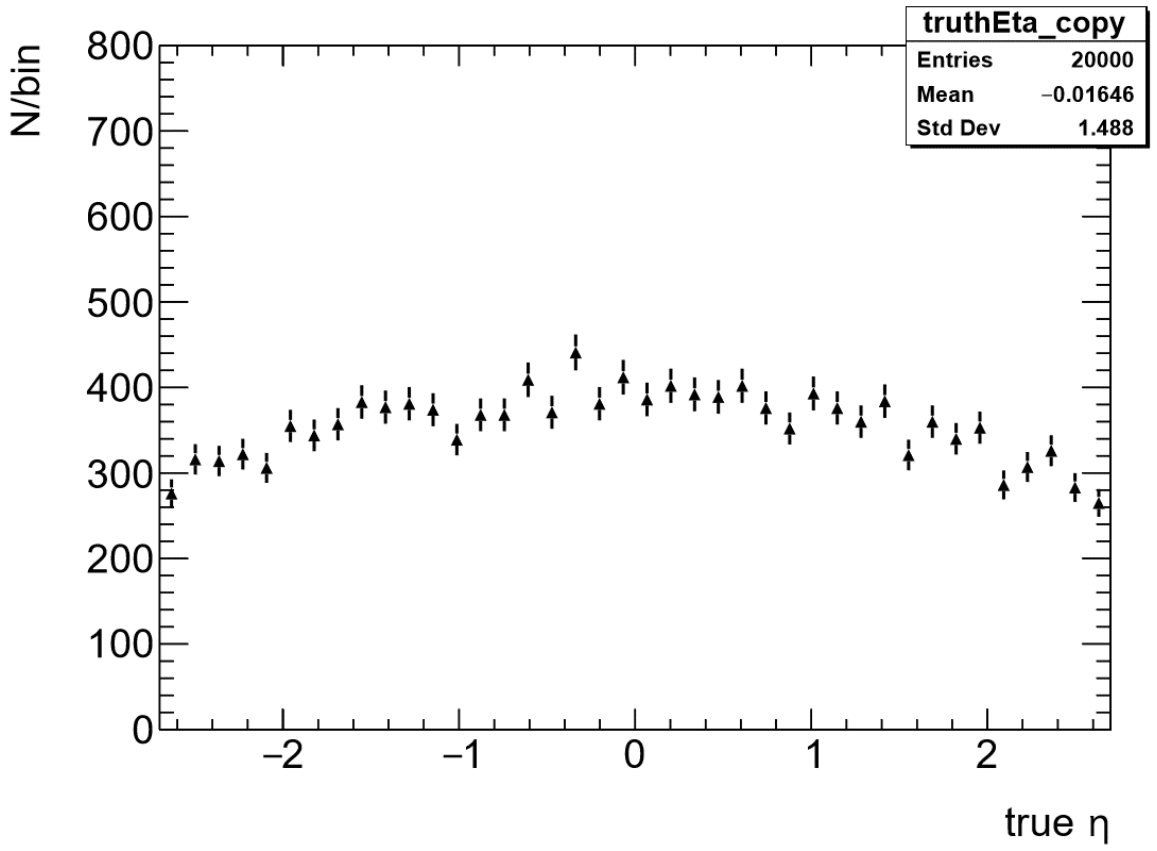

Figure 18: η from muons in truth information

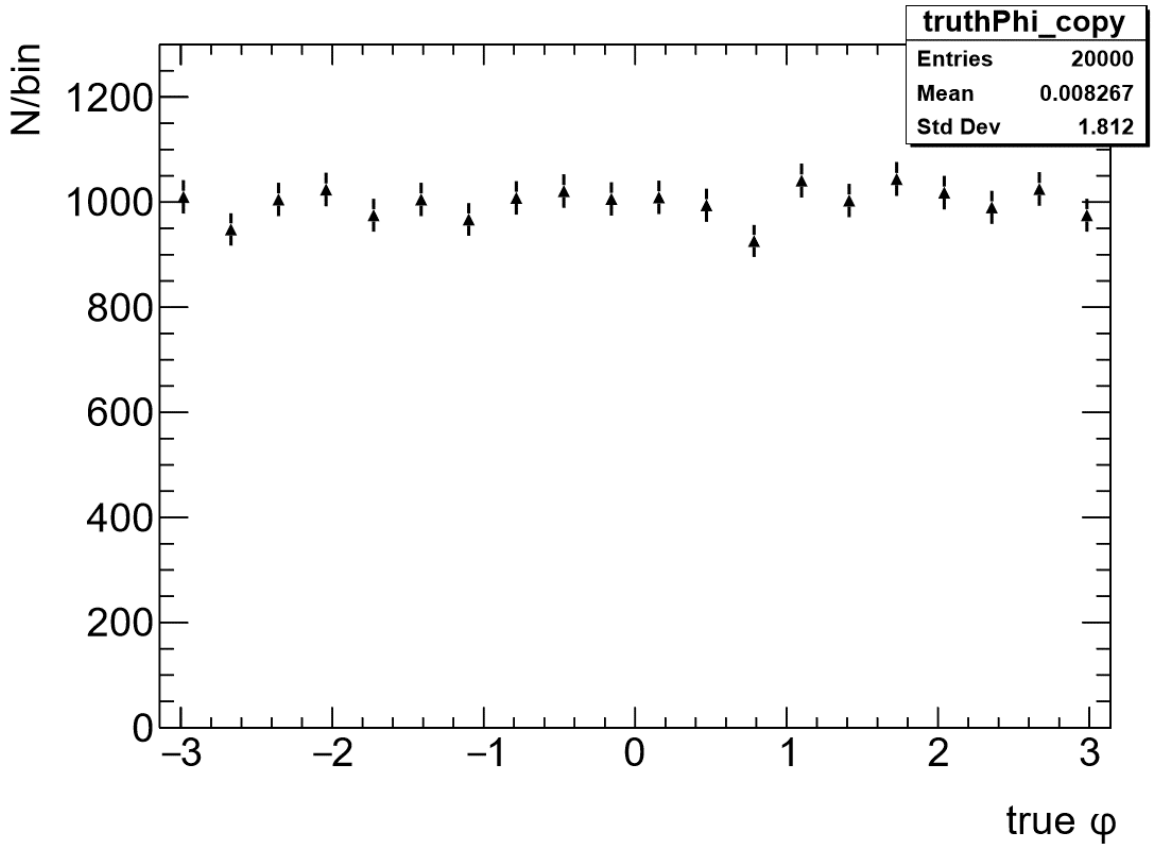

Figure 19: ϕ from muons in truth information

The η distribution in figure 18 looks significantly different from the reconstructed distribution in figure 10, which must come from the muons in the minimum bias having a particular direction compared to the muons coming from the Z^0. The ϕ distribution in figure 19 looks the same as in figure 11, which is interesting, because it can help us isolate the background from the signal, which will be helpful in the future. More important are the p_T distributions, which will give a better picture of the Z^0 itself.

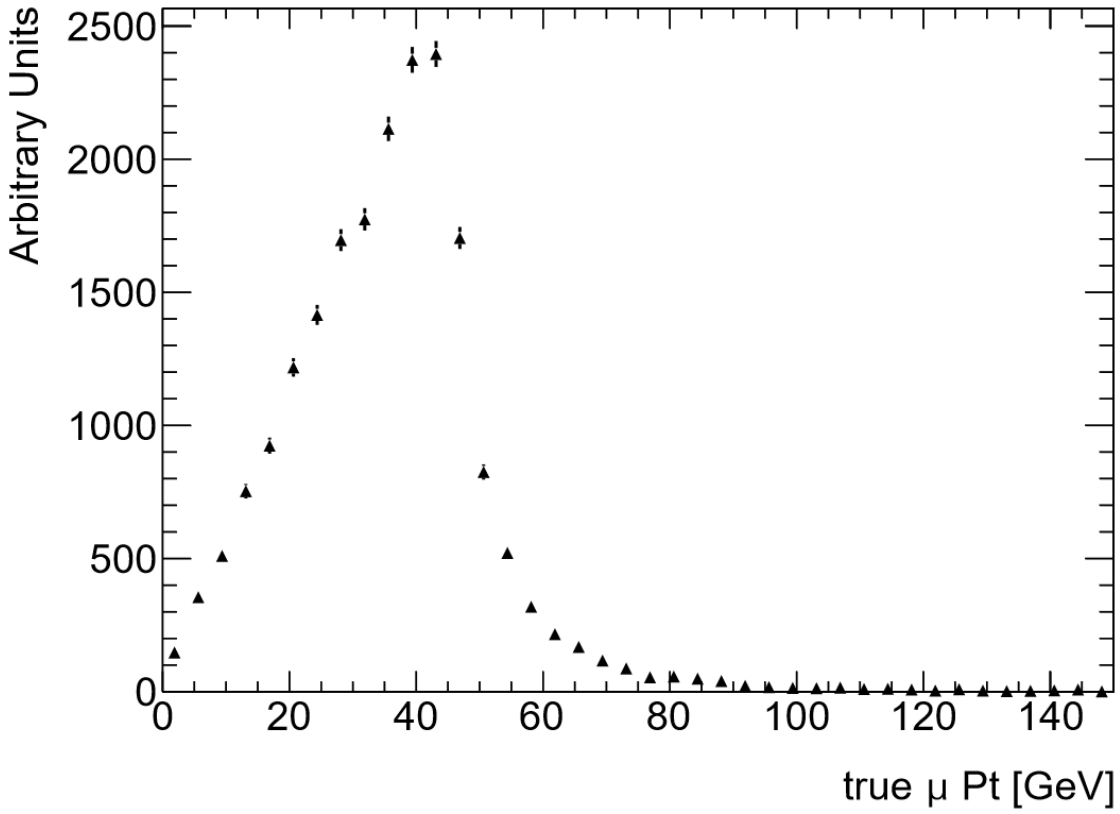

Figure 20: p_T from both muons in each event in truth information

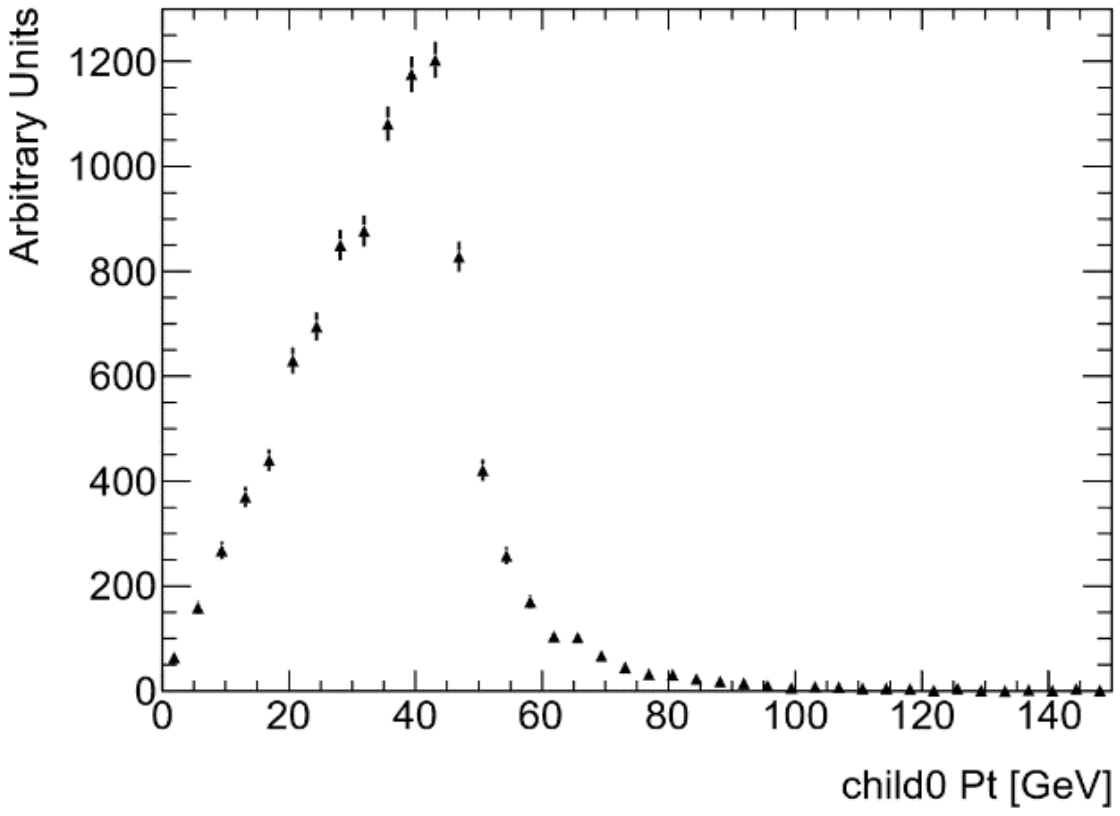

Figure 21: p_T from muon 1 in truth information

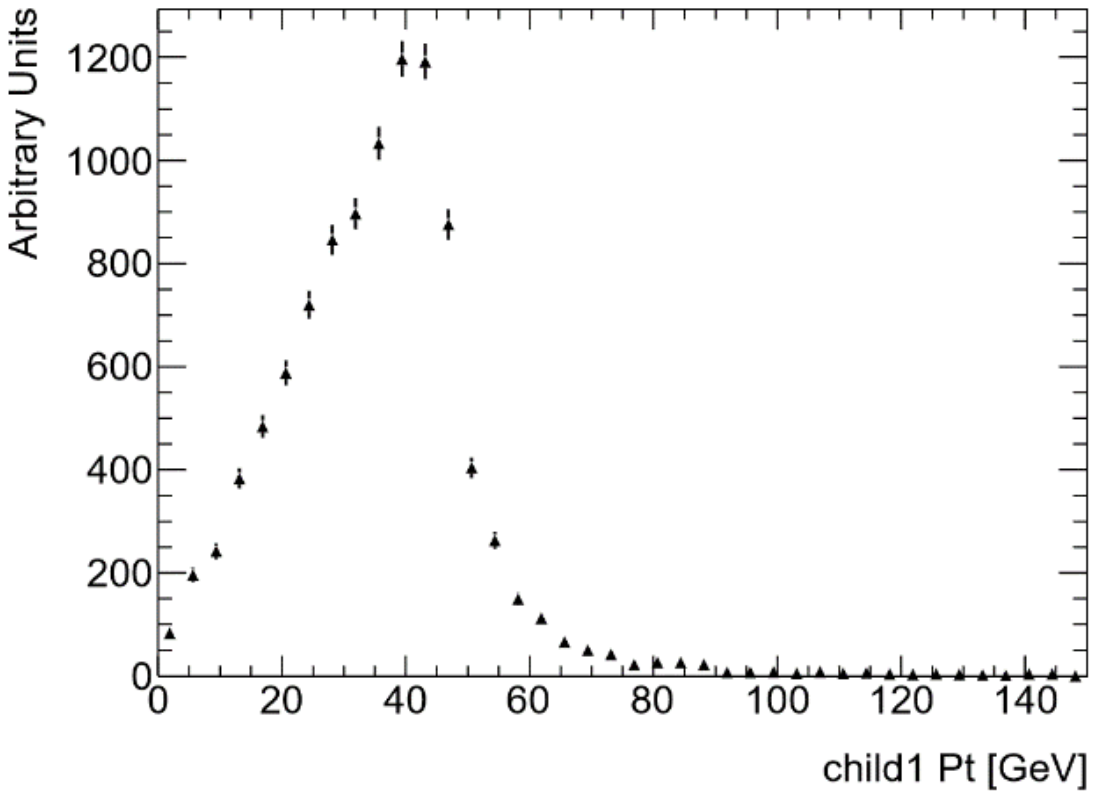

Figure 22: p_T from muon 2 in truth information

All three plots in figures 20, 21 and 22 look very similar, for good reason, since the Z^0 decay produces two muons with p_T adding up to the same value. This means the p_T distribution for each of the muons should be identical. These p_T distributions also look similar to the p_T-distribution for the leading muon in figure 15, since the leading muon in the reconstruction is highly likely to be one of the children coming from the Z^0. Doing the same with the two children as we did with the leading and sub-leading muons, gives this Z^0 mass distribution:

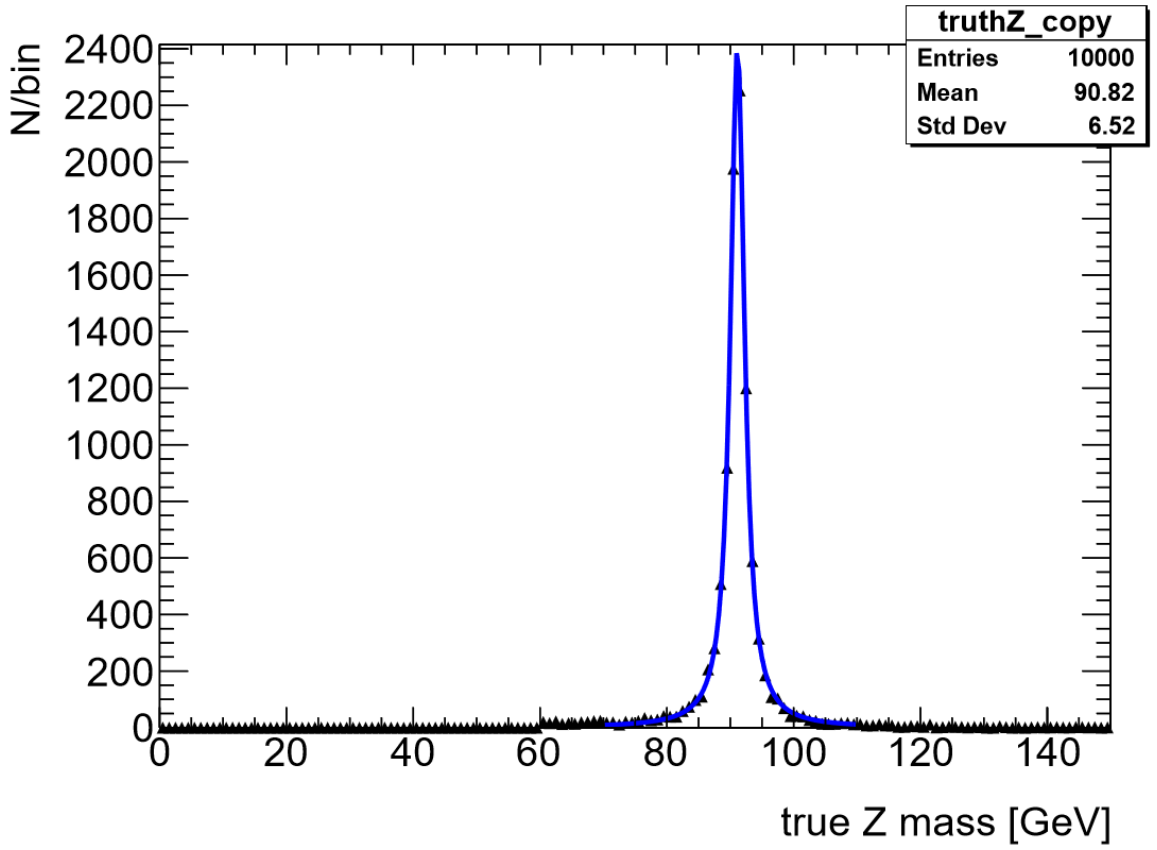

Figure 23: Z mass from muons in truth information with Gauss+BW convolution

The fit on the distribution in figure 23 gives the following parameters:

Table 6: parameters for Gauss+BW convoluted fit for truth information

Parameter	Value	Error
Mass	91,1351	0,0186190
FWHM	2,55158	0,0592204
Area	9976,59	102,521
Sigma	0,242672	0,121223

Where the Z^0 mass is estimated to $m_Z = 91{,}14 \pm 0{,}02\ GeV$, and confirming the width of the peak at $2{,}55 \pm 0{,}06\ GeV$, as shown in table 6. This is very close to what we would expect and confirms the results of previous experiments on the Z^0.

Having looked at the distribution of muons both as they were produced and how they were reconstructed, we made some good comparisons, however the minimum bias in the reconstruction makes it difficult to directly compare the two. If we can eliminate that, we can see directly how the distributions of the muons change as they are reconstructed. That would enable us to analyse the detector efficiency and resolution. Luckily for us, the AOD-file allows us to go through the muons and only plot the ones that actually was produced by the Z^0 decay. This will be referred to as truth matching, where we plot the muons that are matched to a Z^0.

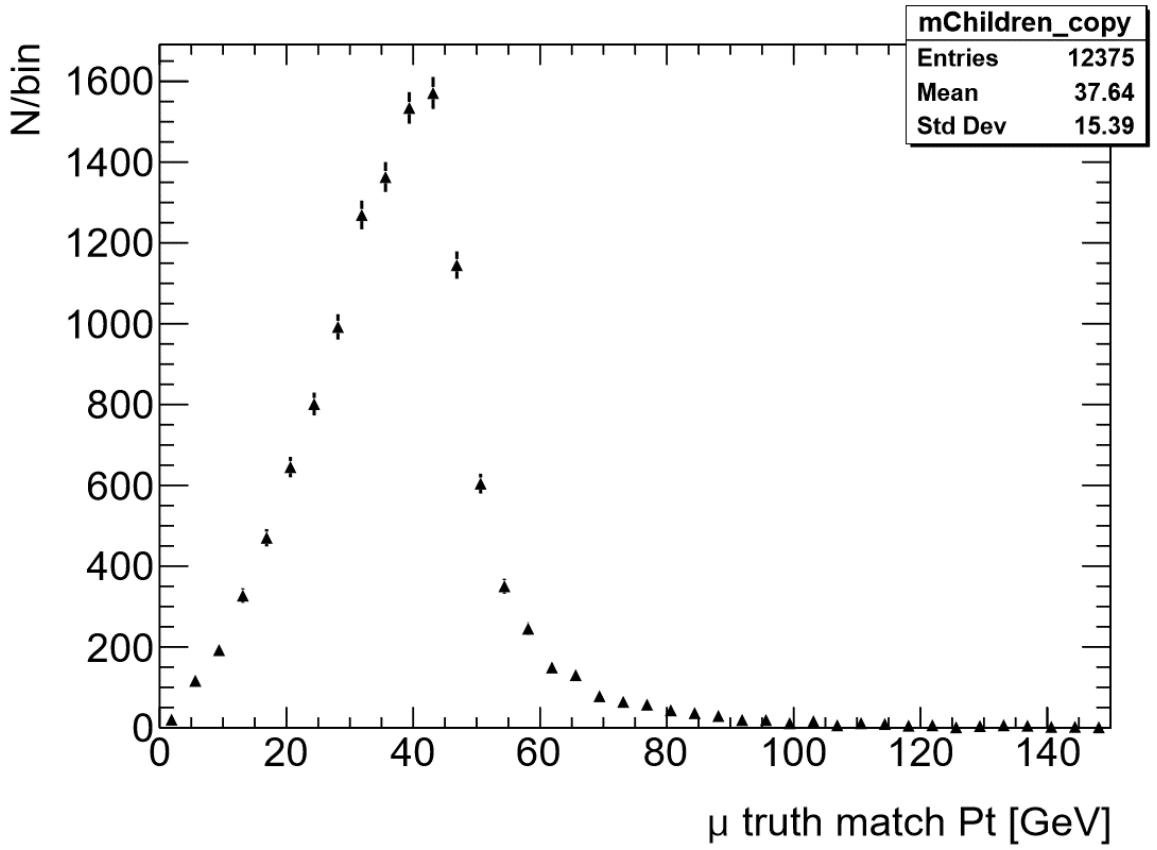

Figure 24: p_T of reconstructed and truth matched muons

The p_T distribution here in figure 24 confirms our expectation, as it looks similar to the true muon p_T distribution from figure 20, and the reconstruction in figure 12, except the tail produced by the minimum bias. After matching both muons produced by the Z^0 in each event, we add them together as explained earlier, to get the mass distribution:

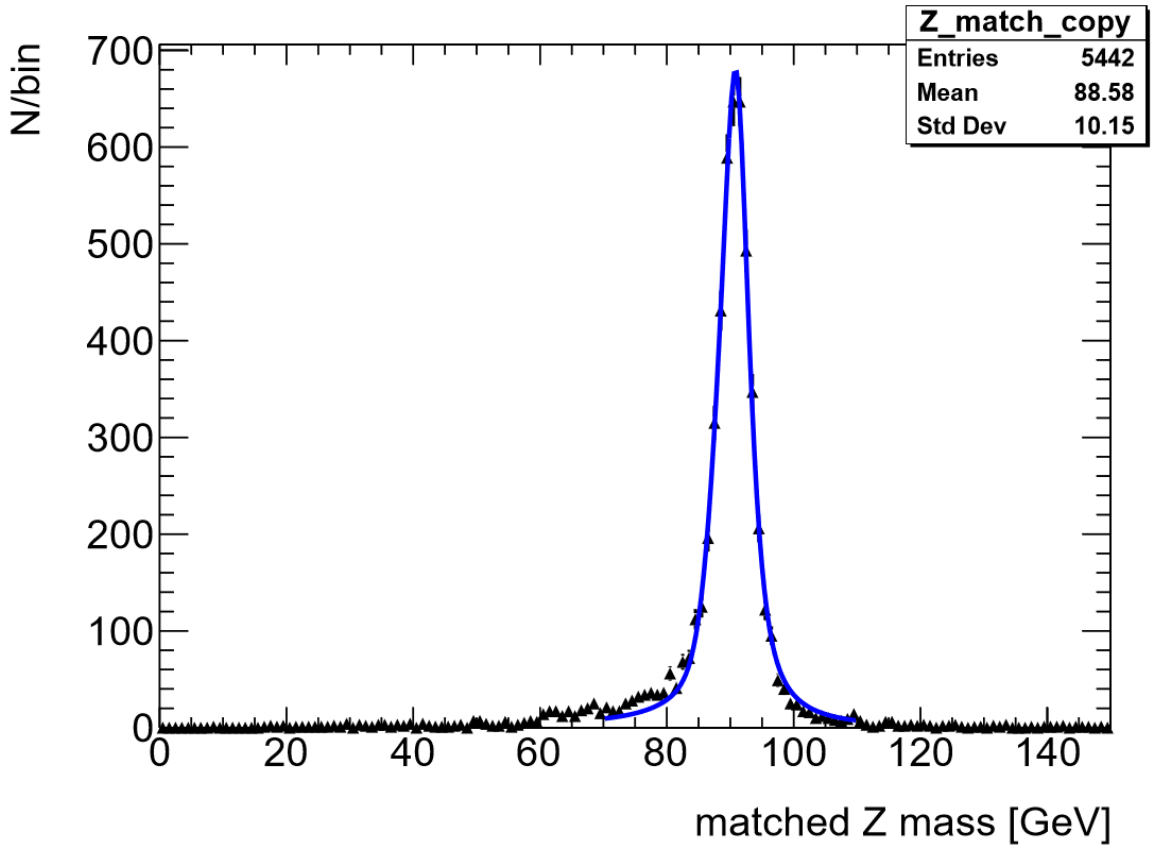

Figure 25: Z mass from truth matched muons with Gauss+BW fit

The fit on the distribution in figure 25 gives us the following parameters:

Table 7: Parameters for Gauss+BW convoluted fit on truth matching

Parameter	Value	Error
Mass	90,4998	0,0484629
FWHM	3,59323	0,158569
Area	5240,72	75,8274
Sigma	1,46576	0,109217

This fit gives a mass estimate similar to the original reconstruction in figure 17, around $m_Z = 90{,}50 \pm 0{,}05\ GeV$, the difference being that we eliminated the minimum bias background. Compared to that mass distribution with the minimum bias included, the peak is also narrower here, at only $3{,}6 \pm 0{,}2\ GeV$ in table 7, compared to the width of $4{,}3 \pm 0{,}2\ GeV$ from table 5. What is interesting is that we can use the fits on this distribution and compare it to the truth information to estimate the mass resolution. If we take the fit on the truth matched mass distribution in table 7 and fix the mass and width to the values given by the truth information in table 6, we should get a sigma which is the difference between the width of the peaks in the truth matching compared to the truth information. This should serve as an estimate of the mass resolution of the reconstruction. This gives the following parameters for the truth matching:

Table 8: Parameters for fit from Figure 24 with fixed mass and width from table 6

Parameter	Value	Error
Mass	91,1351	Fixed
FWHM	2,55158	Fixed
Area	4930,63	71,7059
Sigma	1,90030	0,0565553

As mentioned, the mass and full width is fixed to the values given by table 6, giving us a sigma which is the difference in width between truth and reconstruction, hence estimating the mass resolution of the reconstruction. The value we get from table 8 is around $\sigma(m_Z) = 1{,}90 \pm 0{,}06\ GeV$, which is reasonable estimate given what we have seen so far.

Efficiency

What is more useful is to use the truth matching and compare it to the truth information to get a measure of the efficiency of the detector. Since we know that exactly 2 muons were produced in each event, and we can see how many of those were registered in the detector, we can compare these distributions and estimate the reconstruction efficiency of the detector.

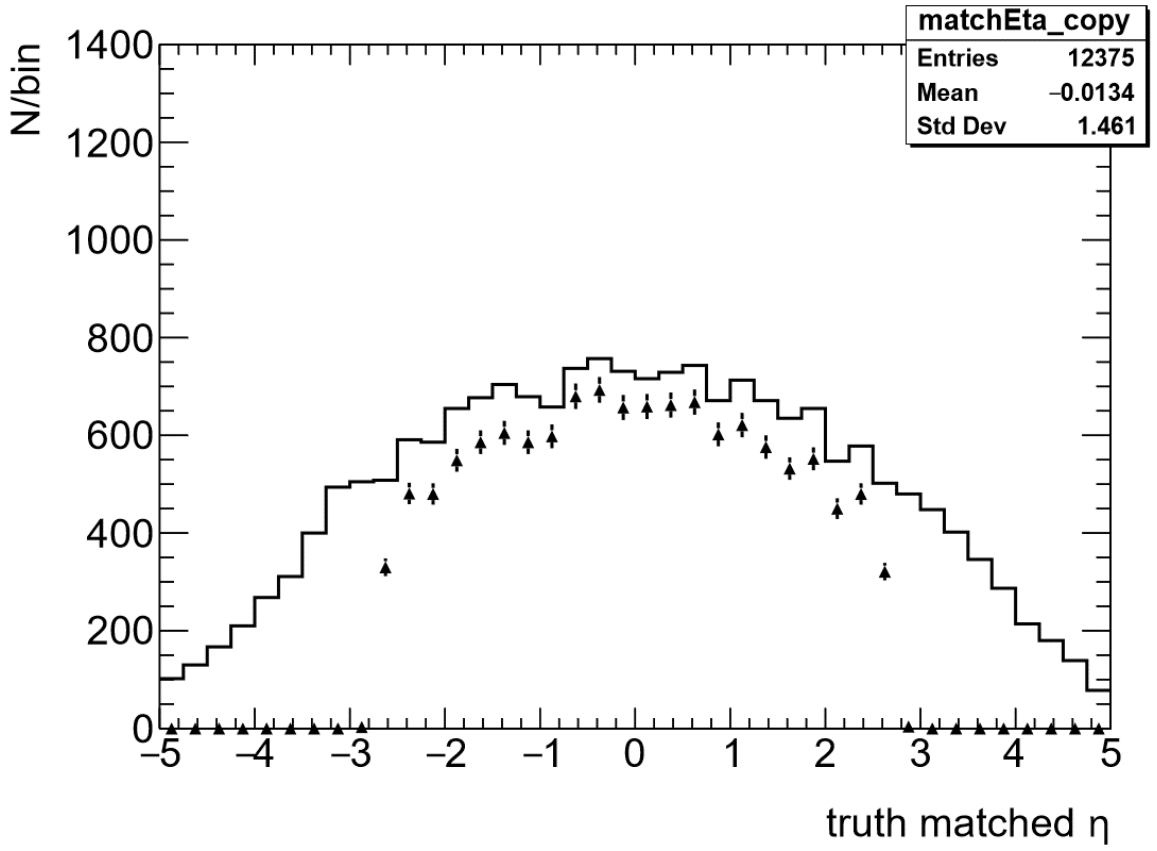

Figure 26: η from muons in truth information (line) and truth matching (dotted)

We can see from this η distribution in figure 26 that the muons are produced across a big interval of η. If we remember eq. 1, we know that this is related to the angle of the muon relative to the beam axis. Since the muon spectrometer sits on the outside of all the other detectors, it means that muons going out at a narrow enough angle will not be detected, and thus fall outside the muon acceptance range. We know that the acceptance range for the ATLAS muon spectrometer is $\eta \in [-2.7,2.7]$. We

can see from figure 26 that most of the muons inside the acceptance range are reconstructed, but we can also see that all muons leaving with a larger η are lost and therefore not reconstructed. If we focus on the muons that do fall inside the acceptance range, we can get a measure of the reconstruction efficiency by computing the fraction of muons that get reconstructed compared to how many actually passed through the detector.

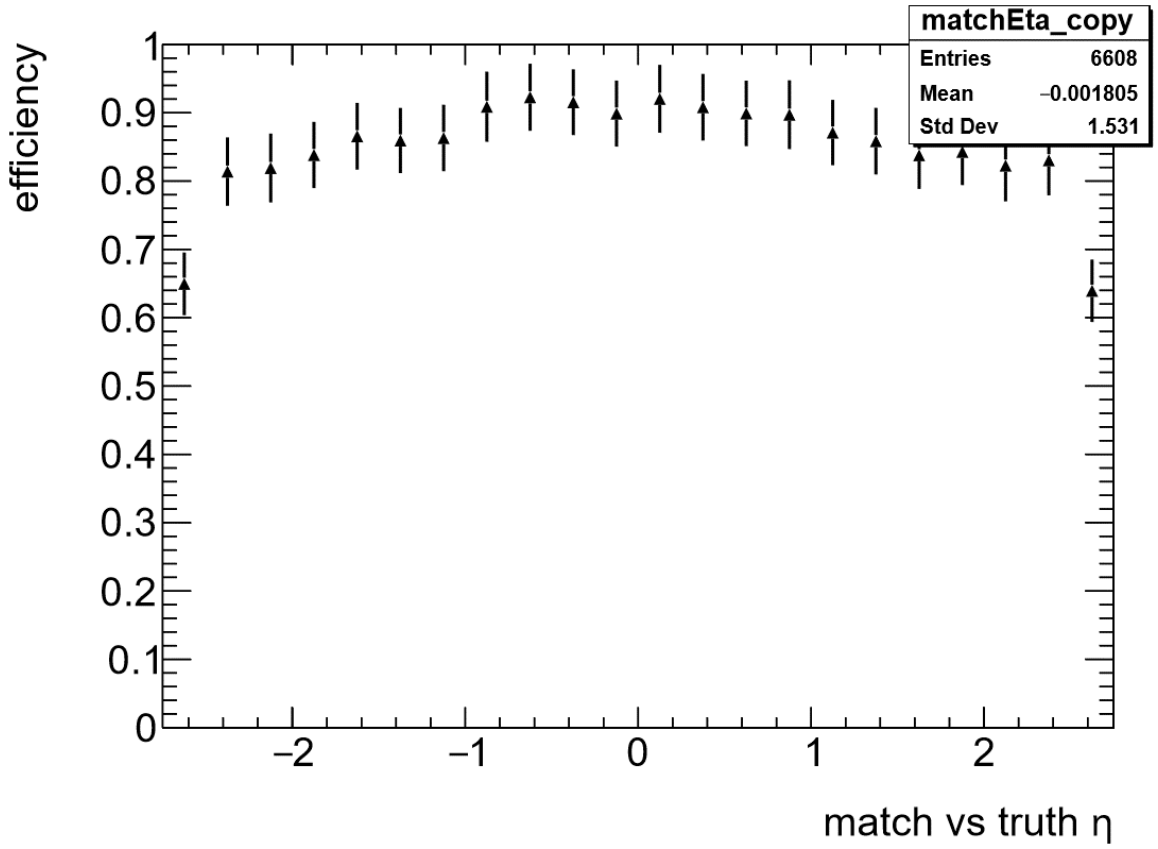

Figure 27: Ratio of η from truth information and truth matched muons inside ATLAS muon acceptance range

Plotting only the ratio match/truth muons in figure 27, the peak efficiency looks to be around 90% around $\eta = 0$, dropping off towards the edges of the range. The average efficiency is easier to estimate knowing that the ϕ distribution is uniform, so plotting the ratio of the ϕ distribution of only the muons inside the eta range of the detector should give a good representation.

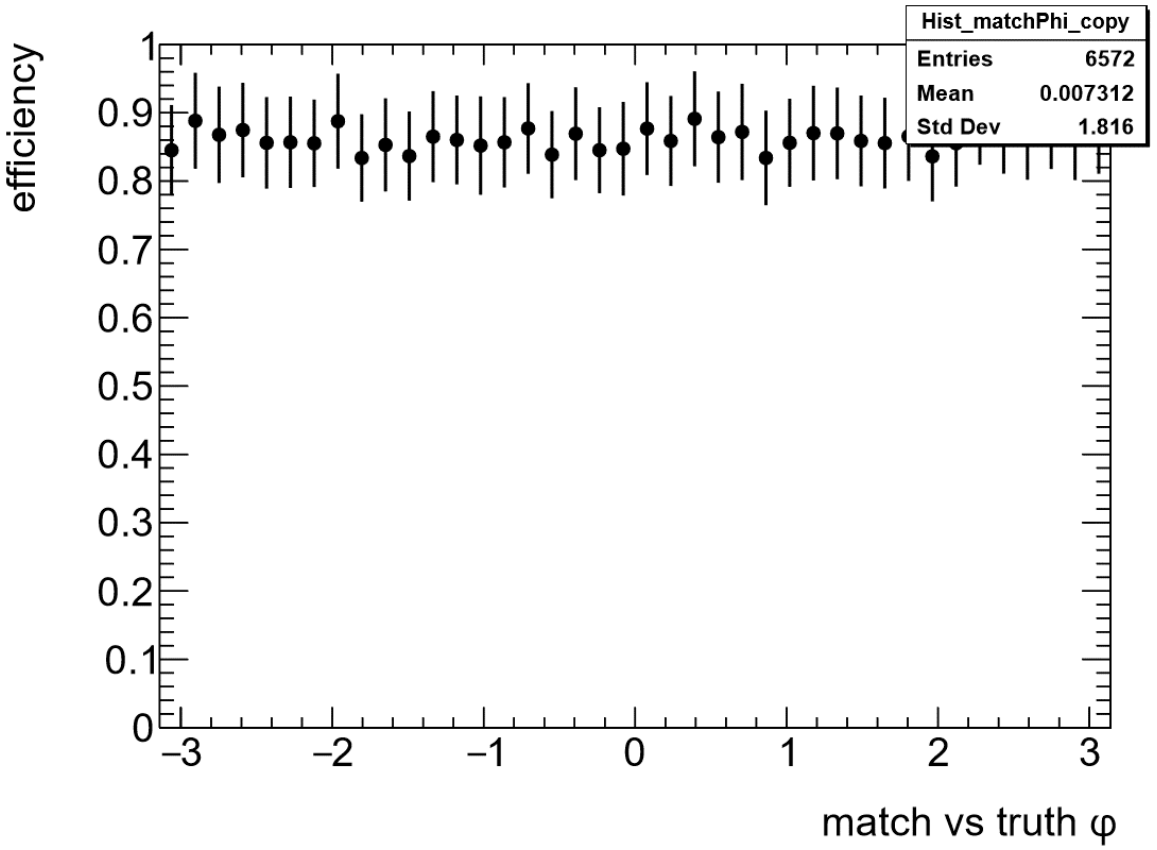

Figure 28: Ratio of ϕ from truth information and truth matched muons inside the ATLAS muon acceptance range

Because we know that ϕ is the angle of the particle relative to a plane perpendicular to the beam axis, the muon spectrometer is wrapped all the way around the barrel. This means that in theory muons leaving at any ϕ should be reconstructed, as long as it is inside the η acceptance range. The uniform nature of the ϕ distribution shown here in figure 28 allows us to estimate the efficiency of the detector to be around 87% for the muons that leave inside the acceptance range.

Momentum resolution

Something else we can do is to estimate the muon p_T accuracy of the detector by dividing the muons into intervals of 10 GeV p_T, and plot $\frac{1}{truth\ p_T} - \frac{1}{match\ p_T}$ for the muons inside each bracket. The difference between the true and measured p_T of the muons should give a good indication of the accuracy of the measurement of the p_T of the muons passing through. This can be made easier to estimate by plotting $\Delta\frac{1}{p_T}$ instead of just the difference itself, because it should produce a gaussian distribution. We can verify this by plotting it for the whole range:

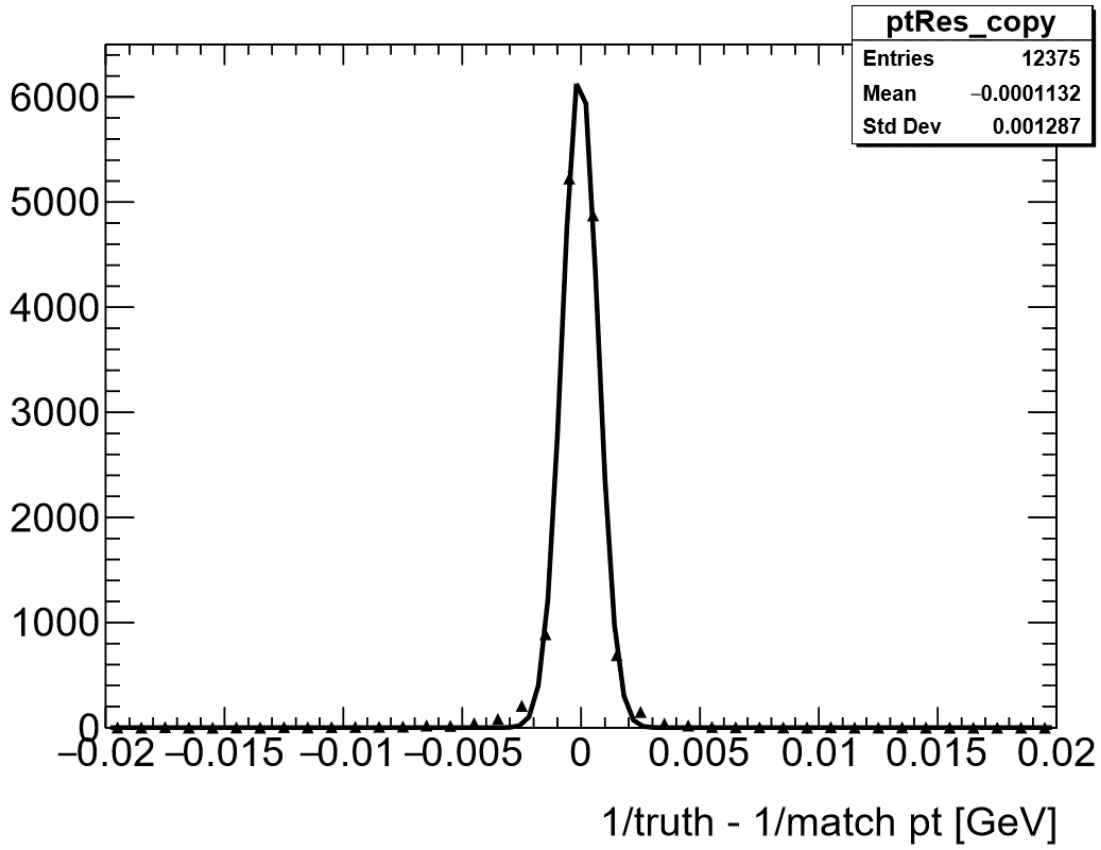

Figure 29: 1/truth p_T - 1/match p_T for 0-100 GeV, with Gaussian fit

The fit in figure 29 does indeed look Gaussian, which means we should be able to use this to estimate the momentum resolution. As we saw from eq. 2, p_T is inversely proportional to the sagitta (s) of the arc that represents the path of the particle. This means that

$$\sigma(p_T) = \frac{dp_T}{ds}\sigma(s) = \frac{K}{s^2}\sigma(s) \tag{13}$$

Where K is some constant number. From that we can deduce that

$$\frac{\sigma(p_T)}{p_T} = \frac{\frac{K}{s^2}\sigma(s)}{\frac{K}{s}} = \frac{\sigma(s)}{s} = \frac{p_T}{K}\sigma(s) \tag{14}$$

However, because we are plotting $\sigma\left(\frac{1}{p_T}\right)$, the momentum resolution becomes

$$\sigma(p_T) = p_T^2\sigma\left(\frac{1}{p_T}\right) \rightarrow \frac{\sigma(p_T)}{p_T} = p_T\sigma\left(\frac{1}{p_T}\right) \tag{15}$$

If we go through and plot this for each interval of p_T, the width of the gaussian indicates the accuracy of $\frac{1}{p_T}$ in this region, thus if we take the product of this standard deviation and p_T in that region and plot it for each of the intervals, it should represent the p_T resolution across the range.

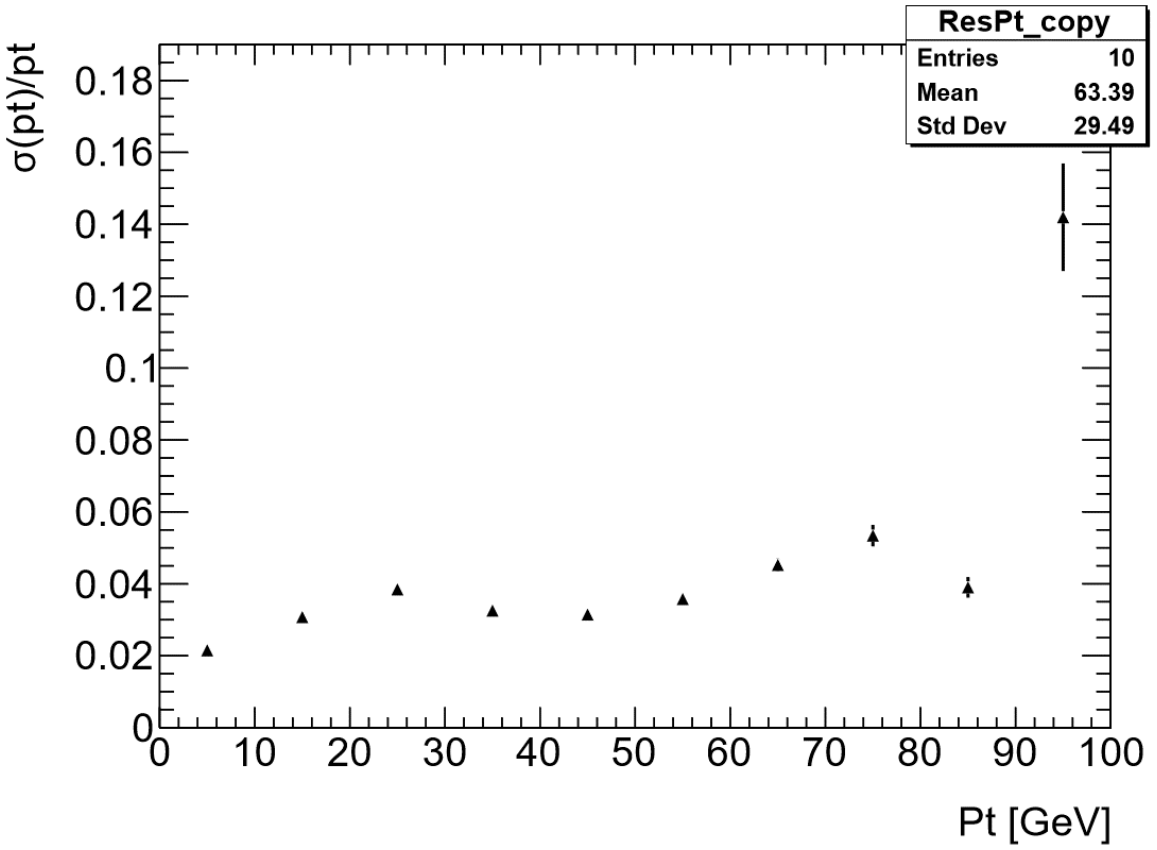

Figure 30: Momentum resolution calculated from standard deviation of 1/truth pt - 1/match pt for pt intervals

The smaller this value is, the more accurate the reconstruction, the higher the resolution. We would expect the resolution to be bad at low p_T because of multiple scattering, but this does not show up here, which may be a consequence of the wide 10 GeV intervals we are using, as this is mostly a problem below 5 GeV. Above this the resolution should be better, however it gets worse again as p_T continues to rise, because it gets more difficult to measure the curvature of the path. Because of the relationship between p_T and the sagitta, as the p_T gets higher, the path becomes straighter and thus the p_T must become more uncertain as it becomes increasingly difficult to distinguish from a straight line 57(32). Figure 30 seems to confirm this, although it is very sensitive at the high end of the p_T range, due to the scarcity of entries above 70 GeV. This is particularly clear above 90 GeV, as there are so few data points to base this measurement on, that the resolution varies more from bin to bin.

Comparing to real data

Because real events happening in ATLAS are far more chaotic than the Monte Carlo simulation used so far gives the impression of, we need to add more events with various interactions in addition to the $Z^0 \rightarrow \mu^+\mu^-$ sample we have used up until now. Normally in any given real event, looking for a $Z^0 \rightarrow \mu^+\mu^-$ interaction is a lot more difficult because it will be buried under lots of other interactions involving other particles also producing muons. This can make the process of identifying which muons come from the Z^0 difficult, because muons have p_T and η across the range. However, the benefit of choosing $Z^0 \rightarrow \mu^+\mu^-$ decays is that it is one of the more common sources of muons, so it is actually not too difficult to find it when analysing a few events from ATLAS. In order to make the MC signal more realistic, we will consider the most common sources of background normally found in $Z^0 \rightarrow \mu^+\mu^-$ events. The most common background sources are $Z^0 \rightarrow \tau^+\tau^-$, diboson, single top, $t\bar{t}$ and Drell-Yan. Drell-Yan interactions is when a quark and anti-quark from different hadrons

interact and annihilate, producing a photon or a Z^0 that then creates a pair of muons. Background from double semileptonic decays from bottom and charm quarks were also considered, but that contribution was not significant enough to be included. Until now we have used truth matching to get rid of the minimum bias from the Z^0 reconstruction in figure 17. However, this is now impractical, because later in this chapter we will need to compare the MC to real data, and since we cannot truth match that, we need a different method to compare them. For that reason, we will from now on use the ATLAS muon selector to select the muons coming from the Z^0. The muon selector uses various criteria like η and p_T to determine which muons should be kept and which should be discarded in order to get the best possible reconstruction of an event. The selector also gives us the opportunity to choose how strict we want to be when selecting muons. This corresponds to different working points like loose, medium or tight. In the first part of this chapter we will use the $Z^0 \rightarrow \mu^+\mu^-$ sample filtered with a medium working point. In order to get a more accurate view of the distribution the different components have been scaled by the reconstruction efficiency for each sample, as well as the cross section for the given source. As we will see later, this should give us a plot which is normalized with respect to luminosity, which will also be helpful once we start comparing it to real data. Adding all the contributions together we get the following distribution:

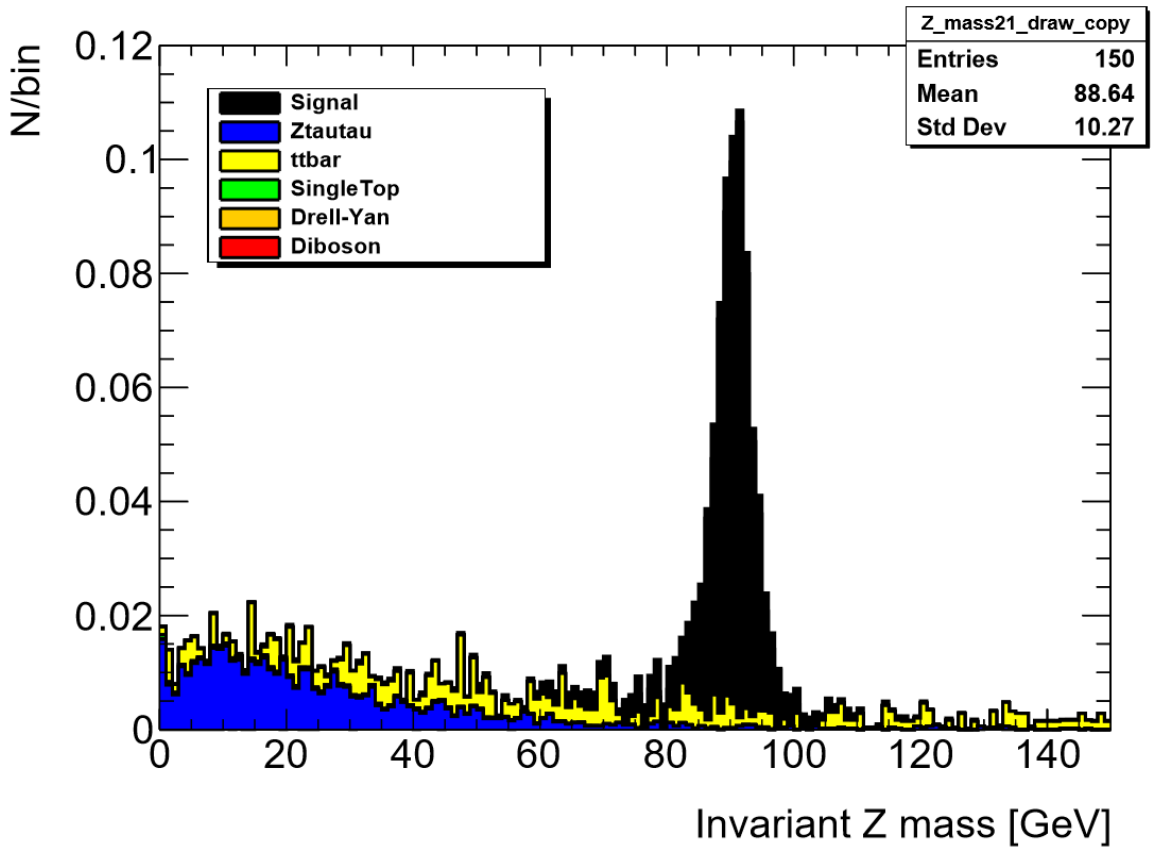

Figure 31: Signal with background with different colours for each contribution, normalized with respect to luminosity

As we can see from figure 31 the signal from the Z^0 is very clear, with most of the background coming from low-p_T muons primarily from $Z^0 \rightarrow \tau^+\tau^-$. $t\bar{t}$ interaction contributes background across the range, while diboson, single top and Drell-Yan contributes less because they have very small cross section compared to the rest. If we draw the distribution with the Y-axis on a log scale, we can see more clearly how much the different sources contribute to the total:

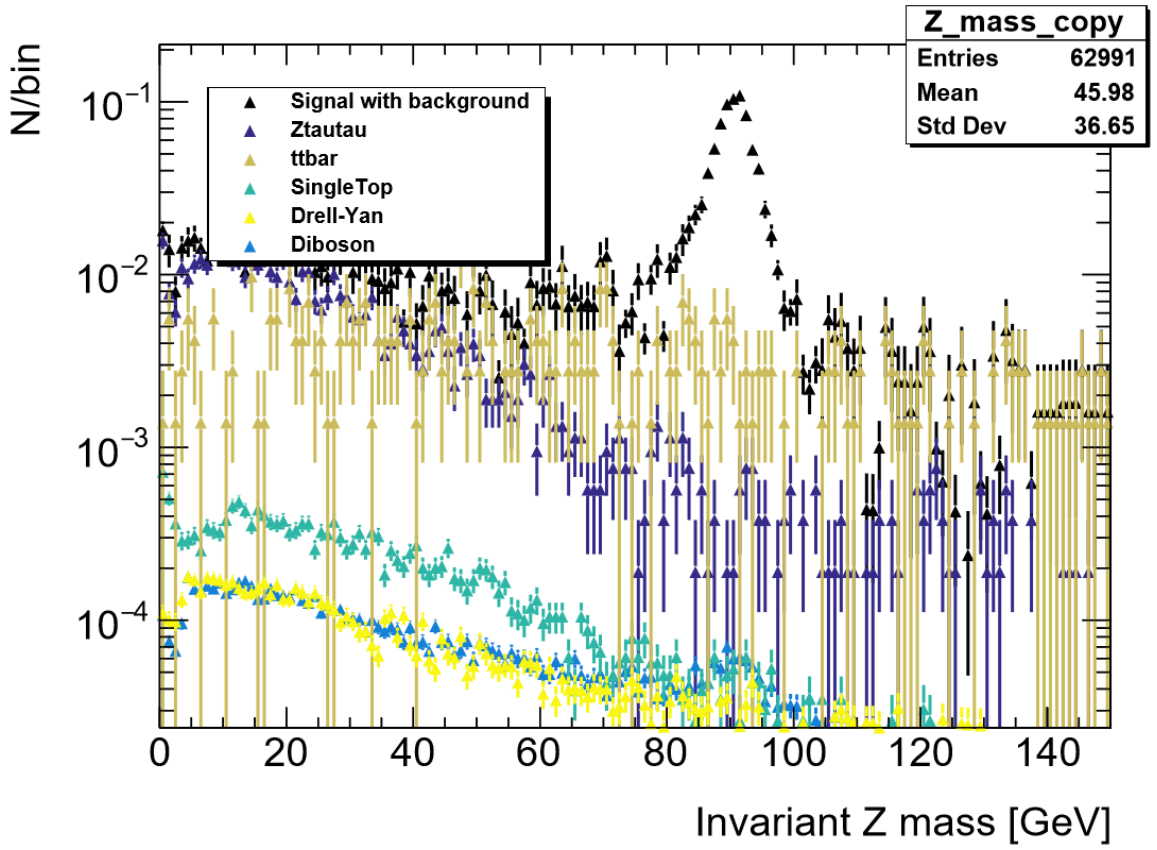

Figure 32: Signal with background contributions, log Y-axis

Shown here in figure 32, we can more clearly see the contributions from the single tops, diboson and Drell-Yan, and verify that they do indeed contribute, albeit only by about 1/100th of the sum. Next, we compare to a real data sample, containing muons from various different interactions. The goal here is to verify that the sets of backgrounds selected and added up in the Monte Carlo looks sensible and give a representative indication of a real event in ATLAS. If we look at a sample of real data containing about 50k events, take the muons satisfying a medium working point, and plot the mass, we get the following distribution:

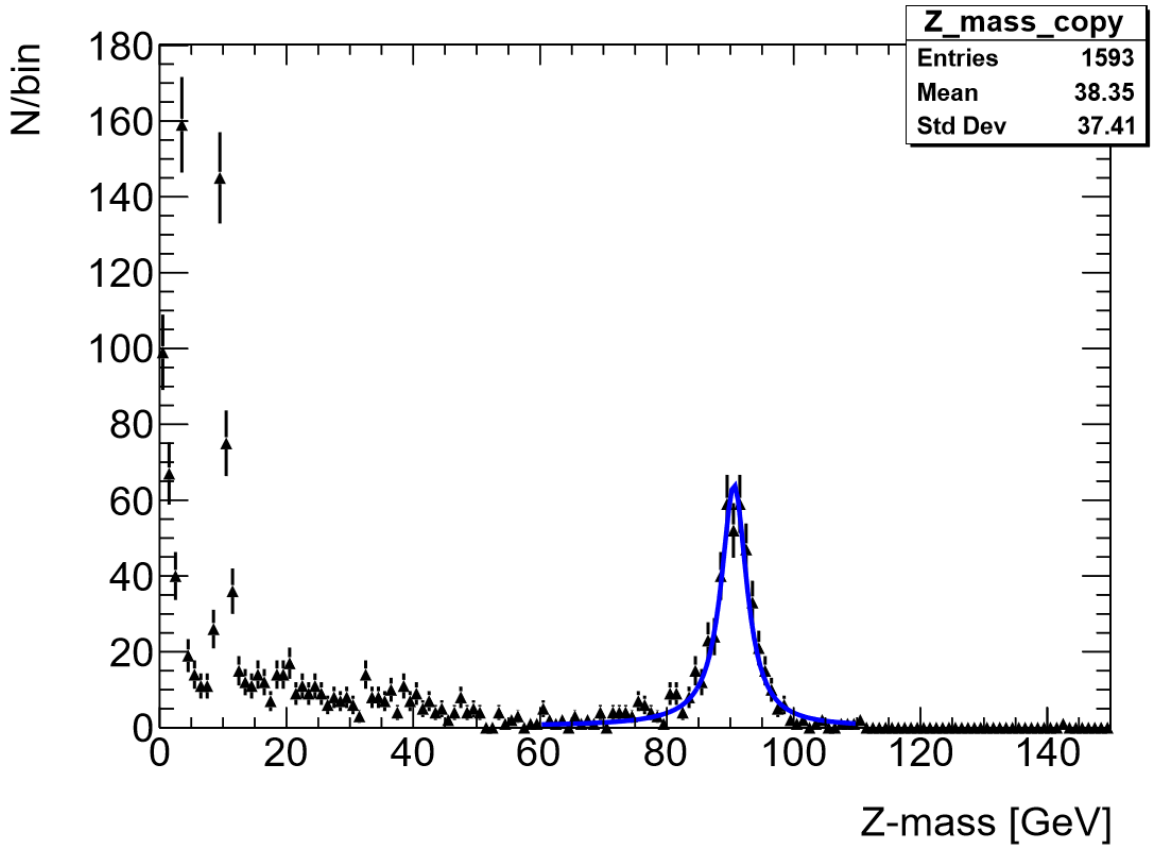

Figure 33: Invariant mass from a real data sample, with Gauss/BW convoluted fit on Z-peak

We can see from figure 33 that the level of background looks reasonable compared to the Z^0 peak, except for certain peaks below 15 GeV, which we will discuss later. It is useful to compare the peak we see in the data to the same peak in the MC, therefore we try to fit the peak with the previously used Gauss+BW convolution, which gives us the opportunity to compare the parameters for the fits. Fitting the data in figure 33 gives us the following parameters:

Table 9: parameters from Gauss+BW convoluted fit on Z peak in data

Parameter	Value	Error
Mass	90,4713	0,169497
FWHM	4,06200	0,595387
Area	510,926	23,9532
Sigma	1,47122	0,421362

The parameters given in table 9 are very consistent with what we have seen with the previous MC distributions, which is a good sign. The full width here is very consistent with the value for the original reconstruction from table 5, which makes sense since that also contains background in the form of the minimum bias.

Since we will eventually be looking for a Higgs, it is important to not pre-empt the content in that region, since that could lead to fabricating a signal that is not there. For this reason, all bins in the Higgs region have been set to zero. As we can see, above 15 GeV, the amount of background looks similar to the Monte Carlo. Below that are peaks of muons coming from sources not considered, which will be discussed later. Comparing the fit on the data sample with a similar fit on the Monte Carlo, we should be able to work out a value of luminosity that should make the two plots of comparable size, since

$$N_{reco} = \mathcal{E}_{reco} * \sigma * \mathcal{L} \quad (16)$$

Here, N_{reco} is the number of reconstructed events we see in a given sample, $\mathcal{E}_{reco}$ is the reconstruction efficiency of the sample, and σ and $\mathcal{L}$ is the cross section and luminosity for that sample. The luminosity is what we are trying to find, so if we normalize each component to that by scaling the number of reconstructed events by the efficiency and cross section from eq. 16, we can then approximate how many $Z^0 \rightarrow \mu^+\mu^-$ events we can see in the data. If we divide the number of entries in the data by the normalized MC distribution given by eq. 16 it should give us a reasonable estimate of the luminosity of Z^0 production in ATLAS.

$$\frac{entries\ in\ data\ Z\ peak}{entries\ MC\ Z\ peak} = \frac{N_{data}}{\frac{N_{reco}}{\mathcal{L}}} = \frac{444}{0{,}814} \approx 545\ nb^{-1} = \mathcal{L} \quad (17)$$

444 is the number of entries inside 3 standard deviations of the Z^0 peak in the data, and 0,814 is the normalized number of entries in the equivalent peak in the MC. If we scale the whole MC plot by this luminosity, it should give us an equivalent Z^0 yield:

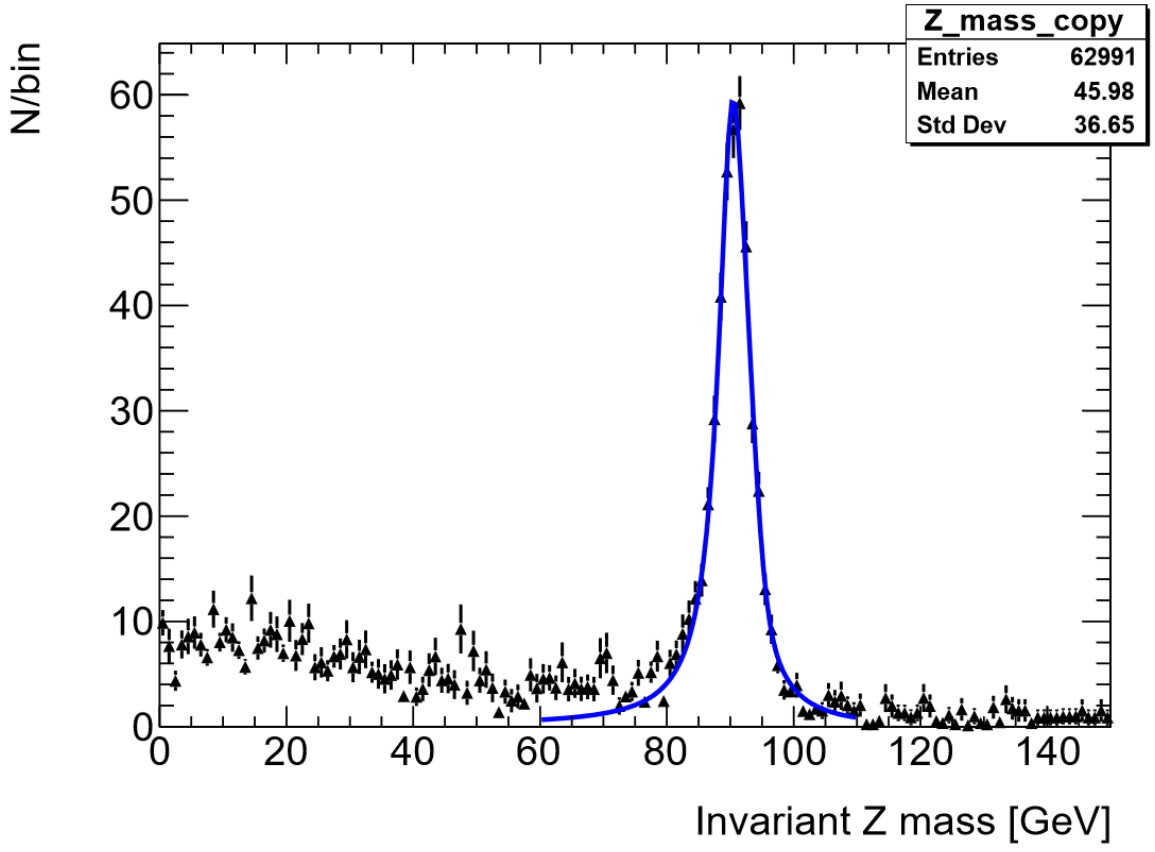

Figure 34: MC Z signal including background with Gauss+BW fit, scaled by luminosity to match data

As mentioned earlier, we want to compare the peaks of the data and MC by fitting them and comparing the parameters. After scaling the MC to the same luminosity in figure 34, we can compare it to the data from figure 33 as they should have the same height. The fit on the MC distribution gives the following parameters:

Table 10: Parameters for Gauss+BW convoluted fit on Z peak in MC

Parameter	Value	Error
Mass	90,4434	0,0642564
FWHM	4,05800	0,235550
Area	515,485	9,30285
Sigma	1,49489	0,161870

The parameters listed here in table 10 look very similar to the parameters for the fit on the data in table 9, which is good news as it suggests the MC distributions we have based this study on are indeed accurate compared to real data.

We can also use the data to estimate how many $Z^0 \rightarrow \mu^+\mu^-$ decays we would expect to see, as well as the effective cross section of this interaction. We already worked out that there are about 444 of those decays in the data, and because the background in that region is small enough to be negligible, we do not worry about that. From the pure $Z^0 \rightarrow \mu^+\mu^-$ MC sample with the selector, we know that of the 10000 events 4596 were reconstructed, giving a reconstruction efficiency of around 46 % (this can be seen in figure 35 below). Note that this reconstruction efficiency is different from the 87% we estimated from figure 28, as that was the efficiency of the detector to register only the muons that passed inside the muon acceptance range. Because we are trying to estimate the total number of Z^0 decays, not just for the muons that actually passed inside the detector, we use the lower but more general efficiency, to also take into account decays producing muons leaving outside the detector acceptance.

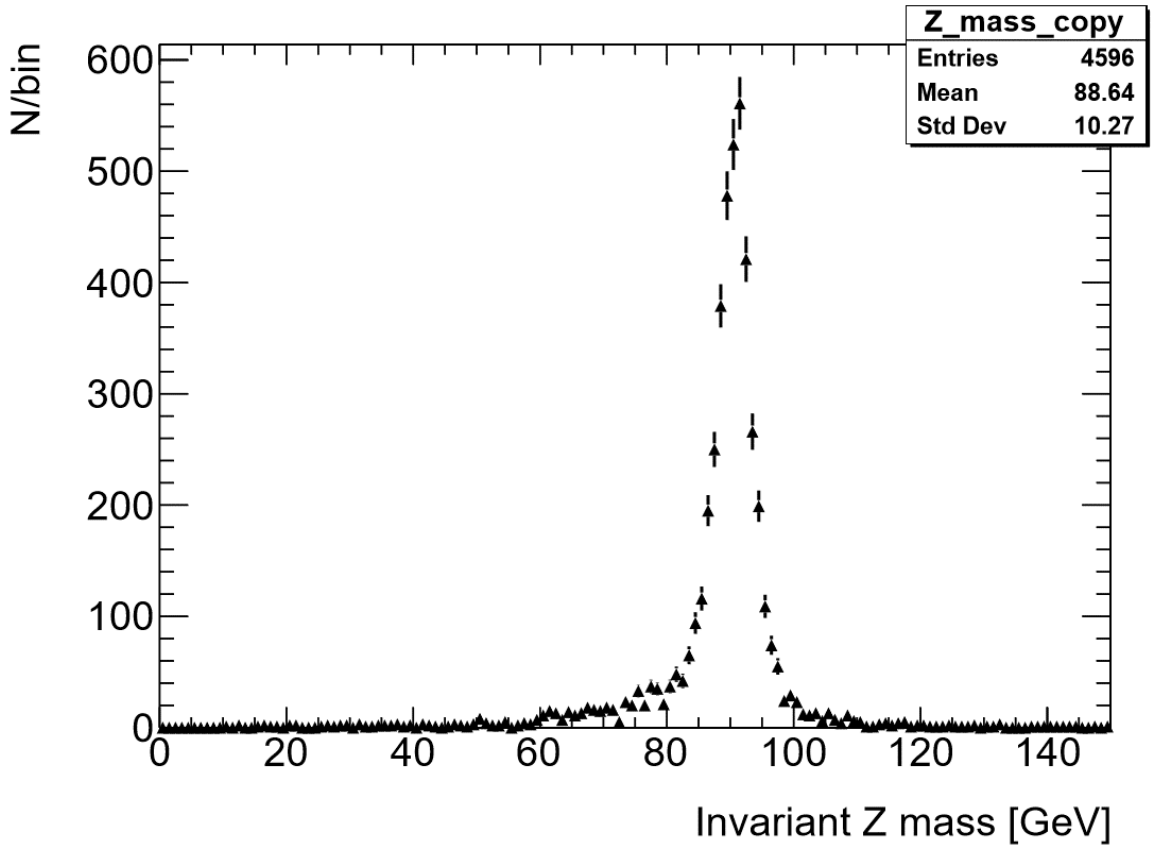

Figure 35: MC $Z \rightarrow \mu\mu$ sample using medium muons

The reconstruction efficiency using the muon selector combined with the number of Z^0 decays in the data means we can estimate that the expected number of Z^0s in the data is approximately

$$N_{true} = \frac{N_{reco}}{\mathcal{E}_{reco}} \approx 966 \tag{18}$$

This means that from the peak we see in the data, we would expect around 966 total number of $Z^0 \rightarrow \mu^+\mu^-$ events. From this we can work out the working cross section as

$$\sigma_{eff} = \frac{N_{true}}{\mathcal{L}} = 1{,}7726\, nb \tag{19}$$

Comparing the estimate given by eq. 19 to the true cross section in the simulated event in the MC of 1,9 nb, this value is in the ballpark, which further strengthens our results based on what we have seen so far. To validate these calculations, we can repeat the calculations from eq. 16-19 with the same samples, but with a loose working point. This should allow slightly more muons through, giving a slightly stronger signal, but also a little more background. Using the same method as previously, we can work out the luminosity to be $\mathcal{L} = 542\ nb^{-1}$. With a loose working point we get 453 entries in the Z^0 data-peak, and a reconstruction efficiency in the MC of 47,31%. This gives us an estimated 958 true Z^0 decays, which is only 8 fewer than the previous estimate. Dividing this by the updated value of luminosity, we get an effective cross section of $\sigma_{eff} = 1{,}7666\, nb$, which is also very close to the previous estimate.

One of the differences it is worth noting is that the real data produced in the events in ATLAS is saved by using triggers as we discussed in the introduction. This could for instance be a threshold on p_T, so that fewer low-p_T muons are stored as these tends to not be too interesting. While we do not have any comparative plots for the MC apart from the first reconstruction we discussed (figures 15 and 16), which contains muons from the Z^0 combined with the minimum bias, it is still a worthwhile discussion because it could point to differences between distributions produced by MC and data.

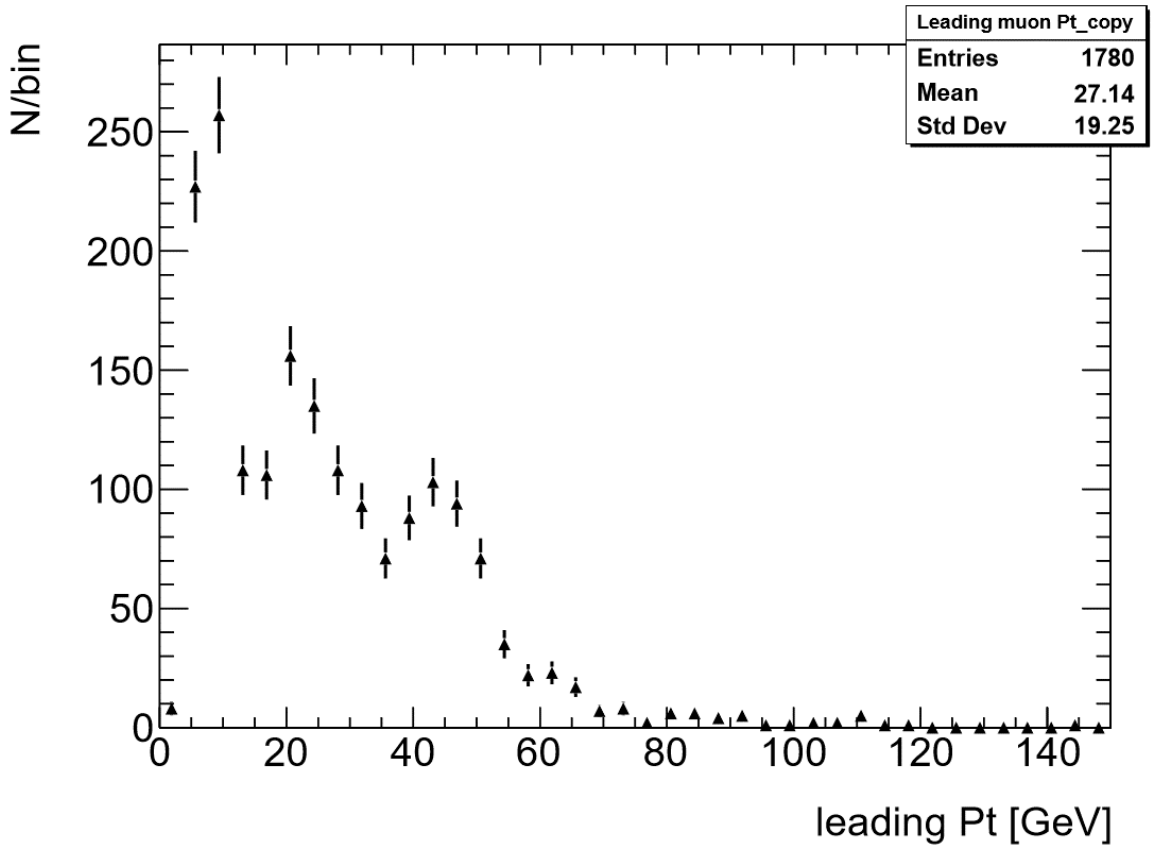

Figure 36: Leading muon pt from data

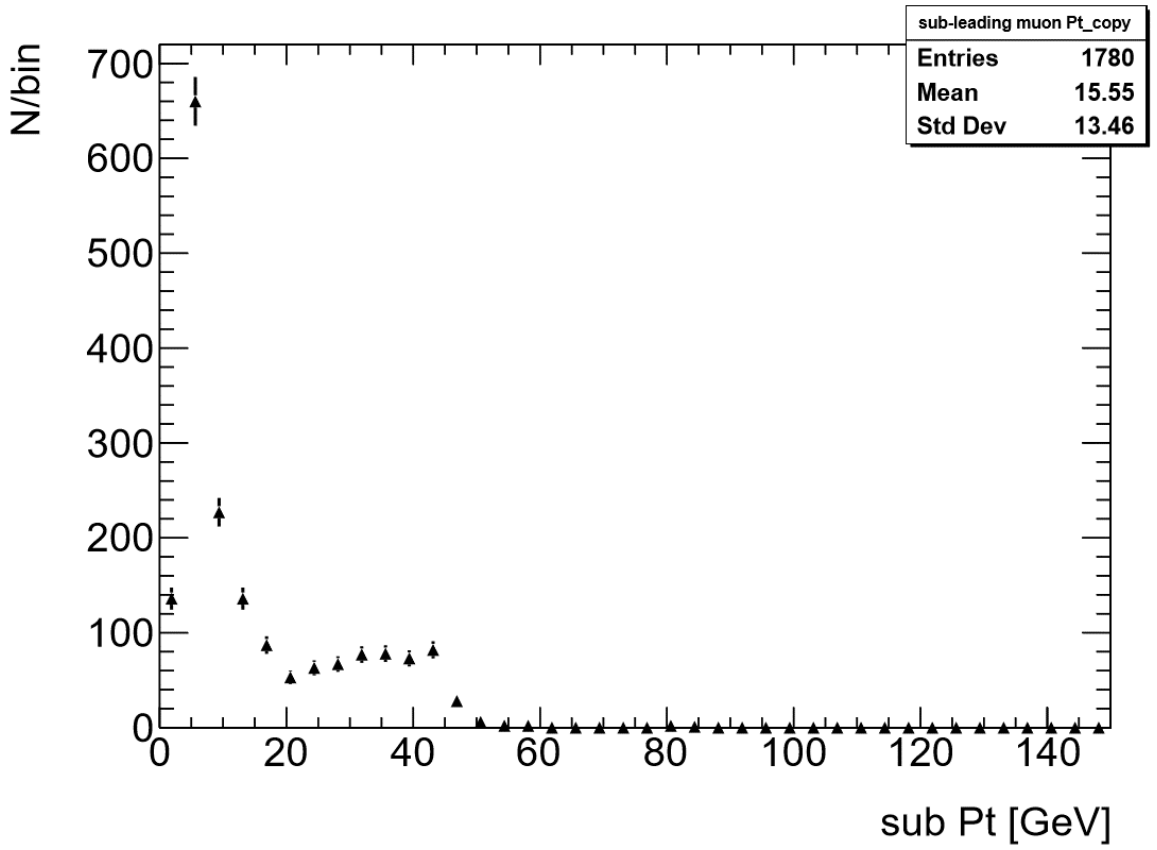

Figure 37: sub-leading muon pt from data

The first difference between the two sets of plots is the amount of low p_T muons. This is mainly because there is a lot more background in the data relative to the Z^0 peak compared to the MC. This is because the data also contains decays from various lighter mesons, which are not in the MC (this will be discussed later). This is very clear if you look at the leading muons, since the MC only contains leading muons coming from the Z^0, shown in figure 15, whereas the data contains leading muons from several different sources, shown in figure 36. However, we can see a difference where there does seem to be a cut in the data, because a lot of muons with $p_T < 5\ GeV$ seem to be dropped and not reconstructed, as can be seen in both figures 36 and 37. Compare that to the minimum bias in the MC sub-leading muons from figure 16, where there does not seem to be any such p_T cuts.

Looking for $H \rightarrow \mu\mu$

Knowing what we know now about the Z^0 such as the mass and width is useful because it can give us more information when looking for the Higgs. The main problem we will run into here is the extremely small cross section of the $H^0 \rightarrow \mu^+\mu^-$ interaction, meaning we will need to run over a lot of data to have a chance of seeing it. To make it a bit easier for ourselves we will also from now on select muons with a loose working point, thus allowing slightly more muon candidates through. If we re-enable the Higgs region in the data, and swich to loose working point, we get the following plot:

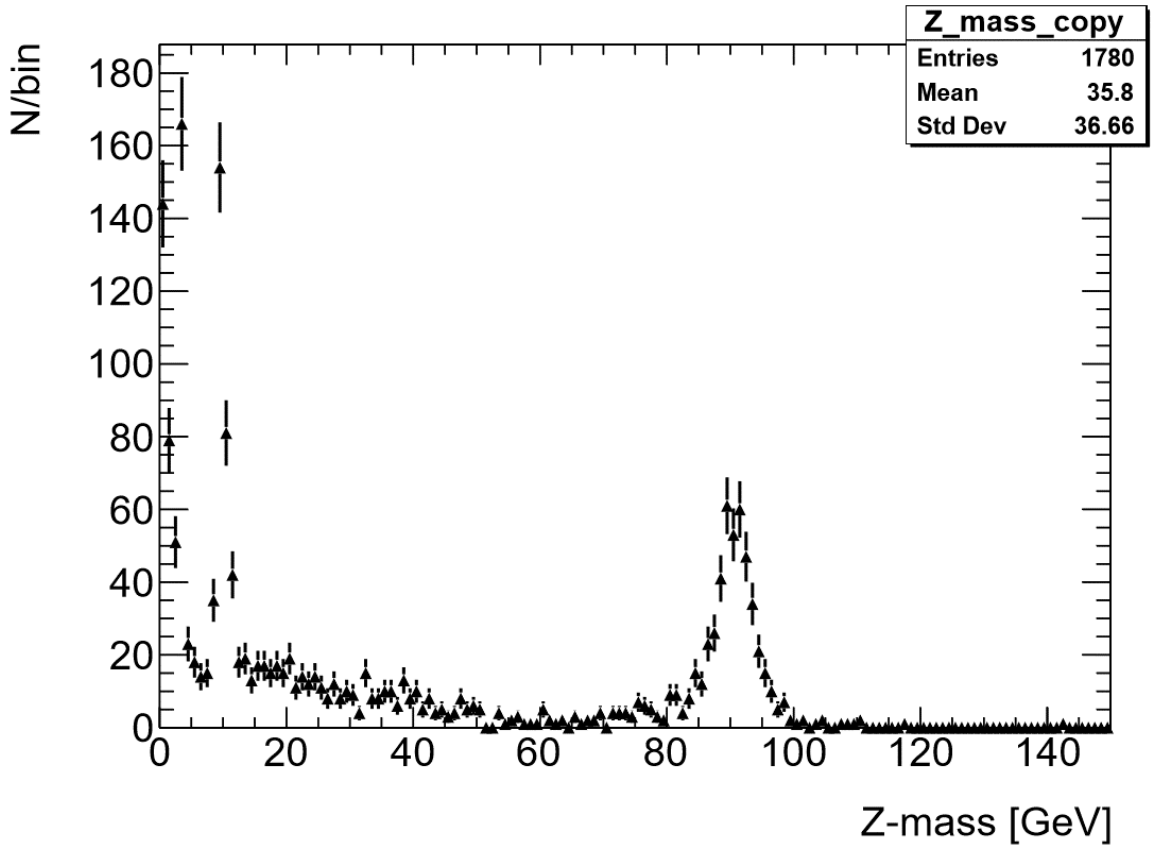

Figure 38: Data mass distribution with loose working point, Higgs region enabled

As we can see from figure 38 there does not appear to be much in the Higgs region. However, 1780 reconstructed events out of 53k total events are not enough to get a good picture of the distribution. If we instead run over 961k events, we end up with around 33k reconstructions:

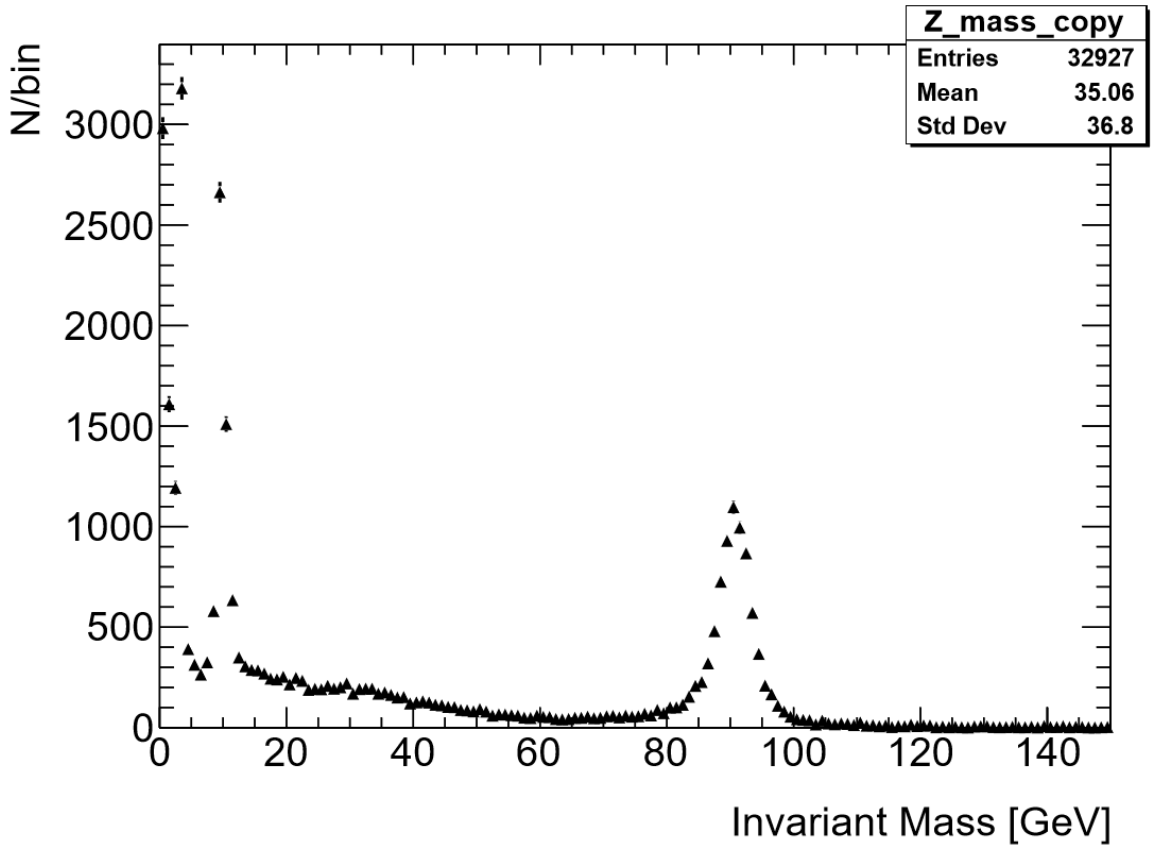

Figure 39: Data mass distribution, 961k events

Worth noting is the low mass background, between 0 and 15 GeV, which we have mentioned earlier:

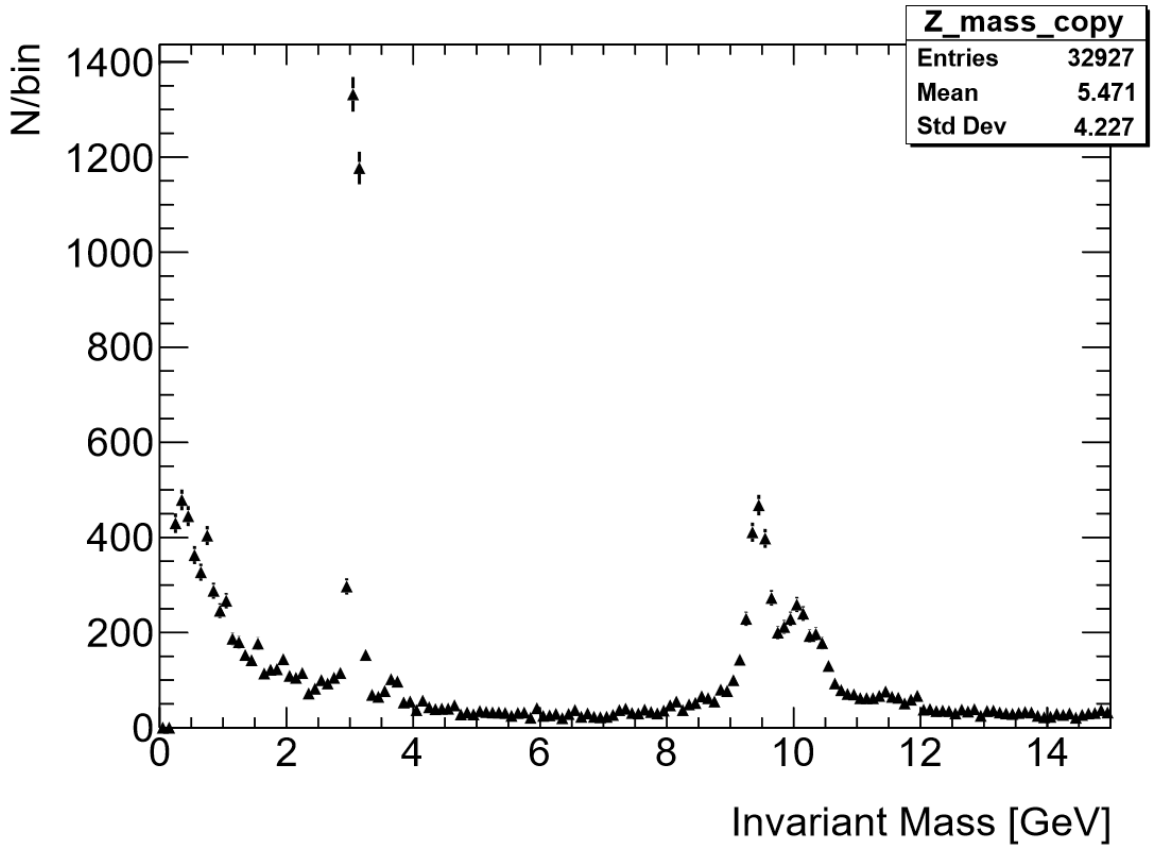

Figure 40: Background from data 0-15 GeV

Here in figure 40, we can see peaks at 3 GeV, and smaller peaks at 9,5 and 10 GeV. These correspond to the J/ψ which is a meson containing a $c\bar{c}$ pair and the ground state and excited state of the ϒ ($b\bar{b}$). If you look closely, you can also see a small peak at around 3,5 GeV, which correspond to the excited state of the J/ψ. Like the Z^0, they all appear here because they also decay to two muons.

If we go back to look at the full range, we can try to fit the full distribution by combining a fit of the background with the peak. In this case we are focusing on the region from 60 GeV up since the background below that is not interesting in our case.

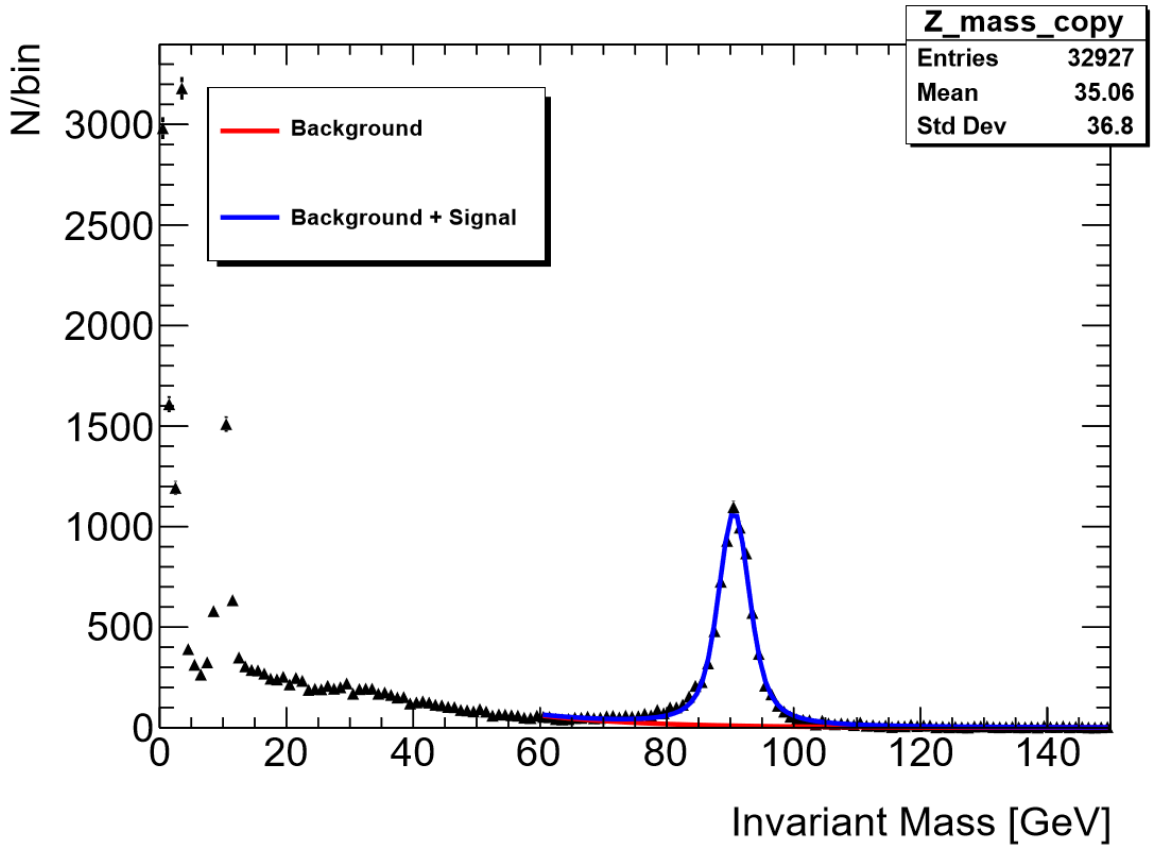

Figure 41: Data with background and signal fits

The red line in figure 41 is an exponential function to fit the background, of the following form:

$$f(x) = e^{p_0 + p_1 x} \qquad (20)$$

Where p_0 is a constant, and p_1 determines the slope of the function. In figure 41, the red line takes the following parameters:

Table 11: Parameters for exponential background

Parameter	Value	Error
Constant	7,75296	0,251061
Slope	-0,0607259	0,00385197

With the blue line using the same function with the parameters in table 11, in addition to the Gauss + BW convolution used to model the peak, with the following parameters:

Table 12: Parameters for Z peak from Gauss+BW convolution

Parameter	value	Error
Mass	90,5916	0,040316
FWHM	3,38597	0,159219
Area	8462,40	114,228
Sigma	1,62786	0,0923036

The red line is just the background for reference, with the blue line combining the exponential function with the Gauss+BW convolution used before. This gives us one last verification of the Z^0

peak, and the parameters are still realistic, even when adding the background into it. It is also promising to see the width listed in table 12 is narrower than for the same peak from table 9, which makes sense, because more data should give an estimate closer to the true value from table 6.

Before we zoom in to the Higgs region in the data, we first need to know what to look for. Therefore, we want to look at an MC sample, to get a hint of what the Higgs peak could look like.

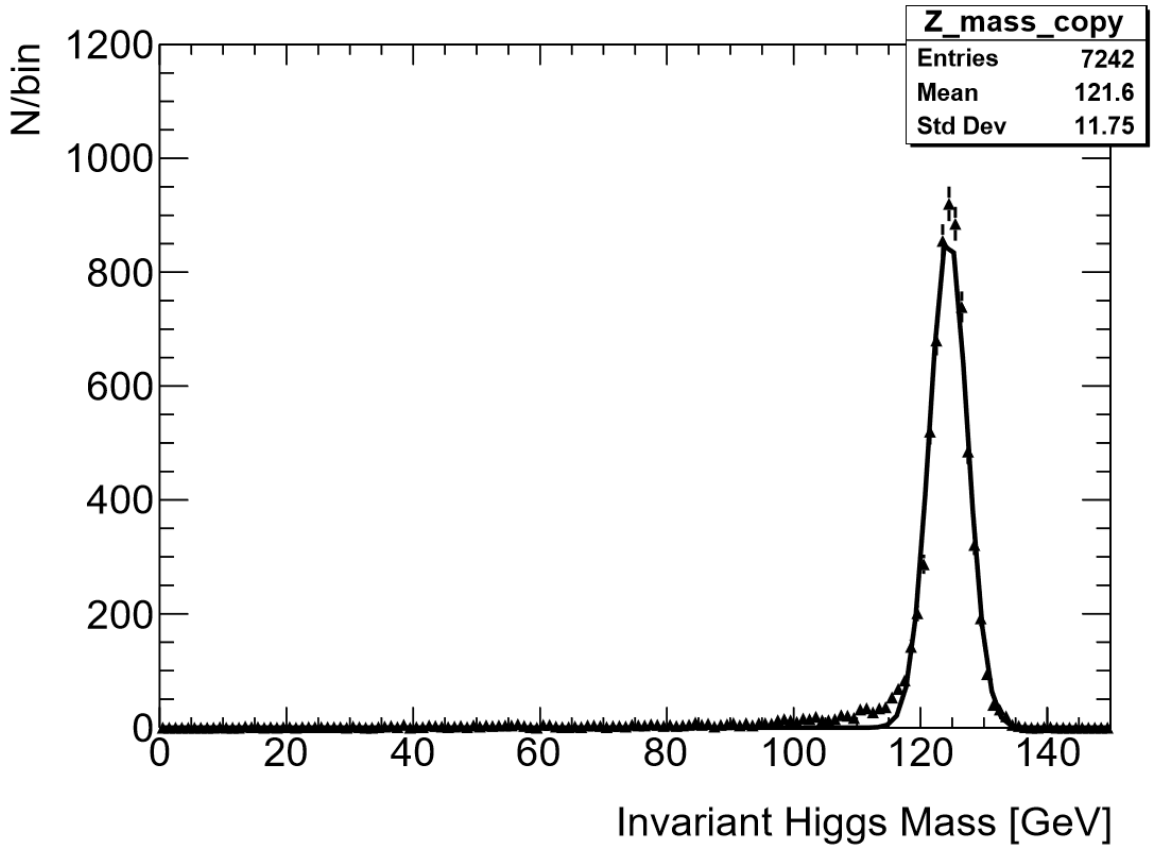

Figure 42: MC Higgs to muon sample with Gaussian fit

At first glance it looks like the Higgs peak in figure 42 is more gaussian than the Z^0, with the fit taking the following parameters:

Table 13: Parameters for Gaussian fit on MC Higgs peak

Parameter:	Value	Error
Constant	867,318	14,6353
Mass	124,417	0,0381396
Sigma	2,99092	0,0339244

The Gaussian listed in table 13 gives a Higgs mass around $m_H = 124{,}42 \pm 0{,}04\ GeV$, which is very much where we would expect it. Based on what we know about the Z^0, we could in theory expect the width of the Higgs to be

$$\sigma(m_Z)\left(\frac{m_H}{m_Z}\right)^2 = 3{,}6\ GeV \tag{21}$$

Where $\sigma(m_Z)$ is the mass resolution we got for the Z^0 from table 8. The width we actually get from the fit on the Higgs is $2{,}99 \pm 0{,}03\ GeV$, which is narrower than the theoretical value based on the resolution of the Z^0, suggesting that the theoretical estimate from eq. 21 was somewhat

conservative. Given these parameters, we can go back to the data and zoom in on the Higgs region and see if there is a hint of the Higgs there:

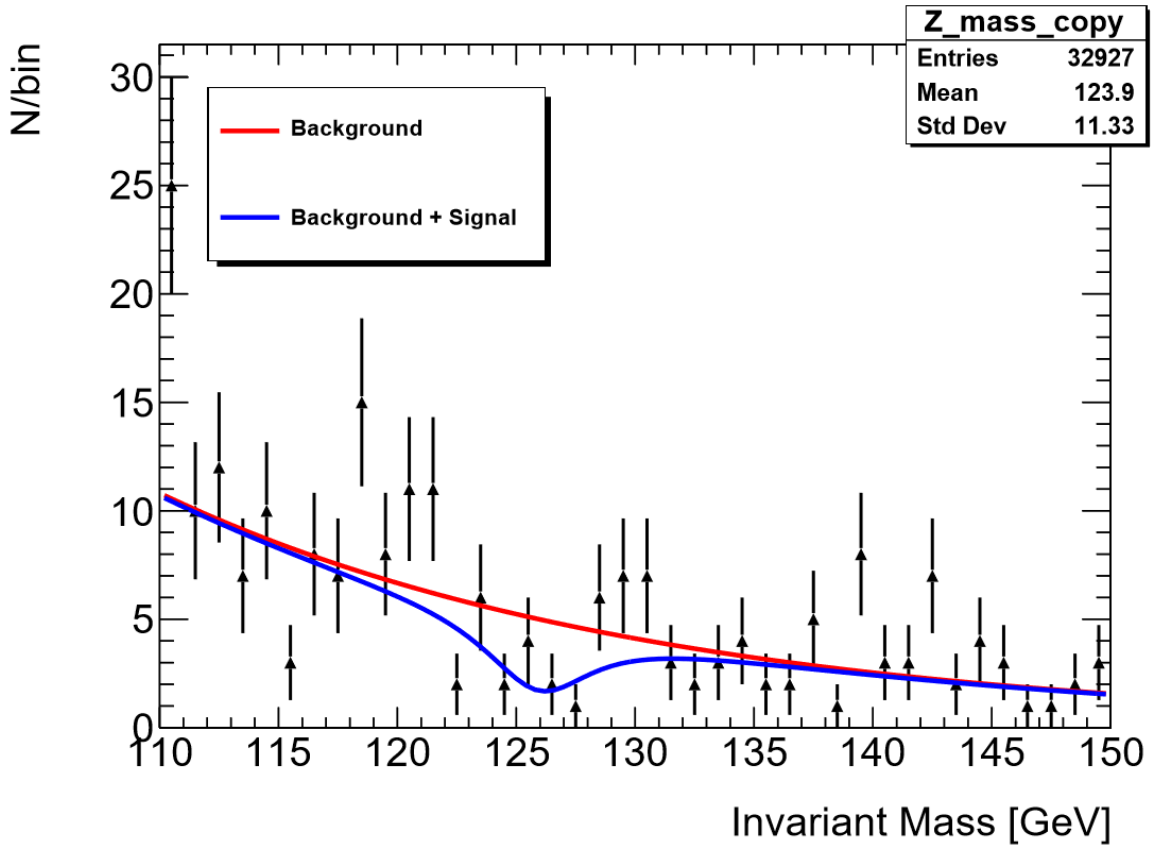

Figure 43: Data in Higgs region with background and signal fits

Here, the red line takes the following parameters:

Table 14: Parameters for exponential background in Higgs region

Parameter	Value	Error
Constant	7,69972	0,0659884
Slope	-0,0483537	0,000519951

And as with figure 41, the blue like takes the same parameters, plus a function to fit the peak. In this case that is a sum of a Gauss and BW function:

Table 15: Parameters for Gauss + BW peak in Higgs region

Parameter	Value	Error
Constant Gauss	-10,6031	10,6066
Mass Gauss	127,049	5,46225
Sigma Gauss	0,00719994	0,0000309034
Constant BW	-1641160	368879
Mass BW	125,926	0,953526
FWHM BW	5,60366	0,771185

The fit from table 15 is different from the previously used convolution, because if we try to estimate the possible mass from the data we have, a normal Gaussian or the Gauss/BW convolution does not give a realistic estimate for the mass and width of the Higgs. Because we just add the two functions together, we get estimates of mass and width for both of them, meaning we can compare how well each of them estimate the Higgs. In this case the BW function gives the best fit for the mass, estimating it to $m_H = 126 \pm 1\ GeV$ where the width of the peak is $5{,}6 \pm 0{,}8\ GeV$ which is around where we would expect it. The Gaussian in comparison estimates a mass higher than what we would expect at $m_H = 127 \pm 5\ GeV$, where the width is also unrealistically narrow at just $0{,}007 \pm 0{,}00003\ GeV$. The estimates given by the two functions combined with the lack of a visible peak in figure 43 does suggest that the peak from the fit is more arbitrary than we would like. This conclusion is also strengthened by the fact that the peak itself is negative compared to the background. Even though there is no clear peak, we can try to use the area enclosed by the two fits to give us an upper estimate of how many Higgs' we could have in the data and use that to estimate the cross section to see if we get something comparable to the MC, like we did earlier for the Z^0 in eq. 19. Since the MC Higgs sample has been fitted with just a Gaussian, in order to get a comparative estimate of the Higgs signal here, we can try to fit the signal with just a Gaussian, while fixing the mass and width based on the values given by the MC shown in table 13. This gives the following plot:

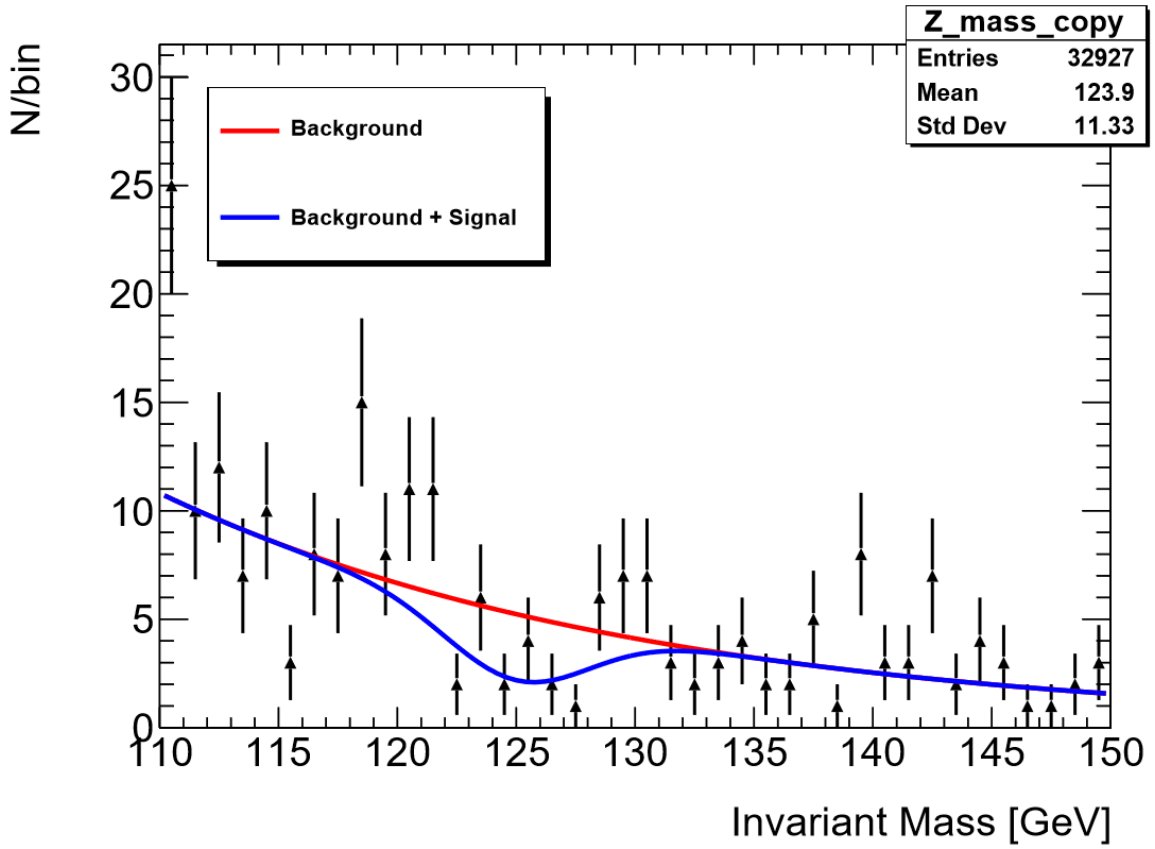

Figure 44: Figure 40 with just a Gaussian fit, mass and sigma fixed

In order to make the estimate as good as possible, we have fixed all parameters except the magnitude of the Gaussian. The background is the same as given by table 14, where the gaussian takes the following parameters:

Table 16: Parameters for Gaussian on Higgs region, with mass and width fixed from MC

Parameter	Value	Error
Constant	-3,04801	0,690487
Mass	125	Fixed
Sigma	2,99092	Fixed

With the mass and width fixed, the magnitude of the Gaussian is $c = -3{,}1 \pm 0{,}7$ as shown in table 16. If we use the area enclosed by the blue and the red line combined with the uncertainty in the magnitude of the Gaussian, we can try to estimate the maximum number of Higgs' we can expect to find. If we assume that the area is proportional to the magnitude, and considering a 95% confidence level, we can estimate the number of Higgs entries:

$$N_H = A \pm 1{,}95 * \frac{A}{c} = -22{,}7914 \pm 10{,}0692 \tag{22}$$

Where A is the area enclosed by the two functions and c is the magnitude of the Gaussian fit from figure 44. Because the magnitude of the peak is negative, the expectation value must also be negative, hence we must assume it to be zero, since we cannot have fewer than 0 Higgs'. Therefore, we can say that with a 95% confidence level that we could maximally expect to see 10 $H^0 \to \mu^+\mu^-$ decays. However, it is worth pointing out that we estimate this while fixing the background function. This means that the uncertainty in the background will also contribute to this, meaning the uncertainty in the area we calculated is bigger in reality than what we found.

In order to work out the luminosity, the method used earlier on the Z using eq. 17 would not give a representative estimate because we would get a luminosity of 0 since there is no visible signal. Our best estimate is therefore to take the luminosity of data generated by ATLAS in 2018 (since that is the data we are using) (33) and scaling by the fraction of the data we are running over. This means we end up with something like

$$\mathcal{L} \approx 58{,}5\ fb^{-1} * \frac{N_{reco}}{N_{total}} = 0{,}0681\ fb^{-1} = 68{,}1 * 10^3\ nb^{-1} \tag{23}$$

The reconstruction efficiency of the $H^0 \to \mu^+\mu^-$ sample is 72,42%, meaning if the data contains maximum 10 Higgs decays, we could expect there to be at most around 14 actual decays. Dividing by the luminosity we get an estimated effective cross section of around $\sigma_{eff} = 0{,}0002\ nb$ based on eq. 19, which is a lot lower than the true value in the MC, which is $\sigma_{true} = 0{,}0283\ nb$. Part of the reason the effective cross section is so low here is likely to be because we have overestimated the luminosity in eq. 23, as that is a very rough estimate. It is also worth noting the higher reconstruction efficiency of the Higgs compared to the Z^0. Using the same working point the $H^0 \to \mu^+\mu^-$ had an efficiency of 72%, compared to only 47% for the Z^0. This could come from the η distribution, where it appears the distribution from the Higgs is more centre loaded than is the case for the Z^0.

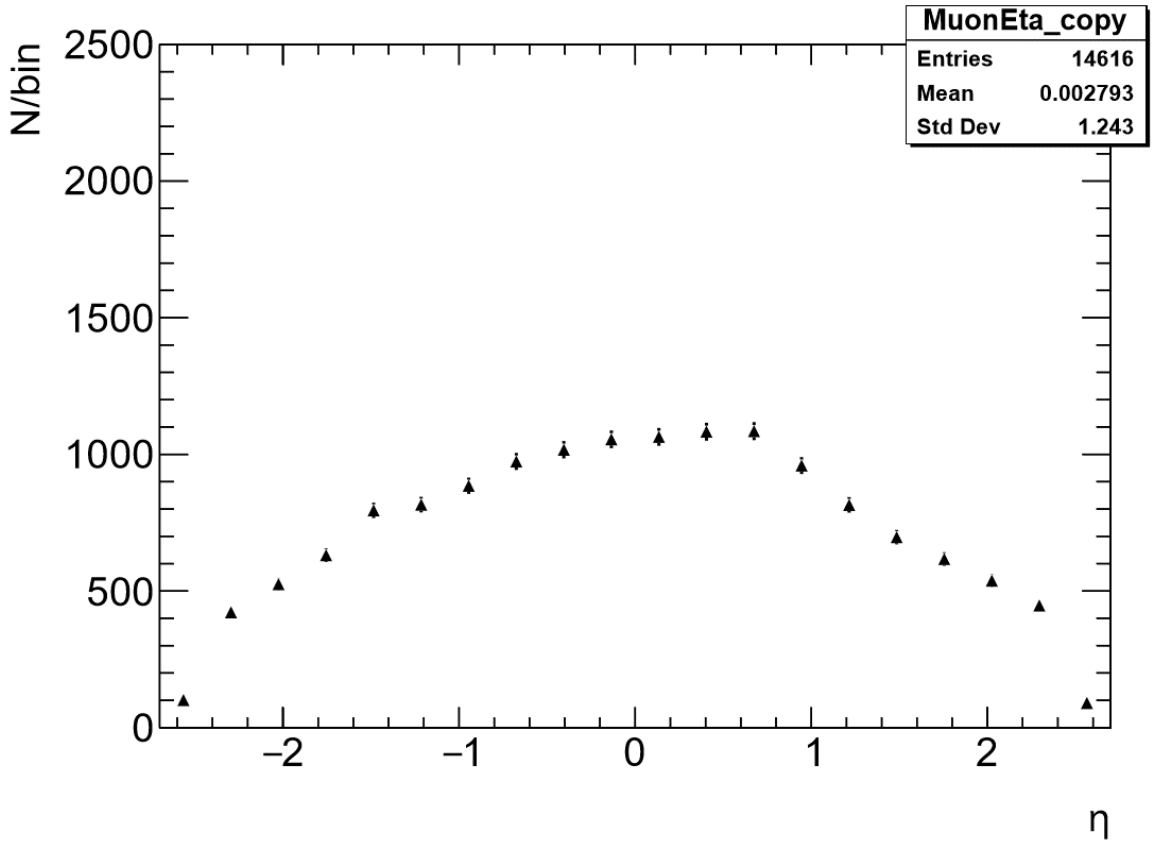

Figure 45: Eta distribution for muons produced by Higgs

Because more of the muons are around the centre here, as shown in figure 45, fewer muons are lost outside the acceptance range of the detector, causing the reconstruction efficiency to go up. This is fewer than for the Z^0, as shown in figure 26, where it is apparent that the η distribution is more evenly distributed than for the Higgs, causing more muons to fall outside the acceptance range.

The main problem with the extremely small cross section of the $H^0 \rightarrow \mu^+\mu^-$ interaction is that you need an absurd amount of data to start seeing a peak. The relationship between cross section, luminosity and number of events is the following

$$N = \mathcal{L} * \sigma \tag{24}$$

Which means that even if we run over the full ATLAS catalogue of data, with a luminosity of $\mathcal{L} = 139\ fb^{-1}$ and a cross section for Higgs production from proton-proton collisions of $\sigma = 55\ pb$ (34), we would expect around $N = 7{,}6 * 10^6$ Higgs bosons produced. The branching ratio for the $H^0 \rightarrow \mu^+\mu^-$ channel can be calculated like this:

$$Br(H^0 \rightarrow \mu^+\mu^-) = \left(\frac{m_\mu}{m_\tau}\right)^2 Br(H^0 \rightarrow \tau^+\tau^-) = 0{,}00025 \tag{25}$$

This means out of the 7,6 million Higgs' produced, only about 1900 of those would decay to two muons. Working backwards from eq. 24 and 25, we can estimate the theoretical number of Higgs' produced in the data we have run over. If we were to see a single $H^0 \rightarrow \mu^+\mu^-$ decay, we would need to produce over 4000 Higgs bosons. Given that of the 1 million events we ran over only 33k were reconstructed, we could maximally expect to see only around 8 $H^0 \rightarrow \mu^+\mu^-$ decays, and that is assuming every one of the reconstructed events produced a Higgs. More importantly, 4000 Higgs

bosons given the cross section for Higgs production mentioned earlier, it would require a luminosity of $\mathcal{L} = 73{,}46\ pb^{-1}$, which is more than the luminosity we estimated to have run over in eq. 23, which was $\mathcal{L} = 68{,}1\ pb^{-1}$. Considering that we also concluded that to be an overestimate, it is unlikely there were even a single Higgs decay in the data we could run over.

Conclusions

It was clear from the outset it was going to be difficult to find anything of significance from the Higgs. Knowing the narrow cross section of Higgs production and especially the $H^0 \to \mu^+\mu^-$ decays, it is so difficult to get a clear measurement of this channel that ATLAS itself is not expected to get a 5 sigma signal until LHC starts its run 3 this year (35). In theory it is possible we could have found a hint of a peak, but time constraints limited the amount of data we could run over. Even if 1 million events seem like a lot, and in the case of the Z^0, J/ψ and ϒ it was enough with only 50k events to establish clear peaks of these decays, the $H^0 \to \mu^+\mu^-$ decay is so rare that even 1 million events is not nearly enough to get a visible signal from this decay channel. Even though we were not successful in finding a clear peak from the Higgs, we were still able to verify several important points about both the ATLAS detector and the Z^0 boson. Starting with a pure MC sample of $Z^0 \to \mu^+\mu^-$ decays, we were able to look at the reconstructed distributions, and pick them apart to separate the minimum bias background to the actual Z^0 decays, and compare the truth information of how the event actually happened to the truth matching of how those muons looked after passing through the detector. Based on this we could get a measure of the muon reconstruction efficiency by comparing the muons that passed inside the muon accepance range of $\eta \in [-2.7,2.7]$, and then by comparing the p_T of the muons for different intervals we were able to verify the momentum resolution of the detector, after realising that the difference in $\frac{1}{p_T}$ is approximately Gaussian, allowing us to use the standard deviation of the Gaussians to estimate the momentum resolution of the detector. Taking this knowledge with us we were able to recreate a good approximation of a real event in the ATLAS detector by adding more MC samples of different events that also produce muons. We could then verify this by comparing to some actual real data. By normalizing the MC plot and comparing to the data, we were able to work out a luminosity corresponding to the Z^0 seen in the data, and we were also able to calculate the effective cross section of the $Z^0 \to \mu^+\mu^-$ from the data. By fitting the Z^0 peak and background, and establishing that it made sense, it allowed us to use it to try to fit the Higgs peak. Even if we established that we overestimated the number of Higgs' in the data, it was still usful to try to estimate the working cross section by comparing it to an MC, like we did with the Z^0. While we were unsuccessful in finding a clear indication of this decay, we know that the teams at ATLAS are hard at work pouring over a lot more data, and hopefully they can confirm this decay channel with greater accuracy once LHC's run 3 starts.

Sources

(1) https://en.wikipedia.org/wiki/CERN (14.01.2021)
(2) https://international-relations.web.cern.ch/stakeholder-relations/Member-State-Relations (14.01.2021)
(3) https://home.cern/science/accelerators/synchrocyclotron (17.03.2021)
(4) https://home.cern/science/accelerators/proton-synchrotron (17.03.2021)
(5) https://home.cern/science/accelerators/super-proton-synchrotron (17.03.2021)

(6) https://home.cern/science/accelerators/large-electron-positron-collider (17.03.2021)
(7) https://home.cern/sites/home.web.cern.ch/files/2018-07/CERN-Brochure-2017-002-Eng_0.pdf (07.04.2021)
(8) https://atlas.cern/discover/detector (23.04.2021)
(9) https://atlas.cern/discover/detector/inner-detector (23.04.2021)
(10) https://atlas.cern/discover/detector/calorimeter (26.04.2021)
(11) https://www.researchgate.net/figure/The-calorimeter-system-in-the-ATLAS-experiment-at-the-Large-Hadron-Collider_fig1_258488732 (26.04.2021)
(12) https://pdg.lbl.gov/2020/listings/rpp2020-list-muon.pdf (08.04.2021)
(13) https://atlas.cern/discover/detector/muon-spectrometer (26.04.2021)
(14) https://cds.cern.ch/record/1457044/files/ATLAS%20fact%20sheet.pdf (26.04.2021)
(15) https://cds.cern.ch/record/1505342 (26.04.2021)
(16) https://en.wikipedia.org/wiki/Pseudorapidity (20.03.2021)
(17) https://en.wikipedia.org/wiki/Sagitta_(geometry) (20.03.2021)
(18) https://home.cern/science/physics/standard-model (05.06.2021)
(19) https://en.wikipedia.org/wiki/Up_quark (04.02.2021)
(20) https://en.wikipedia.org/wiki/Charm_quark (04.02.2021)
(21) https://en.wikipedia.org/wiki/Bottom_quark (04.02.2021)
(22) https://en.wikipedia.org/wiki/Top_quark (04.02.2021)
(23) https://en.wikipedia.org/wiki/Muon (04.02.2021)
(24) https://en.wikipedia.org/wiki/Tau_(particle) (04.02.2021)
(25) https://en.wikipedia.org/wiki/Neutrino (04.02.2021)
(26) https://en.wikipedia.org/wiki/Gluon (04.02.2021)
(27) https://en.wikipedia.org/wiki/W_and_Z_bosons (04.02.2021)
(28) https://en.wikipedia.org/wiki/Photon (04.02.2021)
(29) (Measurements of Cross Sections and Couplings of the Higgs boson Using the ATLAS detector, XXXI International Workshop on High Energy Physics: (HEPFT2017), 5-7 July 2017, B. Stugu et. al, 2017)
(30)https://indico.cern.ch/event/472469/contributions/1982677/attachments/1220934/1785823/intro_slides.pdf (11.06.2021)
(31) https://en.wikipedia.org/wiki/Convolution (12.06.2021)
(32) (Measurement of Muon Momentum Resolution of the ATLAS Detector, A. Salvucci et. al, 2012) https://arxiv.org/pdf/1201.4704.pdf (27.04.2021)
(33) https://twiki.cern.ch/twiki/bin/view/AtlasPublic/LuminosityPublicResultsRun2 (11.06.2021)
(34) (Pixel detector performance and study of CP invariance in H to tau tau decays with the ATLAS detector, Steffen Mæland, 2018) https://bora.uib.no/bora-xmlui/handle/1956/18106 (02.06.2021)
(35) https://home.cern/news/news/accelerators/new-schedule-lhc-and-its-successor (03.06.2021)

Source Code and Data Samples

The algorithm setup is based on the ATLAS software tutorial found here:
https://atlassoftwaredocs.web.cern.ch/ABtutorial/release_setup/

We have used the following sections:

Create your package
Create algorithm
Configuration (Athena)
Add some printouts
xAOD access
Filling histograms
Tool Handles
Making Trees/Ntuples
CP Algorithm Example sequence
Configure your algorithm
Add to our job

The main part of the algorithm is listed below, coming from the “Execute” part of the file “MyxAODAnalysis.cxx”. Everything else is based entirely on the chapters listed above.

```
StatusCode MyxAODAnalysis :: execute ()
{
  // Here you do everything that needs to be done on every single
  // events, e.g. read input variables, apply cuts, and fill
  // histograms and trees.  This is where most of your actual analysis
  // code will go.
  ANA_MSG_INFO ("in execute");
  m_muonSize->clear();
  m_muonEta->clear();
  m_muonPhi->clear();
  m_muonPt->clear();
  m_muonE->clear();
  m_leadingPt->clear();
  m_subPt->clear();
  m_Z_mass->clear();
  m_truthZ->clear();
  m_children->clear();
  m_truthEta->clear();
  m_truthPhi->clear();
  m_mChildren->clear();
  m_Z_match->clear();
  m_MinBias->clear();
  m_matchEta->clear();
  m_matchPhi->clear();
  m_ptRes->clear();
  m_etaRes->clear();
  const xAOD::EventInfo* eventInfo = 0;
  ANA_CHECK(evtStore()->retrieve( eventInfo, "EventInfo"));
  // check if the event is data or MC
  // (many tools are applied either to data or MC)
  bool isMC = false;
  // check if the event is MC
  if (eventInfo->eventType (xAOD::EventInfo::IS_SIMULATION)) {
    isMC = true; // can do something with this later
    ANA_MSG_INFO ("MC is triggering");
    const xAOD::TruthEventContainer* xTruthEventContainer = NULL;
    ANA_CHECK(evtStore()->retrieve(xTruthEventContainer, "TruthEvents"));
    xAOD::TruthEventContainer::const_iterator itr;
    auto tHSevent = xTruthEventContainer->at(0);
    int nPart = tHSevent->nTruthParticles();
    for (int iPart = 0; iPart < nPart; iPart++) {
      const xAOD::TruthParticle* particle = tHSevent->truthParticle(iPart);
      if (particle) {
```

```
      if (particle->pdgId() == 23) {
        double_t truthZ = (particle->p4()).M();
        const xAOD::TruthParticle* child0 = particle->child(0);
        const xAOD::TruthParticle* child1 = particle->child(1);
        if (child0) {
          if (child1) {
            if (child0->pdgId() == 13 && child1->pdgId() == -13) {
              m_truthZ->push_back (truthZ * 0.001);
              m_children->push_back (child0->pt() * 0.001);
              m_children->push_back (child1->pt() * 0.001);
              m_truthEta->push_back (child0->eta());
              m_truthEta->push_back (child1->eta());
              m_truthPhi->push_back (child0->phi());
              m_truthPhi->push_back (child1->phi()); }}}}}}
  const xAOD::MuonContainer* muons = nullptr;
  ANA_CHECK (evtStore()->retrieve (muons, "Muons"));
  m_muonSize->push_back (muons->size());
  if (muons->size() < 2) {          //ignore events with less than 2 muons
```

```
    ANA_MSG_INFO ("No Muons Here");
    tree ("analysis")->Fill ();
    return StatusCode::SUCCESS; }
  const xAOD::Muon* muon_m1 = nullptr;
  const xAOD::Muon* muon_m2 = nullptr;
  const xAOD::Muon* MinBias1 = nullptr;
  const xAOD::Muon* MinBias2 = nullptr;
  Double_t ptRes1 = 0;
  Double_t ptRes2 = 0;
  Double_t etaRes1 = 0;
  Double_t etaRes2 = 0;
  Double_t value1 = 0;
  Double_t value2 = 0;
  for (const xAOD::Muon* muon : *muons) {
    typedef ElementLink<xAOD::TruthParticleContainer>ElementTruthLink_t;
    const xAOD::TruthParticle* tresult = 0;
    if (muon->isAvailable<ElementTruthLink_t>("truthParticleLink")) {
      const ElementTruthLink_t ptruthContainer = muon->auxdata<ElementTruthLink_t>("truthParticleLink");
```

```
      if (ptruthContainer.isValid()) {
        tresult = *ptruthContainer; }}
    if (tresult != 0) {
      int pdgId = tresult->pdgId();
      if (pdgId == 13 || pdgId == -13) {
        const xAOD::TruthParticle* mother = tresult->parent(0);
        if (mother) {
        int pdgIdParent = mother->pdgId();
          if (pdgIdParent == 23) {
            if (muon_m1 == nullptr) {
              muon_m1 = muon;
              ptRes1 = ((1/(tresult->pt() * 0.001)) - (1/(muon_m1->pt() * 0.001)));
              etaRes1 = (tresult->eta() - muon_m1->eta()); }
              else {
              muon_m2 = muon;
              ptRes2 = ((1/(tresult->pt() * 0.001)) - (1/(muon_m2->pt() * 0.001)));
              etaRes2 = (tresult->eta() - muon_m2->eta()); }}}}}
    if (tresult == 0) {
```

```
      if (muon->pt() > value1) {
        value1 = muon->pt();
        MinBias1 = muon; }}}
  for (const xAOD::Muon* muon : *muons) {
    typedef ElementLink<xAOD::TruthParticleContainer>ElementTruthLink_t;
    const xAOD::TruthParticle* tresult = 0;
    if (muon->isAvailable<ElementTruthLink_t>("truthParticleLink")) {
      const ElementTruthLink_t ptruthContainer = muon->auxdata<ElementTruthLink_t>("truthParticleLink");
      if (ptruthContainer.isValid()) {
        tresult = *ptruthContainer; }}
    if (tresult == 0) {
      if (muon->pt() > value2) {
        if (muon->pt() == value1) {continue;}
          value2 = muon->pt();
          MinBias2 = muon; }}}
  if (muon_m1 != nullptr) {
    m_mChildren->push_back (muon_m1->pt() * 0.001);
    m_matchEta->push_back (muon_m1->eta());
```

```
    m_matchPhi->push_back (muon_m1->phi());
    m_ptRes->push_back (ptRes1);
    m_etaRes->push_back (etaRes1);
    if (muon_m2 != nullptr) {
      m_mChildren->push_back (muon_m2->pt() * 0.001);
      m_matchEta->push_back (muon_m2->eta());
      m_matchPhi->push_back (muon_m2->phi());
      m_ptRes->push_back (ptRes2);
      m_etaRes->push_back (etaRes2);
      TLorentzVector muon_m1_p4 = muon_m1->p4();
      TLorentzVector muon_m2_p4 = muon_m2->p4();
      TLorentzVector Zm_p4 = muon_m1_p4 + muon_m2_p4;
      Double_t Z_match = Zm_p4.M();
      m_Z_match->push_back (Z_match * 0.001); }}
  if (MinBias1 != nullptr) {
    if (MinBias2 != nullptr) {
      TLorentzVector MinBias1_p4 = MinBias1->p4();
      TLorentzVector MinBias2_p4 = MinBias2->p4();
      TLorentzVector MB_p4 = MinBias1_p4 + MinBias2_p4;
      Double_t MinBias = MB_p4.M();
      m_MinBias->push_back (MinBias * 0.001); }}
  Double_t pt_value = 0;
  Double_t pt_sub = 0;
  const xAOD::Muon* muon_leading = nullptr;
  const xAOD::Muon* muon_sub = nullptr;
  for (const xAOD::Muon* muon : *muons) {
    ANA_MSG_INFO ("execute(): original muon pt = " << ((muon)->pt() * 0.001) << " GeV");
    if (muon->pt() > pt_value) {                    //find leading muon
      pt_value = muon->pt();
      muon_leading = muon; } }
  for (const xAOD::Muon* muon : *muons) {
    if (muon->pt() > pt_sub) {                      //find sub-leading muon
      if (muon->pt() == pt_value) {continue;}       //ignore leading muon
        pt_sub = muon->pt();
        muon_sub = muon; }}
  TLorentzVector muon_leading_p4 = muon_leading->p4(); //define muon 4-momenta
  TLorentzVector muon_sub_p4 = muon_sub->p4();
  TLorentzVector Z_p4 = muon_leading_p4 + muon_sub_p4;
  Double_t Z_mass = Z_p4.M();                           //calculate Z mass
  const xAOD::EventInfo* ei = nullptr;
  ANA_CHECK (evtStore()->retrieve (ei, "EventInfo"));
  m_runNumber = ei->runNumber ();
  m_eventNumber = ei->eventNumber ();
  for (const xAOD::Muon* muon : *muons) {
    m_muonEta->push_back (muon->eta());
    m_muonPhi->push_back (muon->phi());
    m_muonPt->push_back (muon->pt() * 0.001);   //factor 0.001 to make unit GeV
    m_muonE->push_back (muon->e() * 0.001); }
  m_leadingPt->push_back (muon_leading->pt() * 0.001);
  m_subPt->push_back (muon_sub->pt() * 0.001);
  m_Z_mass->push_back (Z_mass * 0.001);
  tree ("analysis")->Fill ();
}
// if data check if event passes GRL
if (isMC == false) { // it's data!
  ANA_MSG_INFO ("data should trigger");
  if (!m_grl->passRunLB(*eventInfo)) {
    ANA_MSG_INFO ("drop event: GRL");
    return StatusCode::SUCCESS; } // go to next event
  const xAOD::MuonContainer* muons = nullptr;
  ANA_CHECK (evtStore()->retrieve (muons, "AnalysisMuons_NOSYS"));
  m_muonSize->push_back (muons->size());
  if (muons->size() < 2) {          //ignore events with less than 2 muons
    ANA_MSG_INFO ("No Muons Here");
    tree ("analysis")->Fill ();
    return StatusCode::SUCCESS; }
  Double_t pt_value = 0;
  Double_t pt_sub = 0;
  const xAOD::Muon* muon_leading = nullptr;
  const xAOD::Muon* muon_sub = nullptr;
  for (const xAOD::Muon* muon : *muons) {
    ANA_MSG_INFO ("execute(): original muon pt = " << ((muon)->pt() * 0.001) << " GeV");
```

```
    if (muon->pt() > pt_value) {                    //find leading muon
      pt_value = muon->pt();
      muon_leading = muon; } }
  for (const xAOD::Muon* muon : *muons) {
    if (muon->pt() > pt_sub) {                      //find sub-leading muon
      if (muon->pt() == pt_value) {continue;}       //ignore leading muon
        pt_sub = muon->pt();
        muon_sub = muon; }
  }
  TLorentzVector muon_leading_p4 = muon_leading->p4(); //define muon 4-momenta
  TLorentzVector muon_sub_p4 = muon_sub->p4();
  TLorentzVector Z_p4 = muon_leading_p4 + muon_sub_p4;
  Double_t Z_mass = Z_p4.M();                         //calculate Z mass
  const xAOD::EventInfo* ei = nullptr;
  ANA_CHECK (evtStore()->retrieve (ei, "EventInfo_NOSYS"));
  m_runNumber = ei->runNumber ();
  m_eventNumber = ei->eventNumber ();
  for (const xAOD::Muon* muon : *muons) {
```

```
    m_muonEta->push_back (muon->eta());
    m_muonPhi->push_back (muon->phi());
    m_muonPt->push_back (muon->pt() * 0.001);   //factor 0.001 to make unit GeV
    m_muonE->push_back (muon->e() * 0.001); }
  m_leadingPt->push_back (muon_leading->pt() * 0.001);
  m_subPt->push_back (muon_sub->pt() * 0.001);
  m_Z_mass->push_back (Z_mass * 0.001);
  tree ("analysis")->Fill ();
 } // end if not MC
 ANA_MSG_INFO ("keep event: GRL");
 return StatusCode::SUCCESS;
}
```

MC $Z \rightarrow \mu\mu$:

mc16_13TeV.361107.PowhegPythia8EvtGen_AZNLOCTEQ6L1_Zmumu.merge.AOD.e3601_e5984_s3126_s3136_r9364_r9315	
Number of events:	10000
Cross section:	1,9 nb

Background MC samples:

$Z \rightarrow \tau\tau$:

mc16_13TeV.361108.PowhegPythia8EvtGen_AZNLOCTEQ6L1_Ztautau.recon.AOD.e3601_a875_r9364	
Number of events:	10000
Cross section:	1,9 nb

Diboson:

mc16_13TeV.361600.PowhegPy8EG_CT10nloME_AZNLOCTEQ6L1_WWlvlv.recon.AOD.e4616_s3126_r10201	
Number of events:	10000
Cross section:	0,0106 nb

mc16_13TeV.361601.PowhegPy8EG_CT10nloME_AZNLOCTEQ6L1_WZlvll_mll4.recon.AOD.e4475_s3126_r9364	
Number of events:	10000
Cross section:	0,00451 nb

mc16_13TeV.361602.PowhegPy8EG_CT10nloME_AZNLOCTEQ6L1_WZlvvv_mll4.recon.AOD.e4054_s3126_r9364	
Number of events:	10000
Cross section:	0,00278 nb

mc16_13TeV.361603.PowhegPy8EG_CT10nloME_AZNLOCTEQ6L1_ZZllll_mll4.recon.AOD.e4475_s3126_r9364	
Number of events:	10000
Cross section:	0,00127 nb

mc16_13TeV.361605.PowhegPy8EG_CT10nloME_AZNLOCTEQ6L1_ZZvvvv_mll4.merge.AOD.e4054_e5984_s3126_r10201_r10210	
Number of events:	10000
Cross section:	0,000549 nb

Single Top:

mc16_13TeV.410011.PowhegPythiaEvtGen_P2012_singletop_tchan_lept_top.recon.AOD.e3824_s3126_r9364	
Number of events:	10000
Cross section:	0,0437 nb

Ttbar:

mc16_13TeV.410000.PowhegPythiaEvtGen_P2012_ttbar_hdamp172p5_nonallhad.recon.AOD.e3698_s2997_r10423	
Number of events:	500
Cross section:	0,696 nb

Drell-Yan:

mc16_13TeV.301000.PowhegPythia8EvtGen_AZNLOCTEQ6L1_DYee_120M180.merge.AOD.e3649_e5984_s3126_r10201_r10210	
Number of events:	10000
Cross section:	0,0175 nb

mc16_13TeV.301001.PowhegPythia8EvtGen_AZNLOCTEQ6L1_DYee_180M250.merge.AOD.e3649_e5984_s3126_r10201_r10210	
Number of events:	10000
Cross section:	0,00292 nb

mc16_13TeV.301002.PowhegPythia8EvtGen_AZNLOCTEQ6L1_DYee_250M400.merge.AOD.e3649_e5984_s3126_r10201_r10210	
Number of events:	10000
Cross section:	0,00108 nb

mc16_13TeV.301003.PowhegPythia8EvtGen_AZNLOCTEQ6L1_DYee_400M600.merge.AOD.e3649_e5984_s3126_r10201_r10210	
Number of events:	10000
Cross section:	0,000196 nb

mc16_13TeV.301004.PowhegPythia8EvtGen_AZNLOCTEQ6L1_DYee_600M800.merge.AOD.e3649_s3126_r9364_r9315	
Number of events:	10000
Cross section:	0,0000374 nb

mc16_13TeV.301005.PowhegPythia8EvtGen_AZNLOCTEQ6L1_DYee_800M1000.merge.AOD.e3649_e5984_s3126_r10201_r10210	
Number of events:	10000
Cross section:	0,0000106 nb

mc16_13TeV.301006.PowhegPythia8EvtGen_AZNLOCTEQ6L1_DYee_1000M1250.merge.AOD.e3649_e5984_s3126_r10201_r10210	
Number of events:	2000
Cross section:	0,00000426 nb

Dijet:

(contains semileptonic decays, these samples were considered, but not included)

mc16_13TeV.423300.Pythia8EvtGen_A14NNPDF23LO_perf_JF17.merge.AOD.e3848_e5984_s3126_s3136_r10724_r10726	
Number of events:	10000
Cross section:	2430000 nb

mc16_13TeV.423301.Pythia8EvtGen_A14NNPDF23LO_perf_JF23.merge.AOD.e3848_s3126_r10201_r10210	
Number of events:	10000
Cross section:	728000 nb

mc16_13TeV.423302.Pythia8EvtGen_A14NNPDF23LO_perf_JF35.merge.AOD.e3848_s3126_r10201_r10210	
Number of events:	10000
Cross section:	134000 nb

Real Data:

data18_13TeV.00360063.physics_Main.deriv.DAOD_PHYS.f969_m2020_p4150	
Number of files:	15
Number of events:	960976

MC $H \rightarrow \mu\mu$:

mc16_13TeV.345097.PowhegPythia8EvtGen_NNLOPS_nnlo_30_ggH125_mumu.merge.AOD.e5732_s3126_r9364_r9315	
Number of events:	10000
Cross section:	0,0283 nb